Doctoral Dissertation (Shinshu University)

Evaporation-induced surface modification of high performance fibers

Sep. 2018

ZHU PENG

CONTENTS

CHAPTER ONE

General Introduction

Chapter 1: General introduction

1.1 Surface modification of high performance fibers

High performance fibers are engineered for specific uses that require exceptional strength, heat resistance and/or chemical resistance, such as glass fiber, carbon fiber, aramid fiber, PBI (polybenzimidazole) fiber, PBO (polyphenylenebenzobisozazole) fiber and PI (polyimide) fiber, Sulfar (PPS, polyphenylene sulfide) fiber, melamine fiber and HDPE (high-density polyethylene) fiber. In the study, PBO and carbon fiber were selected as research subjects because they had excellent performance, but their shortcomings were also very obvious. Therefore, the surface modification of High performance fibers is needed.

In general, the surface modification methods on high performance fibers can be divided into two types: oxidation and non-oxidation. Oxidation is the method with using an oxidizing agent to improve the activity of functional groups on the fiber surface. Oxidation includes gas phase oxidation carried in air, oxygen or ozone; liquid phase oxidation with nitric acid & sulfuric acid, ammonia, hydrogen peroxide, sodium hydroxide, potassium permanganate, chlorate, hypochlorite, persulfate as the oxidant; anodic oxidation carried with sodium hydroxide, ammonium bicarbonate, sulfuric acid, nitric acid, ammonium nitrate and organic acid or the salts of organic acids as electrolyte. Non-oxidation is the method, with which the structure and surface energy of the fiber surface was regulated with coating, grafting, cleaning, etching and so on. With these methods, such as plasma, chemical grafting, surface cleaning, the weak layer of the fiber interface can be removed to some degree, and the surface roughness of the fibers and the engagement of the interface can be improved. Meanwhile, the surface

energy of the fiber will increase [1].

Poly(p-phenylene benzobisoxazole) (PBO) fibers were developed by the US Air Force and commercialized by Toyobo as Zylon [2]. The company commercially produces two types of PBO fibers; standard type AS and high modulus type HM [3]. As a new structural material, PBO fibers have low density, high strength, high modulus (HM), good chemical resistance, and good thermal stability [4-10]. Because of these favorable features, PBO fibers have great potential applications such as fiber reinforced composites [11-13], tendons for scientific balloon, high strength tethers, tension structures, and body armor [5,14-17].

However, PBO fibers have a critical problem like photodegradation under UV exposure, which can deteriorate structures and properties of PBO fiber and corresponding products [18]. According to the report provided by Toyobo, both AS and HM PBO fibers lost 65 % of their strength after 6 months exposure at Ohtsu, Japan, or after 500 h exposure in a Xenon light weatherometer [15, 19]. Therefore, measures of protecting PBO fibers from UV effects are needed.

To overcome such an undesired characteristic, some researches have been undertaken to protect high performance fibers form UV light [20-22]. Jin et al. prepared a photoaging-resistant PBO fiber containing a light stabilizer (OB-1) by in situ polymerization and dry-jet wet-spinning [15]. Won et al. used low density polyethylene loaded with different content of TiO_2 and white pigment as protective film for high performance fibers from UV light [14]. Song et al. prepared a (polyhedral oligomeric silsesquioxane/TiO_2)$_n$ multi-coating on PBO fibers via layer-by-layer assembly [23]. They also added UV absorbers to PBO fiber surfaces by coordination bond formation and physical adsorption [24]. Zhang et al. focused on the UV shielding efficiency of

PBO fibers with a ZnO nanoparticle/epoxy hybrid coating [17].

Carbon fibers (CFs) have been widely used as reinforcements for advanced composites because of their excellent mechanical properties, high thermal and electrical conductivities, excellent corrosion resistance, low linear thermal expansion coefficient, and low density [25, 26]. CF-reinforced epoxy composites remain the most widely used fiber-reinforced composite materials because of the simplicity and low cost of their production process. However, the potential of CF-reinforced epoxy composites has not yet been fully exploited because of the chemically inert CF surface, which makes it difficult to achieve the desired interfacial adhesion with the matrix [25].

In investigations of this interfacial adhesion, fiber-reinforced composites are considered to consist of three main components: the fibers, which are the load-bearing components; the matrix, which holds the fibers together and transfers the applied load between fibers; and the fiber–matrix interphase, which determines the adhesion property between the fibers and matrix [27]. During the last decade, extensive research has been devoted to improving the fiber–matrix interphase using surface treatment of the CFs using techniques such as chemical grafting, electromechanical methods, plasma treatment, radiation, or surface coating [28-30]. However, in addition to providing a coating, these methods generate oxygen functional groups via strong oxidizing reactions, which lead to drawbacks on the CF surface that cause a decrease of the fiber strength [31, 32]. However, with recent developments in materials science and technology, an increasing number of new materials that have begun to be used as coating components have been invented, such as carbon nanotubes [33-35], graphene oxide [36, 37], and graphene nanoplatelets [26, 38].

In addition to inorganic coatings, research has also been conducted on organic

coatings, including studies on the tensile properties of polyimide-coated CFs [39, 40]; the interfacial shear strength (IFSS) of CFs coated with high-performance polymers such as poly(arylene ether phosphine oxide) (PEPO), Udel®P-1700, and Ultem®1000, water-soluble poly(hydroxy ether ethanol amine), water-dispersed carboxy-modified poly(hydroxyether), and water-insoluble poly(hydroxy ether) [41]; the effect of polyamide coatings on CFs on the mechanical properties of carbon/epoxy composites [42]; the effect of hygrothermal aging on the interlaminar shear strength of carbon–epoxy composites based on fibers coated with Nylon 6,6 [43]; and the role of a polyamide interphase on CFs reinforcing an epoxy matrix [44].

1.2 Polymer grafted nanoparticles

Nanoparticles may be synthesized from many materials by various physical and chemical methods, with the particles differing in their elemental composition, shape, size, and chemical or physical properties [45]. The physical methods generally involve vapor deposition and depend on the principle of sub-dividing bulk precursor materials into smaller nanoparticles. The chemical approach generally involves reduction of metal ions into metal atoms in the presence of stabilizing agents, followed by the controlled aggregation of atoms [46]. The synthesis of nanoparticles by chemical methods has proved to be more effective than the use of physical methods.

At nanoscale dimensions, the properties of the material may change significantly to differ completely from their bulk counterparts. As the size of the material decreases, the proportion of surface atoms increases, which increases the reactivity and makes them highly reactive catalysts with the surface atoms the active centers for elementary catalytic processes [47].

Surface conductivity and electronic surface states in semiconductor nanoparticles

films [48], enhanced photocatalytic reactivity in TiO_2 nanoparticles [49], super-magnetism in magnetic nanoparticles [50], super-hard coatings of metal alloys [51], and size-dependent electrical properties of SnO_2 grains [52] are all among well documented phenomena in nanophases [53].

Many different methods are used for the production of inorganic nanoparticles. For further manipulations, nanoparticles, usually existing as aggregates, are dispersed in a liquid or solid medium. Different mechanochemical approaches including sonication by ultrasound can be used for this purpose. However, the scope of such approaches for dispersing the nanoparticles is limited by reaggregation of the individual nanoparticles and the establishment of an equilibrium state under definite conditions, which determines the size distribution of the agglomerate of dispersed nanoparticles. Other limitations are related to temperature conditions and the limited stability of some types of inorganic nanoparticles to mechanical impacts. Therefore, the surface modification of nanoparticles is required [53].

In general, surface modification of inorganic nanoparticles means introduction of organic coatings onto the fillers, which can be carried out by utilising physical andchemical interactions between the fillers and the modifiers. Physical treatment (through covering the filler with a low molecular weight surfactant or a high molecular weight polymer) usually results in secondary forces (such as van der Waals, hydrogen and electrostatic forces) between particles and the modifier.

In comparison with physical methods, effect of surface modification based on chemical interaction is more significant because the covalent attachment modifier avoids its desorption from the particles surface. Among the available techniques, coupling agent treatment is the most popular and the easiest to be applied. Grafting

macromolecules onto inorganic particles has some advantages over modification by low molecular surfactants or coupling agents. A series of work has been carried out in this field of growing interest for purposes of improving the dispersibility of the nanoparticles in solvents. Mostly, the graft polymerisation is conducted via two routes: (i) monomers are polymerised from active compounds (initiators or comonomers) covalently attached to the inorganic surface (called 'grafting from'), (ii) ready-made polymers with reactive end groups react with the functional groups on the particles (called 'grafting to'). The latter benefits the control of the molecular weight of the grafting polymer. But generally, the former approach has advantage over the latter one because it is more difficult for polymers to penetrate into the particulate agglomeration than monomers. Besides, the 'grafting to' technique would lead to a polymer coating on the particles, which might hinder the attachments of other polymers [54].

1.3 Fiber surface modification with inorganic nanoparticles

With the increasing application of high performance fiber, the study of high performance fiber surface modification becomes more and more important. There are three aspects of the purpose of fiber surface modification. Firstly, overcoming the own defects of high performance fiber. Some high performance fibers themselves have obvious defects, such as poor UV resistance of PBO fibers. Secondly, overcoming the defects produced in the manufacturing process. The surface flaws or notches created during manufacturing process act as stress concentrators for crack propagation, which lead to fiber fracture. Thirdly, high performance fiber should have some specific performances for specific applications. For example, in the field of fiber reinforced composites, the interface is very important, which requires fiber surface modification to improve the interfacial strength between the fiber and the specified resin.

L. Liu divided the fiber so many surface modification methods into two types: oxidation and non-oxidation [1]. Oxidation is the method with using an oxidizing agent to improve the activity of functional groups on the high performance fiber surface. Oxidation includes gas phase oxidation carried in air, oxygen or ozone, liquid phase oxidation with nitric acid & sulfuric acid, ammonia, hydrogen peroxide, sodium hydroxide, potassium permanganate, chlorate, hypochlorite, persulfate as the oxidant, anodic oxidation carried with sodium hydroxide, ammoniumbicarbonate, sulfuric acid, nitric acid, ammoniumnitrate and organic acid or the salts of organic acids as electrolyte. Non-oxidation is the method, with which the structure and surface energy of the high performance fiber surface was regulated with coating, grafting, cleaning, etching and so on. With these methods, such as plasma, chemical grafting, surface cleaning, the weak layer of the high performance fiber interface can be removed to some degree, and the surface roughness of the high performance fiber and the engagement of the interface can be improved. Meanwhile, the surface energy of the high performance fiber will increase, so that the interface infiltration effect can be improved. Fibers surface functional groups will increase to promote the interfacial reactions.

M. Sharma covered the major CF surface modification techniques under the three main categories: ‘wet’ chemical, ‘dry’ and, ‘multi-scale’/‘multi’-functional modification [55]. Sizing, acidic modification, electrochemical modification and electro-polymer were all belong to ‘wet’ chemical methods. Plasma surface modification, high energy irradiation modification, nickel surface coating, thermal modification and miscellaneous dry treatment were all classified as ‘dry’ methods. Nano particles modification and carbon nano-tube coating were defined as‘multi-scale’/‘multi’-functional modification.

In the classification of M. Sharma, nano particles modification was scientifically

classified as one category. With the development of nanomaterials, the nano particles modification will become the main research direction of fiber surface modification. In addition, nanoparticles can be physically adsorbed on the fiber surface and also can be chemically connected to the fiber surface, so it is difficult to categorize the nano particles modification as a physical or chemical method.

Inorganic nanoparticles surface modification on fiber surface can be divided into two types: chemical connection and physical adsorption.

1.3.1 Chemical connection methods in inorganic nanoparticles surface modification on fiber surface

Chemical connection methods are the most widely used methods in inorganic nanoparticles surface modification on fiber surface, because organic nanoparticles with chemical bonding have better wear resistance than physical adsorption.

1.3.1.1 Reaction groups introduce method

One of these methods, high performance fibers are modified to introduce some reaction groups and then they can react with the surface groups on nanoparticles surface to form chemical bonds. For example, in G.D. Zhao`s study, poly(1,4-phenylene diisocyanate) (PPDI) polymer and silica nanoparticles functionalized CFs were facilely prepared by in situ polymerization and chemical grafting methods. PPDI polymer layer was formed on the surface of the CFs by addition polymerization. PPDI itself contained numerous unreactive isocyanate groups, which could be used as a macromolecule coupling agent to react efficiently with silica nanoparticles in a continual process. The CFs were functionalized by the combination of nanosilica with isocyanates through the reaction between isocyanate groups on the PPDI polymer and silanol groups of nanosilica [56].

In addition, high performance fibers and nanoparticles can be both modified for introducing some reaction groups and then these reaction groups can react with each other to form chemical bonds. For example, B. Gao has reported their works that amino-functionalized graphene oxide (GO-NH_2) was directly grafted onto the acyl chloride functionalized carbon fiber (CF-COCl), that amino groups of functionalized GO were reacted with the acyl chloride groups of the carbon fiber surface [57, 58].

1.3.1.2 Layer by layer assembly

Layer-by-layer assembly, a prevalent method for building functional thin coating or films, has obtained considerable attention in the past 20 years. By absorbing oppositely charged materials alternatively onto a substrate, this repeated process will obtain a multilayer film with a specific structure. Owing to the flexible designability and high level of controllability in a nanoscale single bilayer, as well as the broad adaptability of different substrates such as porous membranes, particles, and biological matter, LBL technologies have seen rapid development and been applied in photoelectric devices, separation or catalysis components, biomedical materials and other new frontiers. Such as W. Luo`s work, he aimed to enhance the interfacial characteristics by applying LBL assembly of graphene oxide and poly-ethyleneimine (PEI) on the surface of carbon fiber [59].

1.3.1.3 Electrochemical surface modification

When a chemical reaction is caused by an externally supplied current, as in electrolysis, or if an electric current is produced by a spontaneous chemical reaction as in a battery, it is called an electrochemical reaction. Chemical reactions where electrons are transferred directly between molecules and/or atoms are called oxidation-reduction or (redox) reactions. In general, electrochemistry describes the overall reactions when

individual redox reactions are separate but connected by an external electric circuit and an intervening electrolyte. Electrochemical method is also used for the grafting of nanoparticles on fibers surface. For example, G.P. Wu reported in his work that a carbon-oxygen bond was expected to form between a carbon atom of carbon fibers and the oxygen atom of carboxylate at the CNTs during the electrolysis. After binding to carbon surface, the attached carboxylate could be decomposed to form a stable carbon-carbon bond between a carbon fiber and the CNTs by removal of a carbon dioxide molecule [60].

1.3.2 Physical adsorption methods in Inorganic nanoparticles surface modification on fiber surface

Physical adsorption is also widely used in inorganic nanoparticles surface modification on fiber surface, because of its simple process, less expensive and environment-friendly.

1.3.2.1 Dip-coating method

In dip-coating method, nanoparticles are dispersed in a solvent by a mechanical dispersion method or chemical modification to form the treatment solvent, and then high performance fibers are dipped in the treatment solvent, then dry out the solvent, and the nanoparticles will be adsorbed on the surface of high performance fibers [38, 61-64]. For example, W.Z. Qin reported in his work that a novel method consisting of coating carbon fibers (CF) with graphite nanoplatelets (GnP) is investigated for its ability to modify the mechanical properties in the interphase region. Coating the CF was achieved by immersing CF in a solution of GnP dispersed in an epoxy-based solution for a few seconds [26].

1.3.2.2 Electrophoretic deposition method

A characteristic feature of electrophoretic deposition is that colloidal particles suspended in a liquid medium migrate under the influence of an electric field (electrophoresis) and are deposited onto an electrode [31,35]. All colloidal particles that can be used to form stable suspensions and that can carry a charge can be used in electrophoretic deposition. This includes materials such as polymers, pigments, dyes, ceramics and metals. B. Hao reported the preparation of glass fibers (GFs) with carbon nanotubes (CNTs) and graphene coating by using an electrophoretic deposition (EPD) process [65]. In Y.J. Kwon`s work, a graphene/carbon nanotube hybrid material stabilized in an aqueous medium, was coated on carbon fibers by anodic electrophoretic deposition [66].

1.3.2.3 In situ growth of nanoparticles

Chemical vapor deposition (CVD), as the most effective method, has been applied to grow carbon nanoparticles and some other nanoparticles. To achieve different structures and morphologies, some critical parameters of CVD, such as growth time, growth temperature, flow rate of carbon source gas and catalyst concentration can be varied [67]. To improve the mechanical properties of fibers/epoxy composites without sacrificing tensile strength of base fibers, carbon black (CB) was introduced onto the surface of CFs by chemical vapour deposition (CVD) in J.D. Dong`s study [32]. J.S. Li deposited boron nitride (BN) coatings on carbon fibers by chemical vapor deposition (CVD) using borazine as single source precursor [68]. P. Agnihotri has synthesized carbon nanotubes (CNTs) on the surface of carbon fiber/fabric using catalytic chemical vapor deposition (CVD) at a temperature of 550 ^{o}C [34]. And L.M. Zhang has directly produced multiwall carbon nanotubes (CNTs) - carbon fibers (CFs) hybrid materials by growing CNTs on CFs by means of chemical vapor deposition [69].

1.3.2.4 Thermal treatment method

In this method, a layer of coating or sizing is first formed on the surface of carbon fiber. Then materials in the coating or sizing layer are reacted at high temperature to form nanoparticles. For example, M. Ghanbarian reported that boron nitride coating was fabricated onto carbon fiber cloths via dip-coating process with boric acid and urea as precursors, followed by nitriding in a nitrogen flow in different temperatures of 650 and 1000 ^{o}C [70].

1.4 Polymer coating on fiber surface

In commercial carbon fibre production, after electrolytic surface treatment, the fibres usually are coated with a thin layer of polymer sizing to facilitate handling and protecting the fibre during weaving and textile processes by realising strand integrity and protect the individual filaments. This additional polymer sizing strongly affects not only fibre-matrix adhesion, but also can change other parameters like brittleness of the composite. Therefore, the polymer sizing has high research value. The followings are some common polymer coating methods [71].

1.4.1 Polymer-solution method

1.4.1.1 Dip-coating method

This Dip-coating method can be divided into two categories. One is to dissolve thermoplastic particles in a specific solvent to form a treatment solution; the other one is to dilute the thermosetting resin and curing agent into a volatile solvent to form a treatment solution. The fibers are then immersed in the treatment solution and dried to obtain the treated samples. In W.B. Liu`s work, a thermoplastic-sizing agent for CF with poly(phthalazinone ether ketone) (PPEK) resin was prepared by dissolving the PPEK in *N*-methylpyrrolidinone (NMP). The sizing agent satisfies the demand of good

compatibility between fiber and matrix in molding process of carbon fiber-reinforced poly(aryl ether ketone)s (PAEKs) composites [72].

A. Markus reported that an addition of an epoxy fiber sizing increased the Mode I fracture toughness by 50% and 84% for aromatic and aliphatic epoxies respectively over the as-received, unsized fiber composite. In his fiber sizing process, the appropriate amount of epoxy was dissolved in ACS-grade 2-propanol (IPA). Then the appropriate amount of curing agent was dissolved in the epoxy/IPA solution. The sizing solution was obtained after mechanically stirring for 1 h. The fiber tow was drawn through the sizing bath described above. After sizing, the fibers were dried to drive off residual IPA solvent. Then the treated fibers were obtained [27].

1.4.1.2 Spray-coating method

Spray-coating method is a branch of the Dip-coating method. The advantage of spray-coating method is the use of less treatment solution, but the problem is that uniformity of polymer is a congenital defect. I. Giraud used poly(ether imide) (PEI) and poly(ether ketone ketone) oligomer aqueous dispersions as The thermoplastic sizings. Then they sprayed the dispersion directly onto the unsized fiber surface, after the solvent evaporated, the PEI or PEKK coated CF sample was obtained [73].

1.4.1.3 Electrophoretic deposition method

In T. Yamamoto`s work, in order to control the surface adhesion between carbon fibers and the resin in CFRTPs, polymeric particles were adsorbed on the carbon fiber surfaces by performing electrophoresis in polymer colloids. With an increase in the applied voltage, the particles were readily adsorbed on the carbon fiber within a short time and the interfacial shear strength between the modified carbon fiber and the resin was enhanced. The interaction between the carbon fiber and the resin was improved by

the adsorbed PMMA particles, thereby strengthening the surface adhesion between them [74].

1.4.1.4 In-situ polymerization method

High-temperature vapor deposition polymerization (VDPH) and electropolymerization are the two common in-situ polymerization methods. High-temperature vapor deposition polymerization (VDP_H) is a promising approach due to its ability to form a relatively uniform and thin layer on three dimensional objects and porous materials. Using the VDP_H approach, a compliant polyimide nanocoating can be deposited directly on each filament within a fiber bundle [40]. T. Naganuma reported that a compliant polyimide nano-coating deposited by the VDP_H method is effective in improving the tensile strength and Weibull modulus of the T1000GB carbon fiber. The introduction of a ductile and compliant coating is also a promising approach to improve the impact energy absorbing capability of the carbon fiber-reinforced composites [39].

R. V. Subramanian shown that polymer coatings could be formed on carbon fiber electrodes by electropolymerization of a variety of monomers in his work [75]. Electropolymerization of CF has the following advantages: (1) polymerization takes place mainly on the surface; (2) film thickness and homogeneity are easily controlled by the applied current or voltage; (3) wetting of the surface by the monomer will provide a uniform film on the porous surface; (4) the chemical and physical properties of the film can be controlled by proper choice of monomer(s) and reaction conditions; (5) the electrochemical process is simple and rather inexpensive, and therefore can be extended from laboratory to continuous semi-industrial scale without radical technological changes [76].

1.4.2 Polymer-melt method

For example, K. Amit reported that polyacrylonitrile (PAN)-based carbon fiber tows are coated with a commercial, heat-crosslinkable polyetherimide (Ultem®) powder. Then an electrical current is applied across the powder-coated fiber tows (towpreg) to melt the thermoplastic powder and form rigidized composites [77].

1.5 Constitution of this dissertation

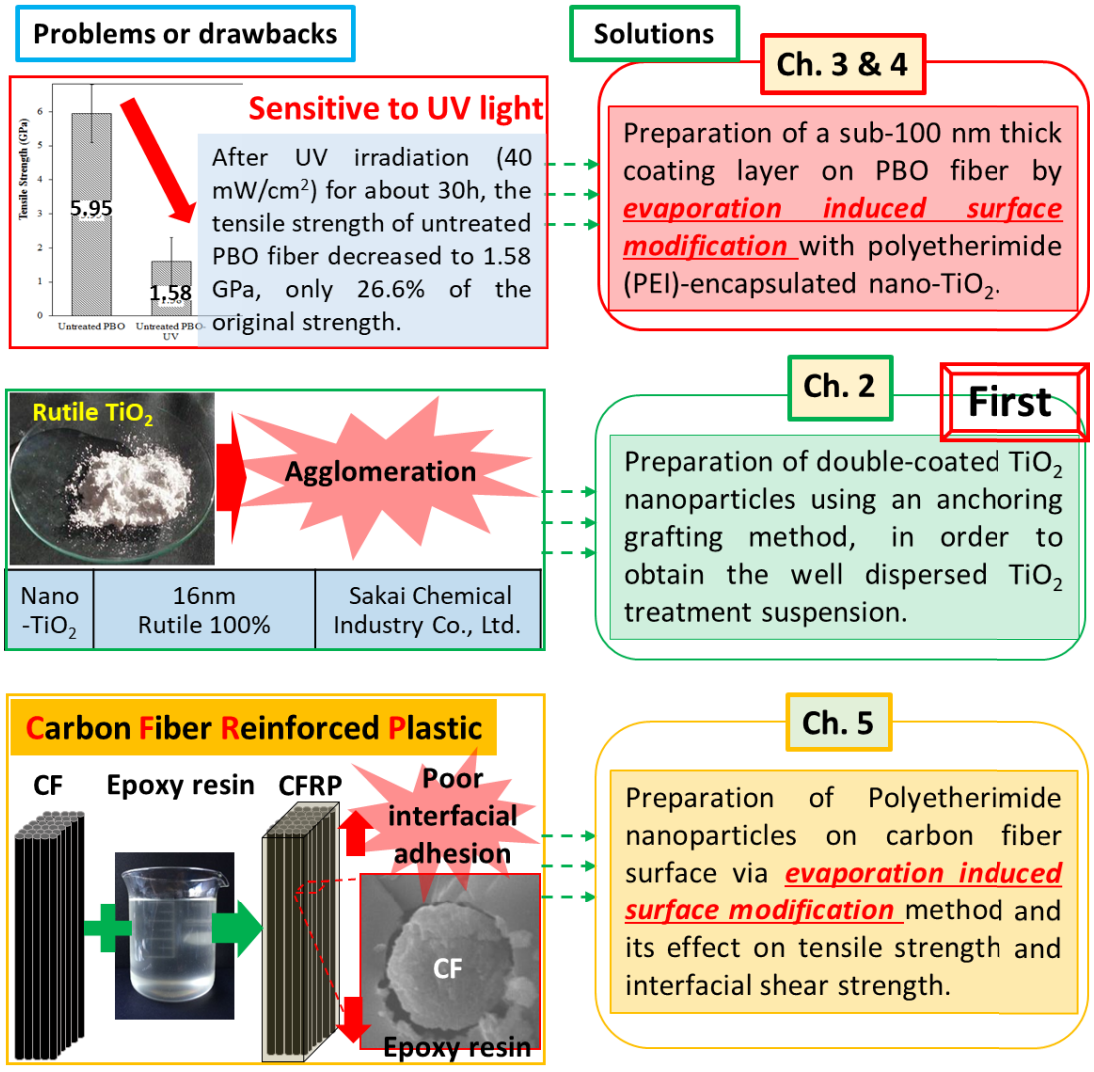

Fig. 1-1. Constitution illustration of this dissertation

As shown in Fig. 1-1, double-coated TiO_2 nanoparticles (TMP) were prepared

using a single-pot fabrication method in NMP in Chapter 2. These particles contained a chemically bonded layer of γ-MPS and a layer of PEI that was absorbed via Van der Waals forces. All fabrication and experimental processes were conducted in NMP, which prevented the agglomeration of particles during the centrifugal drying process. The double-coated TiO_2 nanoparticles (TMP) exhibited improved dispersion in NMP because of steric stabilization of the polymer chains that were absorbed to the particle surface and depletion stabilization of the free polymer in the solvent. In the long-term dispersion stability test, we found that there was a common cycle during the process of the sedimentation in which the suspension shown turbid firstly, then upper clarification and lower turbidity appeared, and then a clear interface layer appeared, and then the part over the interface layer turbid again. The double-coated TiO_2 nanoparticles (TMP) also exhibited improved dispersion within the PEI nanocomposite films and increased interface adhesion between the TiO_2 nanoparticles and the PEI matrix. Therefore, the nanocomposite TMP/PEI film exhibited increased mechanical properties and UV resistance.

In Chapter 3, poly(p-phenylene benzobisoxazole) (PBO) fibers were modified using the evaporation-induced surface coating method. Through this new method, nano-TiO_2 particles encapsulated with polyetherimide (PEI) chains were firmly adsorbed on the fiber surface. The results indicate that besides some nanospheres resulted from the initial agglomeration of PEI-encapsulated nano-TiO_2, a uniform coating layer with thickness of 84 nm was formed by absorption of polyetherimide (PEI)-encapsulated nano-TiO_2. This coating method changed the surface morphology of the PBO fibers, enhanced the surface roughness, and increased the poor UV resistance of untreated PBO fibers.

To improve the UV resistance of poly(p-phenylene benzobisoxazole) (PBO) fibers, a sub-100-nm-thick coating layer was prepared on PBO fibers by evaporating the suspension of polyetherimide encapsulated nano titanium dioxide (TiO_2) particles absorbed around the fiber surface in Chapter 4. The effects of this evaporation-induced surface modification on the structure and properties of PBO fibers were investigated. The content ratio of nano-TiO_2 particles to PEI, the contents of nano-TiO_2 particles and PEI, and the evaporation method greatly influenced the surface modification of the PBO fibers, as confirmed by scanning electron microscopy observation. The ultraviolet (UV) resistance of the PBO fibers was improved after surface modification, which confirmed by single-fiber tensile strength test.

In Chapter 5, PEI nanoparticles were prepared on CF surfaces via an evaporation-induced surface modification method for which the particle diameter could be controlled by changing the PEI concentration. A possible formation mechanism for the PEI particles was proposed: the volatilization process during this modification was very long because of the nonvolatile nature of NMP, the PEI chains could form some separate solvent-containing balls before the evaporation ends, then shrinks with evaporation, eventually forming PEI nanoparticles. When the PEI concentration was not higher than 0.2%, the nanoparticle morphology was almost hemispherical; when the PEI concentration was over 0.2%, many spherical particles appeared above the hemispherical nanoparticles.

References

[1] L. Liu, C.Y. Jia, J.M. He, F. Zhao, D.P. Fan, L.X. Xing, M.Q. Wang, F. Wang, Z.X. Jiang, Y.D. Huang, Interfacial characterization, control and modification of carbon

fiber reinforced polymer composites, Compos. Sci. Technol., 121 (2015) 56-72.

[2] P. Chen, C. Zhang, X. Zhang, B. Wang, W. Li, Q. Lei, Effects of oxygen plasma treatment power on surface properties of poly(p-phenylene benzobisoxazole) fibers, Appl. Surf. Sci. 255 (2008) 3153-3158.

[3] T. Kitagawa, K. Funaki, Morphological studies of poly-p-phenylenebenzobisoxazole (PBO) fibers on the process that determines the direction of the crystal a-axis along the radius direction during the formation of fiber structures, Polymer. 82 (2016) 246-254.

[4] N. Horikawa, Y. Nomura, T, Kitagawa, Tensile fracture behavior of UV light irradiated PBO fiber, J. Solid Mech. Mater. Eng. 3 (2009), 1-9.

[5] B. Song, Q. Fu, L.H. Ying, X.Y. Liu, Q.X. Zhuang, Z.W. Han, Study on photoaging of poly(p-phenylene benzobisoxazole) fiber, J. Appl. Polym. Sci. 124 (2012) 1050-1058.

[6] T. Kitagawa, H. Murase, K. Yabuki, Morphological study on poly-p-phenylenebenzobisoxazole (PBO) fiber, J. Polym. Sci., Part B: Polym. Phys. 36 (1998) 39-48.

[7] C.H. Zhang, W.J. Yuan, S.G. Wang, X.F. Liang, Effect of MWCNTs irradiation grafting treatment on the surface properties of PBO fiber, J. Appl. Polym. Sci. 121 (2011) 3455-3459.

[8] T. Zhang, J.H. Jin, S.L. Yang, G. Li, J.M. Jiang, UV accelerated aging and aging resistance of dihydroxy poly(p-phenylene benzobisoxazole) fibers, Polym. Adv. Technol. 22 (2011) 743-747.

[9] L. Chen, Z. Hu, F. Zhao, L.X. Xing, B. Jiang, Y.D. Huang, Enhanced interfacial properties of PBO fiber via electroless nickel plating, Surf. Coat. Technol. 235

(2013) 669-675.

[10] J.L. Wang, G.Z. Liang, W. Zhao, Z.P. Zhang, Enzymatic surface modification of PBO fibres, Surf. Coat. Technol. 201 (2007) 4800-4804.

[11] C.S. Zhang, P. Chen, D. Liu, B.C. Wang, W. Li, X.T. Kang, Aging behavior of PBO fibers and PBO-fiber-reinforced PPESK composite after oxygen plasma treatment, Surf. Interface Anal. 41 (2008) 187-192.

[12] F. Guo, Z.Z. Zhang, X.H. Xu, W. Jiang, K. Wang, Tribological properties of PBO fabric composites modified by poly (vinyl alcohol), J. Appl. Polym. Sci. 130 (2013) 1313-1320.

[13] J. Qian, J. Wu, X. Liu, Q. Zhuang, Z. Han, Improvement of interfacial shear strengths of polybenzobisoxazole fiber/epoxy resin composite by n-TiO_2 coating, J. Appl. Polym. Sci. 127 (2013) 2990-2995.

[14] J. Won, M.A. Said, A.F.M. Development of UV protective sheath for high performance fibers for high altitude applications, Seyam, Fibers Polym. 14 (2013) 647-652.

[15] J.H. Jin, G. Li, S.L. Yang, J.M. Jiang, Effects of light stabilizer on the ultraviolet stability of poly-p-phenylenebenzobisoxazole (PBO) fibers, Iran. Polym. J. 21 (2012) 739-745.

[16] P.J. Walsh, X.B. Hu, Environmental effects on poly-p-phenylenebenzobisoxazole fibers. II. Attempts at stabilization, J. Appl. Polym. Sci. 102 (2006) 3819-3829.

[17] C.H. Zhang, Y.D. Huang, W.J. Yuan, J.N. Zhang, UV aging resistance properties of PBO fiber coated with nano-ZnO hybrid sizing, J. Appl. Polym. Sci. 120 (2011) 2468-2476.

[18] Y.W. Jang, B.G. Min, K.H. Yoon, Enhancement in compressive strength and UV

ageing-resistance of poly(p-phenylene benzobisoxazole) nanocomposite fiber containing modified polyhedral oligomeric silsesquioxane, Fibers Polym. 18 (2017) 575-581.

[19] ZYLON® (PBO fiber) Technical Information (2005). http://www.toyobo-global.com/seihin/kc/pbo/zylon-p/bussei-p/technical.pdf (accessed April 29, 2018).

[20] Y. Chen, Q. Zhang, Q. Han, Y. Mi, S. Sun, C. Feng, H. Xiao, P. Yu, C. Yang, Synthesis of polysiloxane with 5,5-dimethylhydantoin-based N-halamine pendants for biocidal functionalization of polyethylene by supercritical impregnation, J. Appl. Polym. Sci. 134 (2017) 44721.

[21] A. Naylor, S.M. Howdle, The preparation of novel blends of Ultra High Molecular Weight Polyethylene with polymethacrylate based copolymers using supercritical carbon dioxide, J. Mater. Chem. 15 (2005) 5037-5042.

[22] Y. Chen, X.S. Zhong, Q. Zhang, Synthesis of CO_2-Philic Polysiloxane with N-Halamine Side Groups for Biocidal Coating on CottonInd. Eng. Chem. Res. 51 (2012) 9260-9265.

[23] B. Song, L. Meng, Y. Huang, Preparation and characterization of $(POSS/TiO_2)_n$ multi-coatings based on PBO fiber surface for improvement of UV resistance, Fibers Polym. 14 (2013) 375-381.

[24] B. Song, Q.X. Zhuang, L.H. Ying, X.Y. Liu, Z.W. Han, Photostabilisation of poly(p-phenylenebenzobisoxazole) fibre, Polym. Degrad. Stabil. 97 (2012) 569-1576.

[25] B. Jiang, T. Zhang, L.W. Zhao, Y.D. Huang, Interfacially reinforced carbon fiber composites by grafting modified methylsilicone resin, Compos. Sci. Technol. 140

(2017) 39-45.

[26] W.Z. Qin, F. Vautard, L.T. Drzal, J.R. Yu, Modifying the carbon fiber-epoxy matrix interphase with graphite nanoplatelets, Polym Compos. 37 (2016) 1549-1556.

[27] M.A. Downey and L.T. Drzal, Compos. Toughening of carbon fiber-reinforced epoxy polymer composites utilizing fiber surface treatment and sizing, Appl. Sci. Manuf. 90 (2016) 687-698.

[28] D.I. Chukov, A.A. Stepashkin, M.V. Gorshenkov, V.V. Tcherdyntsev, S.D. Kaloshkin, Surface modification of carbon fibers and its effect on the fibermatrix interaction of UHMWPE based composites, J Alloys Compd. 586 (2014) 459-463.

[29] Yuan X, Zhu B, Cai X, Liu J, Qiao K, Yu J, Improved interfacial adhesion in carbon fiber/epoxy composites through a waterborne epoxy resin sizing agent, J Appl Polym Sci. 134 (2017) 44757.

[30] J. Jiang, X. Yao, C. Xu, Y. Su, L. Zhou, C. Deng, Influence of electrochemical oxidation of carbon fiber on the mechanical properties of carbon fiber/graphene oxide/epoxy composites, Compos. Part A: Appl. Sci. Manuf. 95 (2017) 248-256.

[31] S.A. Song, C.K. Lee, Y.H. Bang, S.S. Kim, A novel coating method using zinc oxide nanorods to improve the interfacial shear strength between carbon fiber and a thermoplastic matrix, Compos. Sci. Technol. 134 (2016) 106-114.

[32] J.D. Dong, C.Y. Jia, M.Q. Wang, Improved mechanical properties of carbon fiber-reinforced epoxy composites by growing carbon black on carbon fiber surface, Compos. Sci. Technol. 149 (2017) 75-80.

[33] W. Liu, S. Zhang, L. Hao, F. Yang, W. Jiao, X. Li, et al. Fabrication of carbon nanotubes/carbon fiber hybrid fiber in industrial scale by sizing process, Appl Surf

Sci. 284 (2013) 914-920.

[34] P. Agnihotri, S. Basu, K.K. Kar, Effect of carbon nanotube length and density on the properties of carbon nanotube-coated carbon fiber/polyester composites, Carbon. 49 (2011) 3098-3106.

[35] Z. Zhao, K. Teng, N. Li, X. Li, Z. Xu, Mechanical, thermal and interfacial performances of carbon fiber reinforced composites flavored by carbon nanotube in matrix/interface, Compos Struct. 159 (2017) 761-772.

[36] D. Jiang, L. Liu, G. Wu, Q. Zhang, J. Long, Z. Wu, et al. Mechanical properties of carbon fiber composites modified with graphene oxide in the interphase, Polym Compos. 38 (2016) 2425-2432.

[37] F. Li, Y. Liu, C.B. Qu, H.M. Xiao, Y. Hua, G.X. Sui, Enhanced mechanical properties of short carbon fiber reinforced polyethersulfone composites by graphene oxide coating, Polymer. 59 (2015) 155-165.

[38] W.Z. Qin, F. Vautard, L.T. Drzal, J.R. Yu, Mechanical and electrical properties of carbon fiber composites with incorporation of graphene nanoplatelets at the fiber-matrix interphase, Compos Part B. 69 (2015) 335-341.

[39] T. Naganuma, K. Naito, J.M. Yang, J. Kyono, D. Sasakura, Y. Kagawa, The effect of a compliant polyimide nanocoating on the tensile properties of a high strength PAN-based carbon fiber, Compos Sci Technol. 69 (2009) 1319-1322.

[40] K. Naito, Tensile properties of polyimide composites incorporating carbon nanotubes-grafted and polyimide-coated carbon fibers, J. Mater. Eng. Perform. 23 (2014) 3245-3256.

[41] H.M. Kang, T.H. Yoon, M. Bump, J.S. Riffle, Effect of solubility and miscibility on the adhesion behavior of polymer-coated carbon fibers with vinil ester resins, J.

Appl. Polym. Sci. 79 (2001) 1042-1053.

[42] P.C. Varelidis, R.L. McCullough, C.D. Papaspyrides, The effect on the mechanical properties of carbon/epoxy composites of polyamide coatings on the fibers, Compos Sci Technol. 59 (1999) 1813-1823.

[43] T Duvis, C.D Papaspyrides, Carbon-Epoxy Composites Based on Fibers Coated with Nylon 6,6: Hygrothermal Ageing versus Interlaminar Shear Strength, Polym Adv Technol. 5 (1994) 444-450.

[44] T. Skourlis, T. Duvis, C.D. Papaspyrides, The role of a polyamide interphase on carbon fibres reinforcing an epoxy matrix, Compos Sci Technol. 48 (1993) 119-125.

[45] Masala, R. Seshadri, Synthesis routes for large volumes of nanoparticles, Annu Rev Mater Res, 34 (2004) 41-81.

[46] H.M. Chen, R.S. Liu, Architecture of metallic nanostructures: synthesis strategy and specific applications, J Phys Chem C, 115 (2011) 3513-3527.

[47] S. Kango, S. Kalia, A. Celli, J. Njuguna, Y. Habibi, R. Kumar, Surface modification of inorganic nanoparticles for development of organic-inorganic nanocomposites - a review, Prog Polym Sci, 38 (2013) 1232-1261.

[48] A. Rothschild, Y. Komem, A. Levakov, N. Ashkenasi, Y. Shapiro, Electronic and transport properties of reduced and oxidized nanocrystalline TiO_2 films, Appl Phys Lett, 82 (2003) 574-576.

[49] K. Hashimoto, H. Irie, A. Fujishima, TiO_2 photocatalysis: a historical overview and future prospects, Jpn J Appl Phys, 44 (2005) 8269-8285.

[50] S.I. Nikitenko, Y. Koltypin, V. Markovich, E. Rozenberg, G. Gorodetsky, A. Gedanken, Synthesis of air-stable iron-iron carbide nanocrystalline particles

showing very high saturation magnetization, IEEE J Quant Electron IEEE Trans Magn, 38 (2002) 2592-2594.

[51] S. Veprek, M. Jilek, Super- and ultrahard nanacomposite coatings: generic concept for their preparation, properties and industrial applications, Vacuum, 67 (2002) 443-449.

[52] A.C. Bose, P. Thangaduran, S. Ravasamy, Grain size-dependent electrical studies of nanocrystalline SnO_2, Mater Chem Phys, 95 (2006) 72-78.

[53] B.A. Rozenberg, R. Tenne, Polymer-assisted fabrication of nanoparticles and nanocomposites, Prog. Polym. Sci., 33 (2008) 40-112.

[54] M.Z. Rong, M.Q. Zhang, W.H. Ruan, Surface modification of nanoscale fillers for improving properties of polymer nanocomposites: a review, Mater Sci Tech, 22 (2006) 787-796.

[55] M. Sharma, S. Gao, E. Mäder, H. Sharma, L.Y. Wei, J. Bijwe, Carbon fiber surfaces and composite interphases, Compos Sci Technol, 102 (2014) 35-50.

[56] G.D. Zhao, P. Hu, S.B. Zhou, G.Q. Chen, Y.M. An, Y.H. Cheng, J.D. An, X.H. Zhang, W.B. Han, Ordered silica nanoparticles grown on a three-dimensional carbon fiber architecture substrate with siliconborocarbonitride ceramic as a thermal barrier coating, ACS Appl. Mater. Inter., 8 (2016) 4216-4225.

[57] R.L. Zhang, B. Gao, Q.H. Ma, J. Zhang, H.Z. Cui, L. Liu, Directly grafting graphene oxide onto carbon fiber and the effect on the mechanical properties of carbon fiber composites, Mater Des, 93 (2016) 364-369.

[58] B. Gao, R. Zhang, M. He, L. Sun, C. Wang, L. Liu, et al. Effect of a multiscale reinforcement by carbon fiber surface treatment with graphene oxide/carbon nanotubes on the mechanical properties of reinforced carbon/carbon composites,

Compos. Part A Appl. Sci. Manuf., 90 (2016) 433-440.

[59] W. Luo, B. Zhang, H.W. Zou, M. Liang, Enhanced interfacial adhesion between polypropylene and carbon fiber by graphene oxide/polyethyleneimine coating, J. Ind. Eng. Chem., 51 (2017) 129-139.

[60] G.P. Wu, Y.Y. Wang, D.H. Li, C.X. Lu, W.Z. Shen, X.T. Li, et al., Direct electrochemical attachment of carbon nanotubes to carbon fiber surfaces, Carbon, 49 (2011) 2152-2155.

[61] Y. Yang, C.X. Lu, X.L. Su, X.K. Wang, Effects of emulsion sizing with nano-SiO_2 on interfacial properties of carbon fibers/epoxy composites, J Mater Sci, 42 (15) (2007) 6347-6352.

[62] H. He, F. Gao, Resin modification on interlaminar shear property of carbon fiber/epoxy/nano-$CaCO_3$ hybrid composites, Polym Compos, 38 (2015) 2035-2042.

[63] L. Chen, H. Jin, Z.W. Xu, M.J. Shan, X. Tian, C.Y. Yang, et al., A design of gradient interphase reinforced by silanized graphene oxide and its effect on carbon fiber/epoxy interface, Mater Chem Phys, 145 (2014) 186-196.

[64] P. Ma, J. Liu, S. Gao, E. Mader, Development of functional glass fibers with nanocomposite coating: a comparative study, Composites Part A, 44 (2013) 16-22.

[65] B. Hao, Q. Ma, S. Yang, E. Mader, P.C. Ma, Comparative study on monitoring structural damage in fiber-reinforced polymers using glass fibers with carbon nanotubes and graphene coating, Compos Sci Technol, 129 (2016) 38-45.

[66] Y.J. Kwon, Y. Kim, H. Jeon, S. Cho, W. Lee, J.U. Lee, Graphene/carbon nanotube hybrid as a multi-functional interfacial reinforcement for carbon fiber-reinforced composites, Compos Part B Eng, 122 (2017) 23-30.

[67] F. Ghaemi, R. Yunus, M.A.M. Salleh, S.A. Rashid, A. Ahmadian, H.N. Lim,

Effects of the surface modification of carbon fiber by growing different types of carbon nanomaterials on the mechanical and thermal properties of polypropylene, RSC Adv., 5 (2015) 28822.

[68] J.S. Li, C.R. Zhang, B. Li, Preparation and characterization of boron nitride coatings on carbon fibers from borazine by chemical vapor deposition, Appl. Surf. Sci., 257 (2011) 7752-7757.

[69] L. Zhang, N. De Greef, G. Kalinka, B. Van Bilzen, J.P. Locquet, I. Verpoest, et al., Carbon nanotube-grafted carbon fiber polymer composites: damage characterization on the micro-scale, Compos Part B Eng, 126 (2017) 202-210.

[70] M. Ghanbarian, E. Taheri-Nassaj, A. Kariminejad, Synthesis of nanostructural turbostratic and hexagonal boron nitride coatings on carbon fiber cloths by dip-coating, Surf. Coat. Technol., 288 (2016) 185-195.

[71] F. Gnädinger, P. Middendorf, B. Fox, Interfacial shear strength studies of experimental carbon fibres, novel thermosetting polyurethane and epoxy matrices and bespoke sizing agents, Compos. Sci. Technol., 133 (2016) 104-110.

[72] W.B. Liu, S. Zhang, L.F. Hao, W.C. Jiao, F. Yang, X.F. Li, et al., Properties of carbon fiber sized with poly(phthalazinone ether ketone) resin, J Appl Polym Sci, 128 (2013) 3702-3709.

[73] I. Giraud, S. Franceschi, E. Perez, C. Lacabanne, E. Dantras, Influence of new thermoplastic sizing agents on the mechanical behavior of poly (ether ketone ketone)/carbon fiber composites, J. Appl. Polym. Sci., 132 (2015) 42550.

[74] T. Yamamoto, K. Uematsu, T. Irisawa, Y. Tanabe, Controlling of the interfacial shear strength between thermoplastic resin and carbon fiber by adsorbing polymer particles on carbon fiber using electrophoresis, Compos Part A, Appl Sci, 88 (2016)

75-78.

[75] R.V. Subramanian, J.J. Jakubowski, F.D. Williams, Interfacial aspects of polymer coating by electropolymerization. J Adhesion, 9 (1978) 185-195.

[76] B. Zinger, S. Shkolnik, H. Hoecker, Electrocoating of carbon fibers with polyaniline and poly (hydroxyalkyl methacrylates), Polymer, 30 (1989) 628-635.

[77] A.K. Naskar, D.D. Edie, Consolidation of reactive ultem powder-coated carbon fiber tow for space structure composites by resistive heating, J Compos Mater, 40 (2006) 1871-1883.

CHAPTER TWO

Preparation of double-coated TiO_2 nanoparticles using an anchoring grafting method and investigation of the UV resistance of its reinforced PEI film

Chapter 2: Preparation of double-coated TiO_2 nanoparticles using an anchoring grafting method and investigation of the UV resistance of its reinforced PEI film

2.1 Introduction

Polymer composites that consist of well-dispersed nanomaterials within a polymer matrix have attracted significant attention because of their unique electronic, antibacterial, optical, and mechanical properties [1-6].

The performance of polymer nanocomposites depends on the dispersion of a nanofiller material and the nature of the interphase between the nanofillers and the polymer matrix [7]. Surface modification of inorganic nanoparticles has been shown to increase their interactions with a matrix and improve their dispersion within the matrix [8]. Grafting polymerization is a common method for fabrication of nanocomposites and generally occurs via two routes [6,9,10]: (i) monomers are polymerized from initiators or co-monomers that are covalently attached to the inorganic surface (called "grafting from"); and (ii) polymers that contain reactive end groups are attached to functional groups on particles ("grafting to") [11]. The second approach allows the molecular weight of the grafting polymer to be controlled. However, it is easier for monomers to penetrate into a particulate agglomeration than it is for polymers, which is an advantage of the first approach [9].

In this work, we have modified a PEI matrix by the addition of rutile titanium dioxide nanoparticles. We modified TiO_2 nanoparticles using an anchoring grafting method, which was both convenient and economical (Fig. 2-1). Anchoring PEI (without

reactive end groups) to the TiO_2 nanoparticles (which have been modified with γ-MPS) surface by the Van der Waals force. Thus, the TiO_2 nanoparticles were subsequently coated with γ-MPS and PEI. All fabrication and experimental processes were conducted in NMP, which prevented the agglomeration of particles during the centrifugal drying process. The dispersion-sedimentation mechanism that occurred during the modification of TiO_2 nanoparticles was examined using the dispersion stability test. Finally, TMP/PEI films were fabricated using a novel process. The films' mechanical properties and UV resistance, before and after exposure to UV radiation, were also investigated.

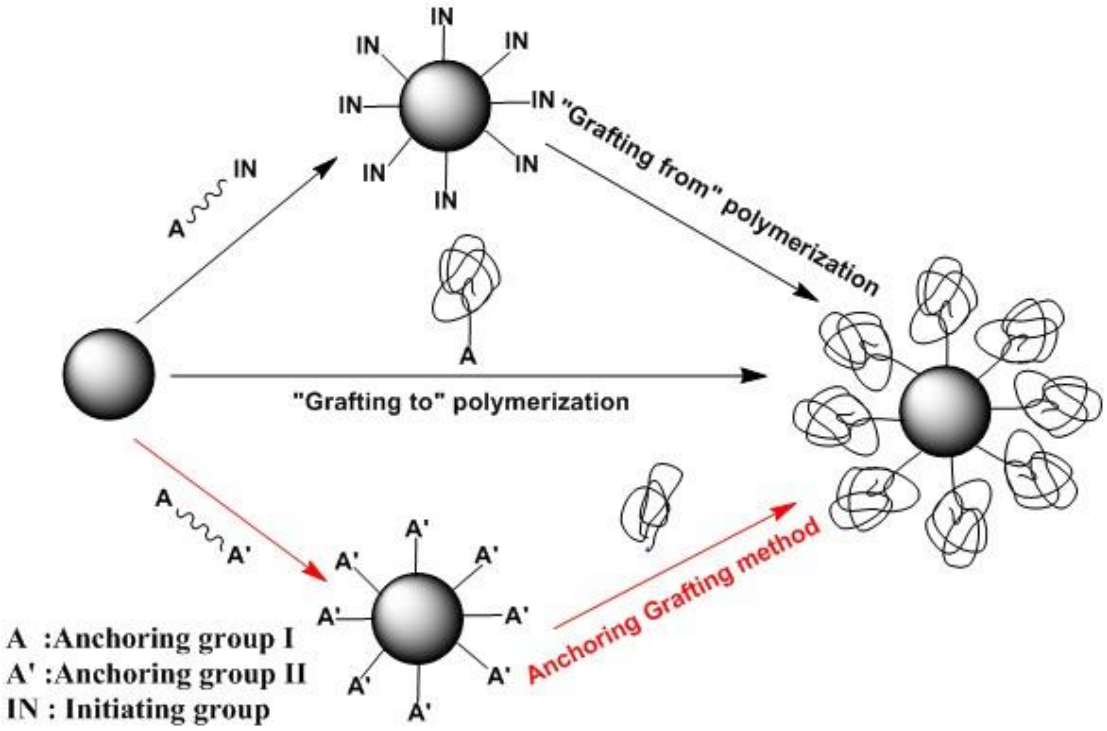

Fig. 2-1. Schematic showing the anchoring grafting method comparing with other two methods.

2.2 Experimental

2.2.1 Materials

TiO_2 nanoparticles (STR-100N, TiO_2 Content >95%, Crystal structure: Rutile 100%) with an average particle size of 16 nm and a specific surface area of 100 m^2/g were supplied by SAKAI CHEMICAL INDUSTRY CO., LTD, Japan. *N*-Methyl-2-pyrrolidone (NMP) was purchased from KANTO CHEMICAL CO., LTD, Japan. 3-(Trimethoxysilyl)propyl methacrylate (γ-MPS, 98%) was obtained from ACROS ORGANICS, USA. Polyetherimide (PEI) was purchased from Sigma-Aldrich Co. LLC, USA. All commercial chemicals were used without further treatment.

2.2.2 Double layer coating of TiO_2 nanoparticles

The surface modification of the TiO_2 nanoparticles was performed in NMP. TiO_2 nanoparticles were added to NMP (100 mL) and then they were subjected to ultrasonication in an ice bath for 25 min. The silane coupling agent γ-MPS (100 wt.% of the TiO_2 nanoparticles) was added dropwise to the mixture . The reaction mixture was stirred at 200 rpm for 6 h at ambient temperature. After the TiO_2 nanoparticles were modified with γ-MPS, pure PEI particles (100 wt.% of the TiO_2 nanoparticles) were added into the mixture. The mixture was stirred at 200 rpm at 70 °C for approximately 6 h. Any remaining free γ-MPS or PEI was removed from the dispersion using centrifugation and redispersion cycles with acetone three times. Then the treated nanoparticles were dried at 80 °C for 24 h. The amounts of each component used to prepare the different particle samples are shown in Table 2-1.

Table 2-1. Formulation of modified nanoparticles.

Sample	TiO_2 (g)	γ-MPS (g)	PEI (g)	NMP(mL)
Ref	0.093	-	-	-
TM	0.093	0.093	-	100
TMP	0.093	0.093	0.093	100

2.2.3 Dispersion stability test

The dispersion stability test was performed on the different TiO_2 nanoparticles in NMP at a concentration of 0.1 wt.% (nanoparticles:solvent). Following ultrasonication in an ice bath for 30 min, γ-MPS (100 wt.% of the TiO_2 nanoparticles) was added and then stirred for 6 h. PEI particles (100 wt.% of the TiO_2 nanoparticles) were added to the mixture and stirred until dissolved. We removed samples at the volume of 10 mL from the mixture every 2 h, and these were allowed to stand for 140 days before the particle sedimentation was evaluated.

2.2.4 Characterization of the modified TiO_2 nanoparticles

The TMP nanoparticles described in section 2.2 was evaluated using FTIR, XPS, TG and TEM. FTIR absorption spectra were recorded between 3600 and 600 cm^{-1} using a Shimadzu FTIR, IR Prestige-21 infrared spectrometer (Shimadzu, Japan). XPS spectra were obtained using an AXIS-ULTRA (KRATOS, Japan) X-ray photoelectron spectrophotometer. The binding energies were referenced to the C 1s peak of adventitious carbon at 284.3 eV. The TG-DTA analysis of the modified nanoparticles and grafting percentage were determined using a Thermo plus TG-8120 (RIGAKU, Japan). TEM was performed using a JEOL-2100F transmission electron microscope (JEOL, Japan).

2.2.5 Fabrication of TiO_2 nanoparticles reinforced PEI film

The TiO_2 nanoparticles (0.2 wt.% of total amount of PEI) were modified with

γ-MPS and PEI (Part 1: 0.2 wt.% of total amount of PEI) using the procedure described in section 2.2. The left PEI particles (Part 2: 99.8 wt.% of total amount of PEI)were then added at the total amount of 45 wt.% of the NMP solvent (100 mL). The mixture was stirred at 200 rpm at 70 °C until all of the PEI particles had dissolved. Films were formed from the mixture in a flat container using an auto film applicator, which were then heated at 150 °C for approximately 2 h to remove the NMP. The containers were then heated at 80 °C for 24 h in a drying oven. The films were subsequently pressed under low pressures for 25 minutes at 120 °C, then cooled with the pressures to ambient temperature to eliminate residual stresses. This process is shown schematically in Fig. 2-2.

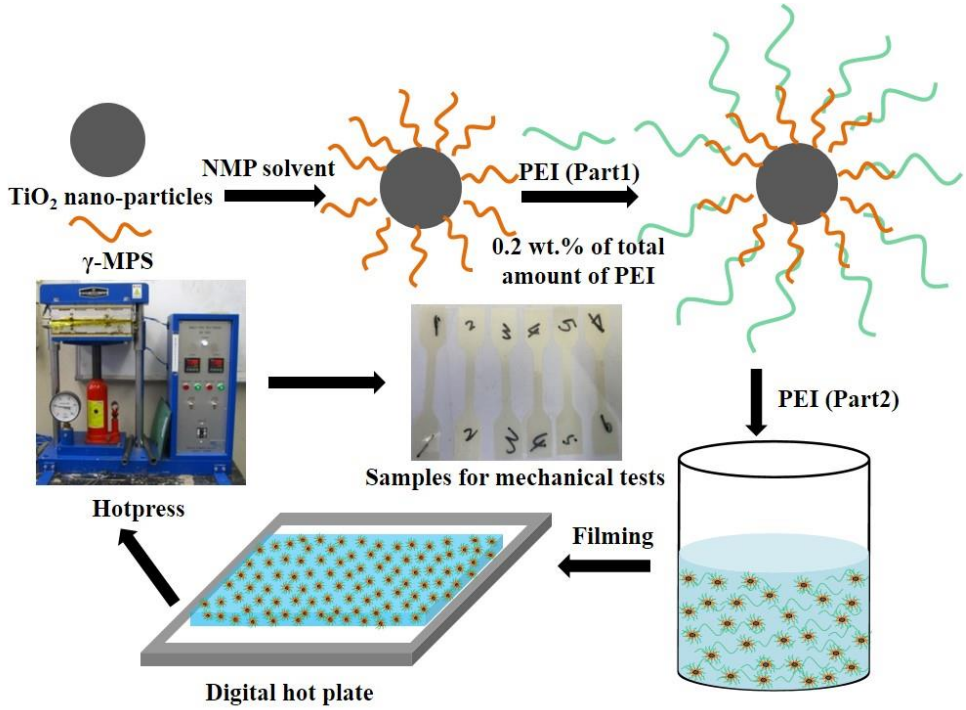

Fig. 2-2. Schematic showing the preparation of TMP nanoparticles and their incorporation into PEI films.

In addition to the TMP/PEI film, four different PEI films were fabricated for

comparison (Table 2-2). A film containing γ-MPS (M/PEI) was fabricated as follows: γ-MPS (0.2 wt.% of PEI) was added to NMP, then the PEI particles were added and the mixture and stirred until the PEI particles had dissolved. Then the film was fabricated in the process as described in fabrication of TMP/PEI before.

A film containing TiO_2 (T/PEI) was fabricated as follows: TiO_2 nanoparticles were added to NMP, after that PEI particles were added into the mixture and stirred until the PEI particles had dissolved. Then the film was fabricated in the process as described in fabrication of TMP/PEI before.

A film containing γ-MPS coated TiO_2 (TM/PEI) that was made in a single step was fabricated as follows: after the TiO_2 nanoparticles were modified with γ-MPS (section 2.2), PEI particles at the amount of 45 wt.% of the NMP solvent (100 mL) were added into the mixture and stirred until all the PEI particles dissolved. Then the film was fabricated in the process as described in fabrication of TMP/PEI before. A neat PEI film (PEI) was also fabricated for comparison in the process as described in fabrication of TMP/PEI before.

The film thickness was approximately 50 μm. All films were then subjected to UV-irradiation (365 nm) using a high-pressure mercury lamp (100 W, HLR100T-2, SEN Light CORP, Japan) under air-cooled conditions. The intensity of incident light (40 mW/cm^2) was measured using an Ultraviolet Radiometer UIT-201 (USHIO, Japan).

Table 2-2. Formulation of various sample films.

Sample	TiO_2 (wt%)	γ-MPS (wt%)	PEI-I (g)	PEI-II (g)	NMP(mL)
PEI	-	-	-	46.26	100
M/PEI	-	0.2	-	46.26	100
T/PEI	0.2	-	-	46.26	100
TM/PEI	0.2	0.2	-	46.26	100
TMP/PEI	0.2	0.2	0.09	46.17	100

2.2.6 Characterization of the TiO_2 nanoparticles reinforced PEI film

The morphology of film surface before and after fracturing (following a tensile strength test) was observed using a JSM-6010LA In Touch Scope scanning electron microscope (JEOL Co. Ltd., Tokyo, Japan).

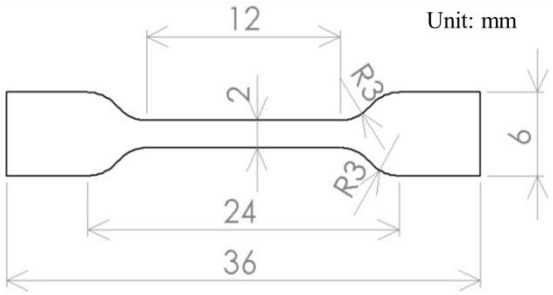

Fig. 2-3. Diagram of tensile test sample

The tensile properties of the films were evaluated referencing the JIS(K-7127) testing method. Dogbone Specimens were prepared by cutting the films to the required shape as shown in Fig. 2-3. The experiments were performed using a universal testing instrument (RTC-1250A, A&D CO., LTD, Japan) with a constant speed of 0.5 mm/min at 23±2 °C. A minimum of five different specimens from each film were tested.

2.3 Results and discussion

2.3.1 FTIR spectroscopy

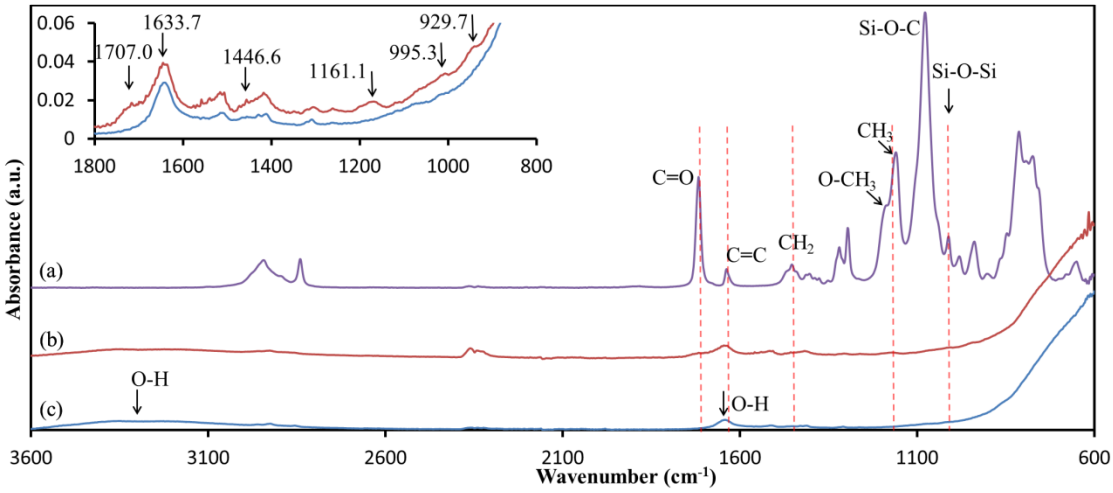

Fig. 2-4. FTIR spectra of (a) γ-MPS, (b) TM and (c) unmodified TiO_2 nanoparticles.

FTIR spectra of γ-MPS, γ-MPS grafted TiO_2 nanoparticles (TM) and unmodified TiO_2 nanoparticles in the region 3600–600 cm^{-1} are shown in Fig. 2-4a, b and c, respectively. The main band assignments for γ-MPS are labeled in the graph [11,12]. The broad absorption band from 3400 to 3200 cm^{-1} and the weak peak at 1616.3 cm^{-1} in the spectrum of the unmodified TiO_2 particles were attributed to the stretching vibration of hydroxyl groups (OH) on the particle surface and absorbed water on the TiO_2 nanoparticles [12]. The inset shows the region from 1800 to 800 cm^{-1}. The bands at 1707.0 and 1633.7 cm^{-1} are characteristic of C=O and C=C stretching vibrations, respectively. The bands at 1446.6 and 1161.1 cm^{-1} are attributed to deformation vibrations of C-H in CH_2 and CH_3, respectively [11]. The presence of a band that is characteristic of Si-O-Si link vibrations (995.3 cm^{-1}) indicated that some condensation of the silane chains had occurred. All of these bands were observed in both γ-MPS and TM. The band at 929.7 cm^{-1} was assigned to the stretching vibration of Ti-O-Si [13-15],

which indicated that a condensation reaction between silane groups and the hydroxyl groups on the TiO_2 nanoparticles had occurred, as shown in Fig. 2-5.

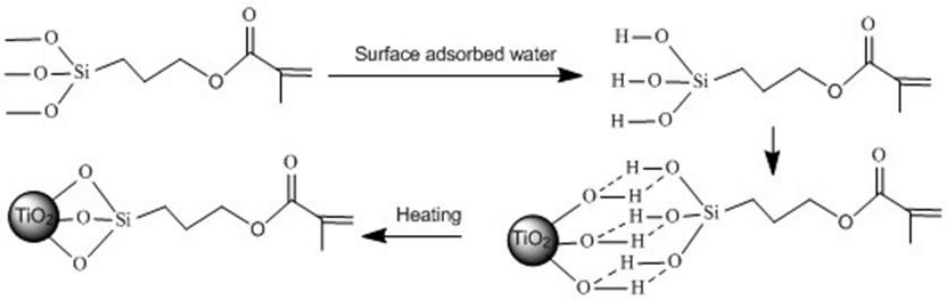

Fig. 2-5. Reaction scheme for the deposition of γ-MPS on TiO_2 nanoparticles.

To confirm whether the residual or physisorbed γ-MPS had been completely washed off, the FTIR spectrum (Fig. 2-6) of the supernatant after three-time wash with acetone was tested. There were no characteristic peaks of γ-MPS shown in spectrum of the supernatant (Fig. 2-6c) after three-time wash. Therefore, there was no free γ-MPS in the supernatant after washing three times. It indicated that the residual or physisorbed γ-MPS had been removed.

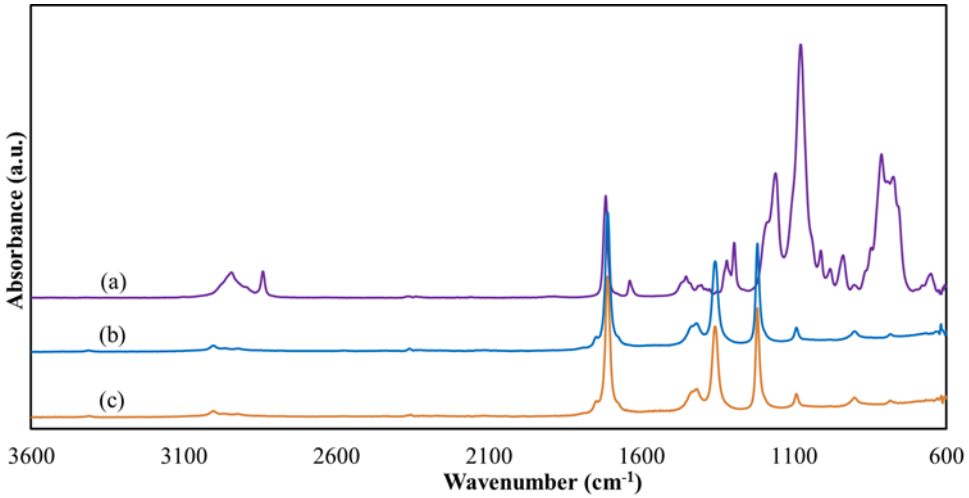

Fig. 2-6. FTIR spectrum of (a) γ-MPS, (b) acetone and (c) the supernatant after three-time wash.

As any residual or physisorbed γ-MPS had been removed, the presence of the peaks described previously in the spectrum of the TM nanoparticles indicated that the grafting of γ-MPS on the surface of the TiO_2 nanoparticles was successful. As water was excluded from the reaction, γ-MPS could only be hydrolyzed by water that had absorbed to the surface of the nanoparticles, which would lead to hydrogen bonding between the silanols and the nanoparticles (Fig. 2-5). Any peaks that corresponded to γ-MPS in the spectrum of TM were very weak.

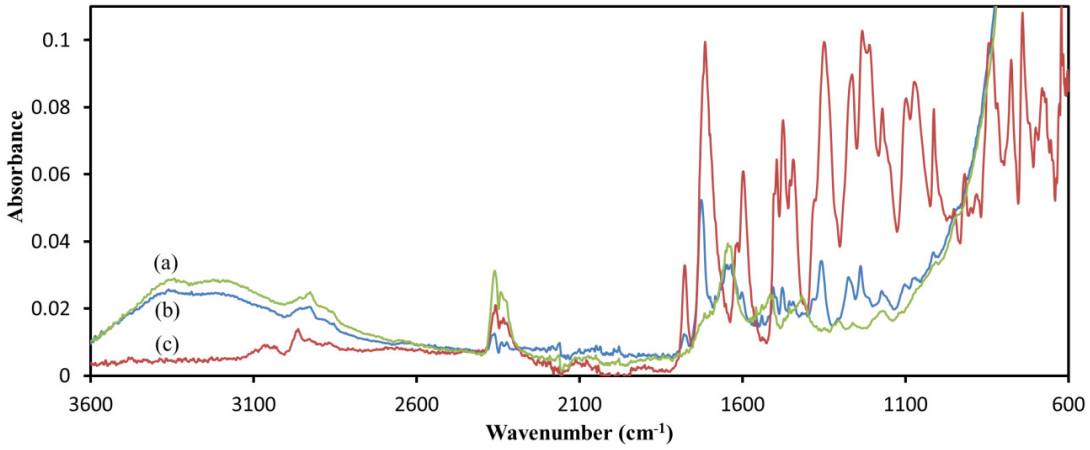

Fig. 2-7. FTIR spectrum of (a) TM, (b) TMP and (c) neat PEI.

The FTIR spectra of TM, TMP and neat PEI are shown in Fig. 2-7. In addition to the characteristic peaks of γ-MPS, almost all of the peaks from PEI appeared in the spectrum of TMP. Additionally, no new peaks were present (Fig. 2-7b). These results indicated that the PEI chains were not chemically bonded to the TM nanoparticles but absorbed by the Van der Waals force, which acted to anchor the PEI chains to the TM nanoparticles in NMP. When the critical concentration of absorbed PEI chains on the nanoparticle surface was reached, the TMP space structure were formed in the NMP solvent, as shown in Fig. 2-2.

2.3.2 XPS spectroscopy

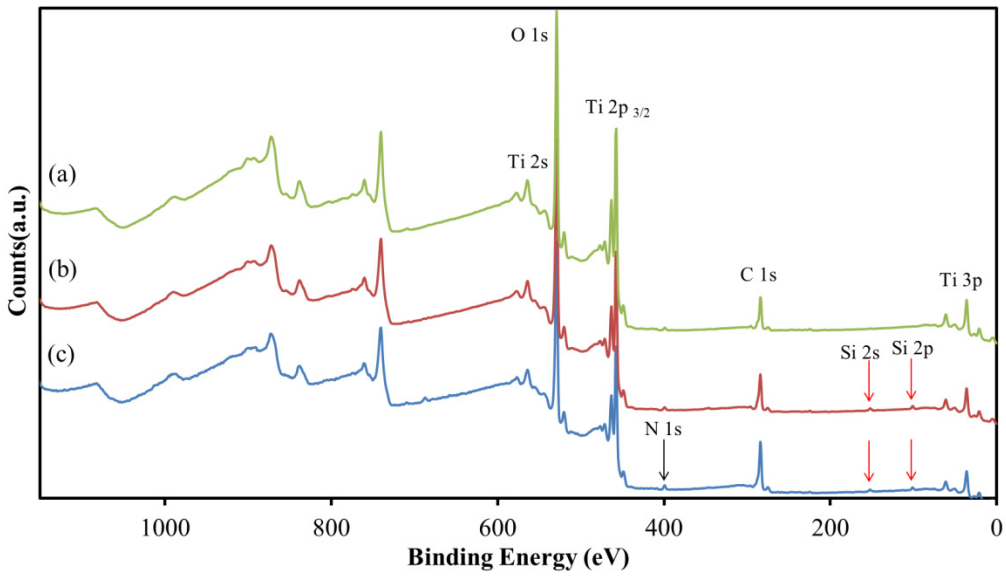

Fig. 2-8. XPS spectra of (a) unmodified TiO_2 nanoparticles, (b) TM and (c) TMP.

The XPS and C 1s spectra of the unmodified TiO_2 nanoparticles, TM and TMP are shown in Fig. 2-8. The XPS spectra indicated that titanium, oxygen, nitrogen, carbon and silicon were present in TM and TMP (Fig. 2-8). The presence of Si 2s and Si 2p transitions in the XPS spectra of TM (Fig. 2-8b) indicated that the TiO_2 nanoparticles had been successfully modified with γ-MPS. Following the double coating process the relative intensity of the N signal in the spectrum of TMP increased, which could confirm that PEI was anchored to the surface. Therefore, the atomic ratio between N 1s and Ti 2p throw the XPS spectrum was calculated as follows:

$$\frac{C_{N\,1s}}{C_{Ti\,2p}} = \frac{\frac{A_{N\,1s}}{ASF_{N\,1s}}}{\frac{A_{Ti\,2p}}{ASF_{Ti\,2p}}} = \frac{A_{N\,1s}\times ASF_{Ti\,2p}}{A_{Ti\,2p}\times ASF_{N\,1s}} = \frac{A_{N\,1s}\times 1.2}{A_{Ti\,2p}\times 0.42} \qquad (1)$$

A: Peak area

ASF: Atomic Sensitivity Factor

$ASF_{N\ 1s} = 0.42$; $ASF_{Ti\ 2p} = 1.2$ [16]

Table 2-3. N 1s/Ti 2p atomic ratio of modified nanoparticles.

sample	TM	TMP
N 1s/Ti 2p ratio	9.3×10^{-3}	1.2×10^{-2}

The N 1s/Ti 2p atomic ratio increased from 9.3×10^{-3} to 1.2×10^{-2} after double coated reaction as shown in Table 2-3. As the atomic concentration of Ti 2p cannot change with the reaction, the atomic concentration ratio between N 1s and Ti 2p can reflect changes in the content of N element. Therefore, we inferred that the introduction of PEI chains containing N element increased the content of N element. It indicated that the PEI chains were anchored to the particle surface, which had been also proved by previous FTIR experiment in section 2.3.1.

2.3.3 TG analysis

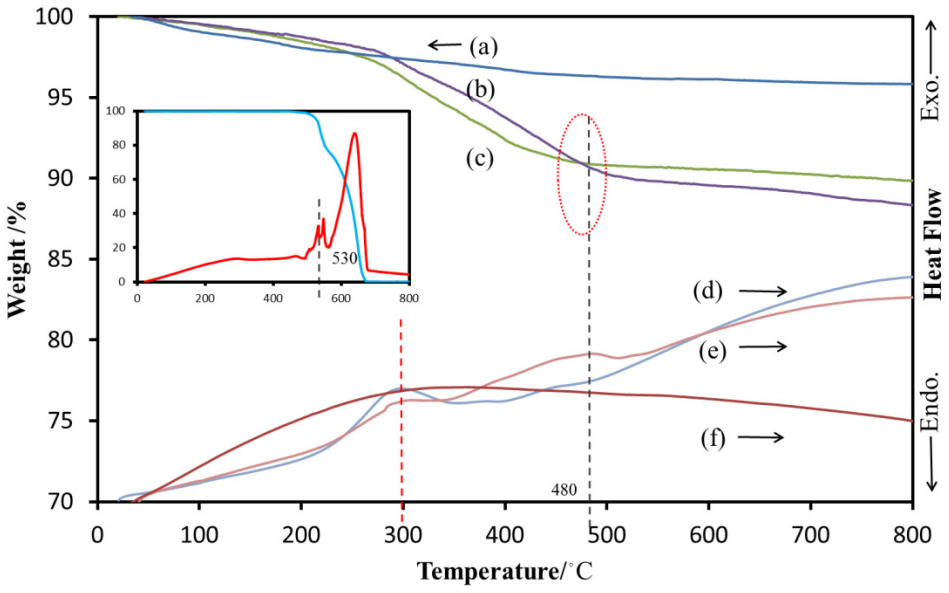

Fig. 2-9. TG curves of (a) unmodified TiO_2 nanoparticles, (b) TMP and (c) TM. DTA curves of (d) TM, (e) TMP and (f) unmodified TiO_2 nanoparticles.

To estimate the amount of γ-MPS and PEI on the surface of the nanoparticles, TG-DTA analysis was performed between ambient temperature and 800 °C in air at a rate of 10 °C/min. The thermal behavior of the unmodified TiO_2 nanoparticles (without drying) is shown in Fig. 2-9a and f. Curve f only show a slow exothermic reaction which caused by decomposition of organic components [15,17-19]. It cannot be observed the obvious endothermic peak caused by desorption of physisorbed water, or the endothermic peak caused by the loss of water from surface hydroxyl groups (TiOH) which led to the formation of Ti-O-Ti bonds [7]. The total weight loss for unmodified TiO_2 nanoparticles was 6.3% until 800 °C.

The TG and DTA curves of TM (Fig. 2-9c and d, respectively) and TMP (Fig. 2-9b and e, respectively) indicated that TMP had greater thermal stability than that of TM. A sharp weight loss occurred near 300 °C that was attributed to the oxidative thermal decomposition of γ-MPS. The decomposition of PEI chains began at 480 °C, even though the decomposition temperature of pure PEI occurs at 530 °C (shown in the inset). The lower decomposition temperature can be explained by the strong interactions between the γ-MPS and PEI layers, which weakened the interactive forces between the PEI chains [20]. In addition, at the decomposition temperature of PEI (480 °C) the weight loss of both TM and TMP were almost identical (ellipse in Fig. 2-9). This indicated that the γ-MPS grafting rate for TMP was almost the same as for TM. The total weight loss for TM and TMP was 10.1% and 11.7%, respectively.

The γ-MPS grafting rate of TM was calculated by subtracting the weight loss of the unmodified particles from the total weight loss of TM [7,15,21]. As the γ-MPS grafting rate of TMP was almost the same as that of TM, the PEI grafting rate of TMP was also calculated by subtracting the weight loss of TM from the total weight loss of TMP. The

grafting rates of γ-MPS and PEI were 3.8% and 1.6%, respectively.

2.3.4 TEM observation

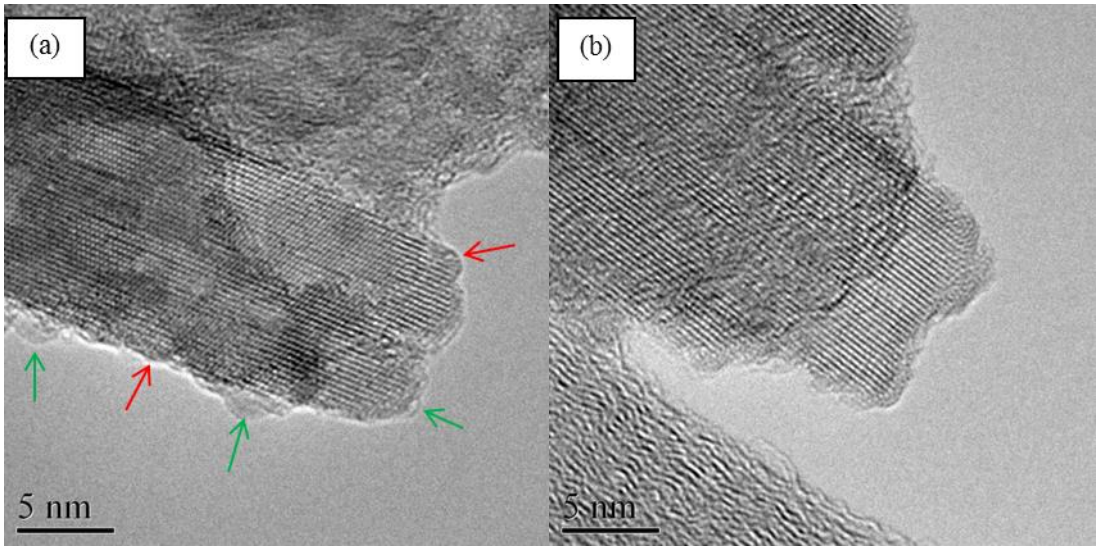

Fig. 2-10. TEM images of (a) TM and (b) TMP.

A combination of both FTIR spectroscopy and TEM gave clear evidence that the particles were coated with the polymer [22-24]. TEM images of TM and TMP are shown in Fig. 2-10, in which the area with organized mesoporosity is inorganic particle and the translucent area is organic compound [22-24]. The surface of the pristine TiO_2 nanoparticles appeared rough when grafted with γ-MPS (Fig. 2-10a). As any unreacted γ-MPS was removed from the particle surface by centrifugation and washing, it is evident that γ-MPS was chemically bonded to the particle surface. The particles were not completely or uniformly coated with γ-MPS (red and green arrows, Fig. 2-10a). This may have been because the rate of hydrolysis of γ-MPS was very low because of the exclusion of water, which led to a very low γ-MPS grafting rate on the particle surface. Optimization of the reaction conditions, including reaction time and reaction temperature, will be the direction of future work.

The outermost layer on the TMP nanoparticles (Fig. 2-10b) appeared to be more uniform than that on the TM nanoparticles (Fig. 2-10a). Because of the long chains of PEI, the part without grafting γ-MPS on the particle surface all covered with PEI after the concentration of absorbed PEI reached the critical concentration, which was explained in the next section.

2.3.5 Dispersion stability test

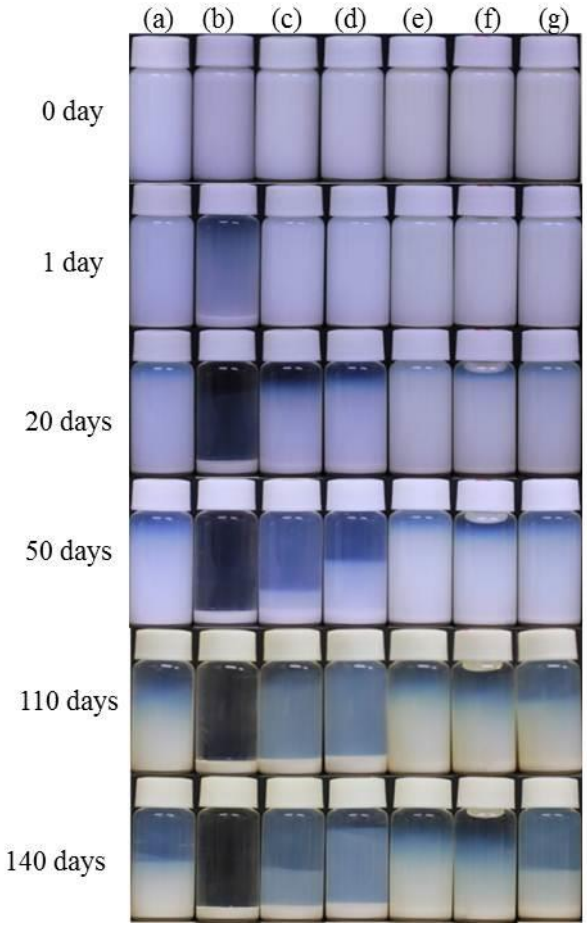

Fig. 2-11. Time-dependent sedimentation of an unmodified TiO_2 nanoparticle suspension, suspensions of TiO_2 nanoparticles exposed to γ-MPS for different times and suspensions of TiO_2 nanoparticles modified with γ-MPS and exposed to PEI for different times.

Table 2-4. Formulation of various sample suspensions.

Samples	a	b	c	d	e	f	g
γ-MPS modification time/h	-	2	4	6	6	6	6
PEI coating time/h	-	-	-	-	2	4	6

The sedimentation behavior of suspensions taken at 2-h intervals during the fabrication of the TMP nanoparticles are shown in Fig. 2-11. The formulations of the different sample suspensions are shown in Table 2-4. The reference sample (the suspension within unmodified TiO_2 nanoparticles, Fig. 2-11a) was dispersed effectively owing to the particle size (16 nm) in the organic solvent. The rate of hydrolysis between γ-MPS and the surface hydroxyl groups increased with time, which was evidenced by the trends that can be seen in Fig. 2-11b~d. But with the lowest hydrolysis reaction rate the nanoparticles (Fig. 2-11b) were covered with the least amount of γ-MPS, which enabled linking between the particles and led to aggregation and settling under the force of gravity [26]. Samples (c) and (d) exhibited better dispersion than sample (b), but worse than sample (a). This indicated that the hydrolysis of γ-MPS at reaction times less than 6 h promoted the flocculation of the colloidal dispersion because the particle surface was not completely covered, which was consistent with the TEM observations. The sedimentation behavior of the samples exposed to PEI for different coating times after being modified with γ-MPS for 6 h are shown in Fig. 2-11e~g. Significant improvements were observed in the dispersion behavior of these samples, because the particles were completely covered with PEI, which was consistent with the TEM observations. The particles were covered with a layer of PEI via Van der Waals forces with chains that extended into solution [27]. Thus, the system was stabilized because of repulsive forces. However, with increased reaction time this stabilization decreased. The PEI concentration on the particle surface in sample (e) was high enough to cause steric

stabilization or even there was amount of non-adsorbed PEI. Therefore, an additional stabilization mechanism may have existed, such as depletion stabilization because of the free polymer molecules that may have promoted the flocculation or stabilization of the colloidal dispersions. This occurs via a depletion interaction that depends on the concentration of the free polymer [27]. The concentration of free PEI in sample (e) must have been less than the critical concentration (C^+) for the onset of depletion flocculation, which exhibited depletion stabilization. The concentration of free PEI in sample (g) must have been greater than C^+ for the onset of depletion flocculation, which exhibited depletion flocculation. The different effects of polymers on colloid stability are shown schematically in Fig. 2-12, which explained the experimental phenomena. Fig. 2-12a simulated the bridging flocculation corresponding to sample (b), (c) and (d) as shown in Fig. 2-11b~d. Fig. 2-12b and c simulated steric stabilization and depletion stabilization, respectively, which occurred in formation of sample (e) as shown in Fig. 2-11e. Fig. 2-12d simulated the depletion flocculation corresponding to sample (f) and (g) as shown in Fig. 2-11f~g.

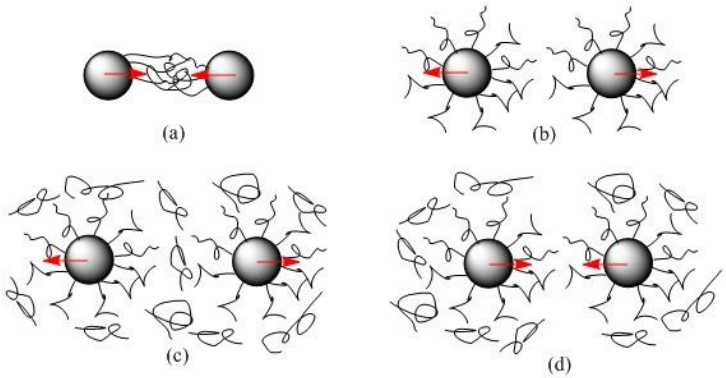

Fig. 2-12. Effects of polymers with different concentrations on colloid stability: (a) bridging flocculation, (b) steric stabilization, (c) depletion stabilization, (d) depletion flocculation.

The long-term suspension behavior also indicated that there were one or more clear interfaces during the sedimentation test. Samples (c) and (d) were used to illustrate this because of their proper cycles in which the suspension shown turbid firstly, then upper clarification and lower turbidity appeared, and then a clear interface layer appeared, and then the part over the interface layer turbid again. Before the appearance of the interfaces, particles that were larger than the limit size had precipitated. The interface was very vague and the supernatant was very clear. Colloid particles with the limit size maintained the steric stabilization and achieved the dynamic equilibrium of deposition. Particles smaller than the limit size were at the top of the suspension which have more obvious Brownian motion. In addition, the constant collision of the smaller particles on the large particles lower resulted in the clear interface. Then the smaller particles became uniform dispersed between liquid level and the interface by Brownian motion. So the supernatant disappeared. As the size of the small particles increased, this process cycled until all of the particles had completely precipitated. After approximately 140 days, there were two clear interfaces in samples (c) and (d). Because of the increased dispersion in samples (a), (e), (f) and (g), the cycle was much longer. Samples (a) and (g) had one clear interface, while there was no clear interface in sample (e) and (f). This phenomenon existed in all samples, even in sample (b). However, it was difficult to observe visually in sample (b) because the concentration of particles that were smaller than the limit size was very low.

2.3.6 Mechanical properties of TiO_2 nanoparticle reinforced PEI films

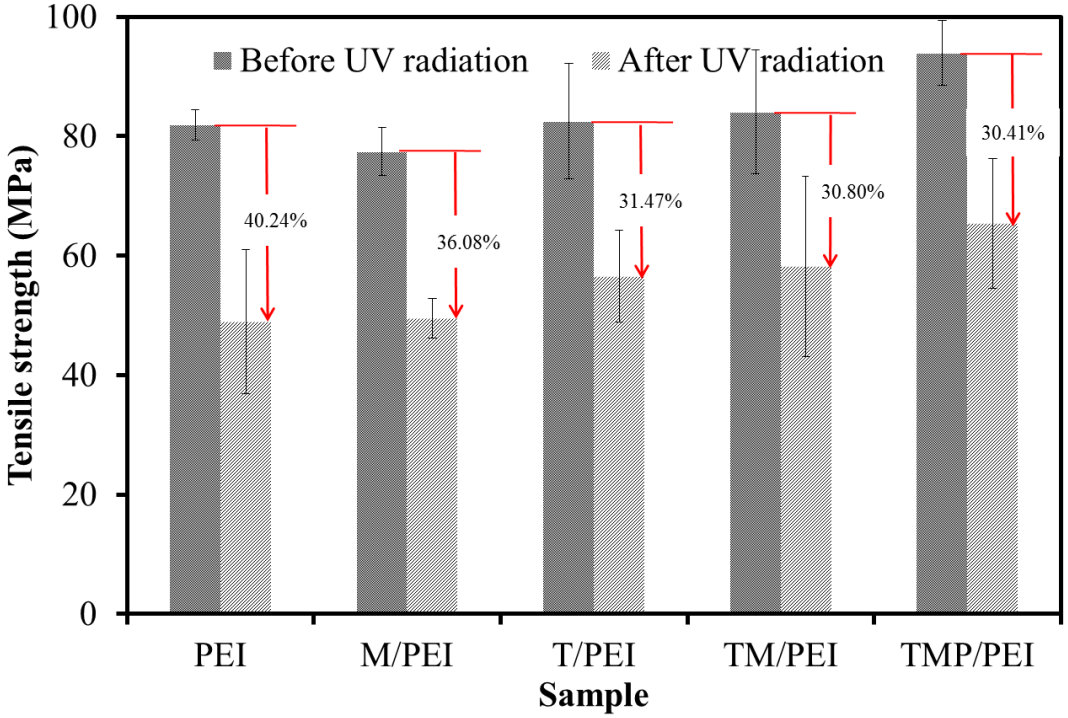

Fig. 2-13. Tensile strength of the films before and after UV radiation.

The tensile strength of the films before and after UV irradiation is shown in Fig. 2-13. Before UV radiation, the tensile strength of the M/PEI film was 5.40% less than neat PEI film. As γ-MPS could not react with PEI to form a cross-linked structure, the tensile strength of M/PEI film decreased because of the formation of micelles via self-hydrolysis of γ-MPS. The tensile strength of the films increased with the addition of the nanoparticles (T/PEI, TM/PEI and TMP/PEI), which was consistent with literature reports [3,5,8]. Poor interfacial adhesion and agglomeration within the T/PEI and TM/PEI films caused the tensile strength to remain similar to the neat PEI film. The double-layered structure of the TMP/PEI film caused enhanced interfacial adhesion and dispersion, which led to an increase in the tensile strength of approximately 14.74%

when compared with the neat PEI film. After 24 hours of UV radiation, the tensile strength of all samples decreased. The fact that the reduction in tensile strength of the M/PEI film was less than that of the neat PEI film indicated that small molecules (γ-MPS) absorbed a portion of the UV energy. The presence of the TiO_2 nanoparticles lessened the reduction in the tensile strength of the films (T/PEI<TM/PEI<TMP/PEI). Among them, the TMP/PEI film exhibited the most resistance to UV damage. The tensile strength of the TMP/PEI film after UV radiation was 33.59% higher than that of neat PEI film.

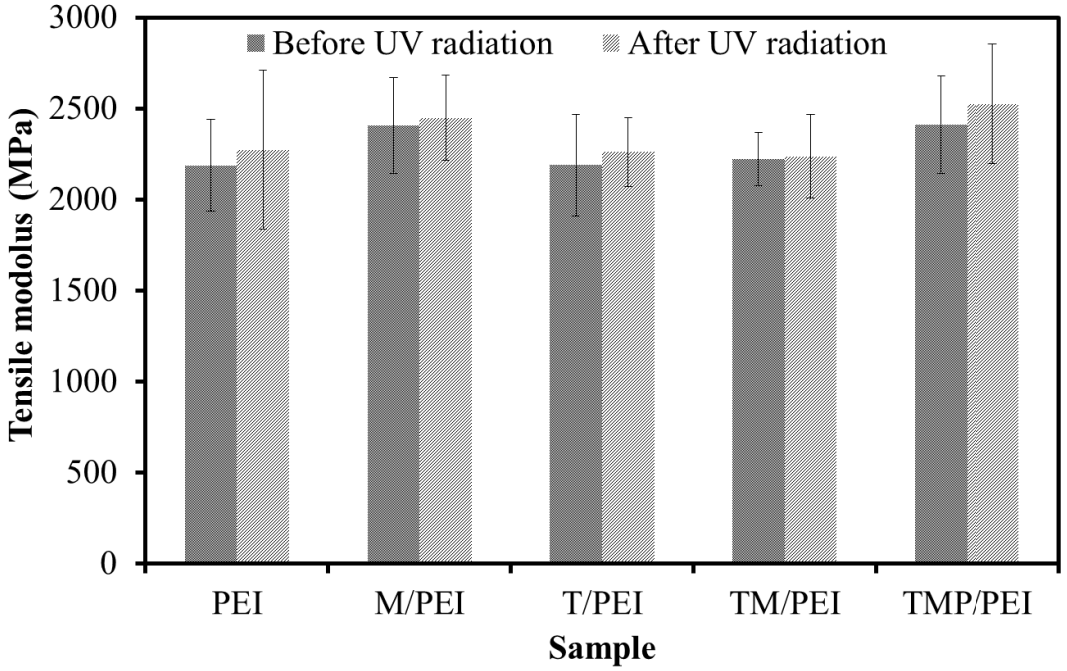

Fig. 2-14. Tensile modulus of the sample before and after UV radiation.

The tensile modulus of each film before and after UV radiation is shown in Fig. 2-14. Before UV radiation, the tensile modulus of the M/PEI film increased when compared with that of the neat PEI film because of the formation of micelles via self-hydrolysis of γ-MPS. TiO_2 nanoparticles are rigid and have a higher modulus than

that of neat PEI. Therefore, the tensile modulus must increase when TiO_2 nanoparticles are added to a polymer matrix [15]. The nanoparticles in the T/PEI and TM/PEI films formed large particles because of poor dispersion. Their influence to tensile modulus could be neglected because of their big size [28], which was in agreement with our experiment results. Following UV radiation, the tensile modulus of all films increased. Although photo-degradation may occur, the increase in tensile modulus can be explained by UV induced cross-linking within the polymer [25]. The mechanical properties of the films are listed in Table 2-5.

Table 2-5. Mechanical properties of the films.

Sample	Tensile Strength (MPa)		Tensile Modulus (MPa)	
	Before UV radiation	After UV radiation	Before UV radiation	After UV radiation
PEI	81.90	48.95	2186.41	2271.73
M/PEI	77.48	49.53	2405.52	2448.13
T/PEI	82.52	56.55	2187.93	2260.47
TM/PEI	84.12	58.22	2220.83	2235.80
TMP/PEI	93.97	65.39	2410.00	2524.14

2.3.7 SEM observation

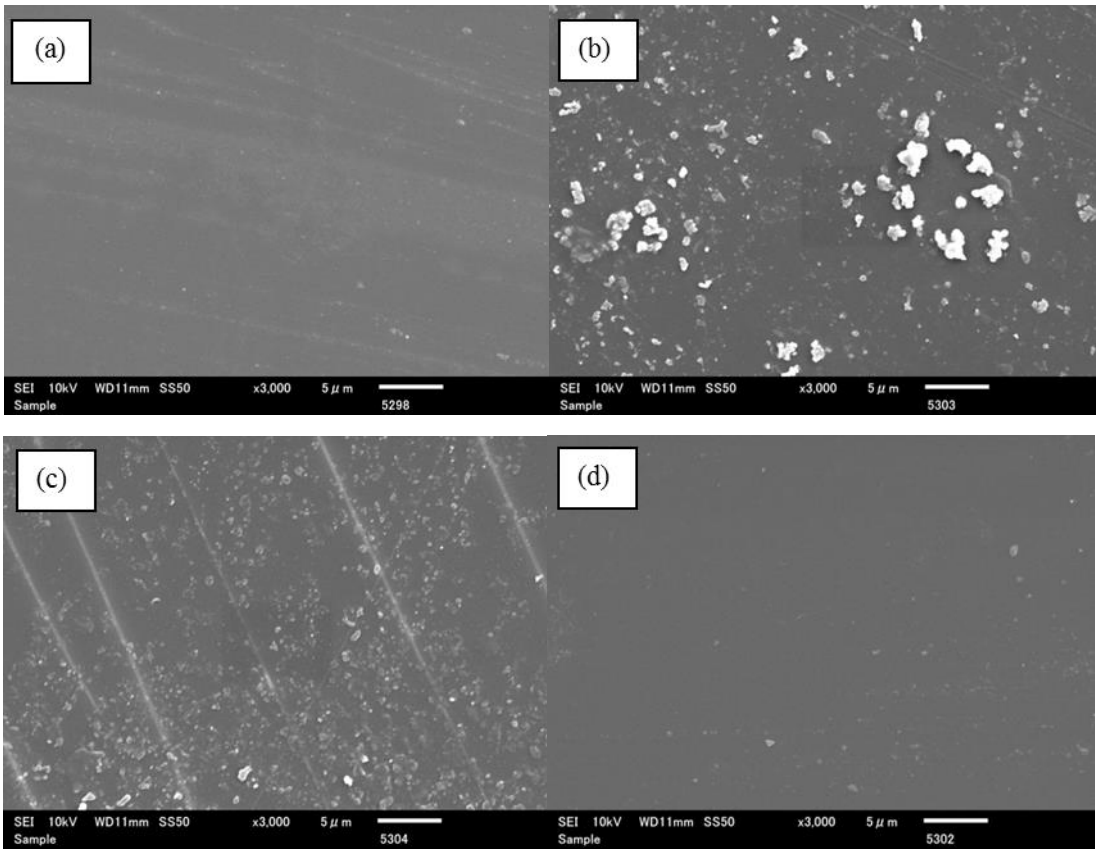

Fig. 2-15. SEM images of surface after 24 h of UV radiation of (a) neat PEI film, (b) T/PEI, (c) TM/PEI and (d) TMP/PEI.

The surface morphology of the films was examined using SEM after 24 h of UV irradiation, as shown in Fig. 2-15. There were no obvious cracks on the surface of the films, which is known to occur in other polymer films [25]. The particle dispersion can be qualitatively assessed by comparing the distribution of particles on the surface of the films. The neat PEI film had a smooth surface (Fig. 2-15a). The agglomeration of particles on the surface of the T/PEI film that was fabricated using the traditional method was the most obvious (Fig. 2-15b), while the surface of the TMP/PEI film that was fabricated using the anchoring grafting method was uniform and smooth. Hence,

the SEM observations confirmed that the fabrication of nanocomposite films using anchoring grafting method was successful in creating smooth films with uniformly distributed particles.

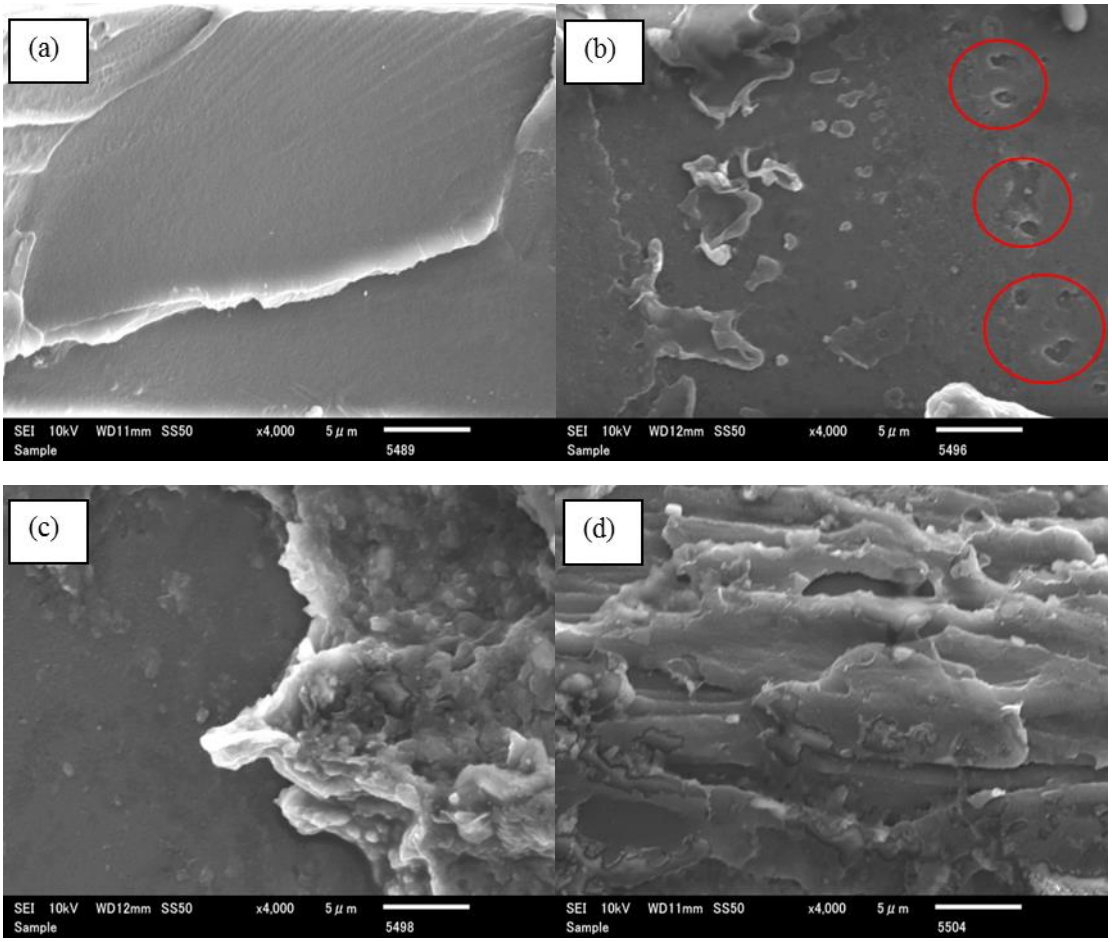

Fig. 2-16. SEM images of fractured surfaces of (a) a neat PEI film, (b) T/PEI, (c) TM/PEI and (d) TMP/PEI.

The fractured surfaces of the neat PEI, T/PEI, TM/PEI and TMP/PEI films after the tensile test were observed using SEM, as shown in Fig. 2-16. These images gave information about the cause and location of failure within the films, and the reinforcement of the films because of the presence of the nanoparticles [15]. The fractured surface of the neat PEI film was very smooth (Fig. 2-16a), while those of the

nanocomposite films were considerably rougher. The T/PEI film that contained untreated TiO_2 nanoparticles had a smoother fractured surface (Fig. 2-16b) than the films that contained treated TiO_2 nanoparticles (Fig. 2-16c and d). Additionally, the holes left by the particles that were pulled-out (red circles, Fig. 2-13b) indicated that the interfacial adhesion between the particles and polymer was poor. Two distinct regions were observed in the image of the fractured TM/PEI film (Fig. 2-16c), one smooth and the other rough. This was because the nanoparticles were only treated with γ-MPS (6 h), which promoted agglomeration. Large shear deformation was obvious in the image of the fractured TMP/PEI film, which indicated that mechanical stress concentrated on the nanoparticles encouraged shear yielding of the film and caused the crack to continue through the entire film. The energy absorbed by this type of shear yielding leads to increased mechanical strength [3,29], which was confirmed by the tensile strength tests.

2.4 Conclusions

Double-coated TiO_2 nanoparticles (TMP) were prepared using a single-pot fabrication method in NMP. These particles contained a chemically bonded layer of γ-MPS and a layer of PEI that was absorbed via Van der Waals forces. All fabrication and experimental processes were conducted in NMP, which prevented the agglomeration of particles during the centrifugal drying process.

The double-coated TiO_2 nanoparticles (TMP) exhibited improved dispersion in NMP because of steric stabilization of the polymer chains that were absorbed to the particle surface and depletion stabilization of the free polymer in the solvent. In the long-term dispersion stability test, we found that there was a common cycle during the process of the sedimentation in which the suspension shown turbid firstly, then upper clarification and lower turbidity appeared, and then a clear interface layer appeared, and

then the part over the interface layer turbid again.

The double-coated TiO_2 nanoparticles (TMP) also exhibited improved dispersion within the PEI nanocomposite films and increased interface adhesion between the TiO_2 nanoparticles and the PEI matrix. Therefore, the nanocomposite TMP/PEI film exhibited increased mechanical properties and UV resistance.

References

[1] J.H. Li, R.Y. Hong, M.Y. Li, H.Z. Li, Y. Zheng, J. Ding, Effects of ZnO nanoparticles on the mechanical and antibacterial properties of polyurethane coatings, Prog, Org. Coat. 64 (2009) 504-509.

[2] Kalfus J, Jancar J, Reinforcing mechanisms in amorphous polymer nano-composites, Compos Sci Technol. 68 (2008) 3444-3447.

[3] C.L. Wu, M.Q. Zhang, M.Z. Rong, K. Friedrich, Silica nanoparticles filled polypropylene effects of particle surface treatment, matrix ductility and particle species on mechanical performance of the composites, Compos Sci Technol. 65 (2005) 635-645.

[4] W.H. Ruan, Y.L. Mai, X.H. Wang, M.Z. Rong, M.Q. Zhang, Effects of processing conditions on properties of nano-SiO_2 polypropylene composites fabricated by pre-drawing technique, Compos Sci Technol. 67 (2007) 2747-2756.

[5] J. Cho, M.S. Joshi, C.T. Sun, Effect of inclusion size on mechanical properties of polymeric composites with micro and nano particles, Compos. Sci. Technol. 66 (2006) 1941-1952.

[6] B.A. Rozenberg, R. Tenneb, Polymer-assisted fabrication of nanoparticles and nanocomposites, Prog. Polym. Sci. 33 (2008) 40-112.

[7] J. Lin, J.A. Siddiqui, R.M. Ottenbrite, Surface modification of inorganic oxide particles with silane coupling agent and organic dyes, Polym Adv Technol. 12 (2001) 285-292.

[8] H. Gu, Y. Guo, S.Y. Wong, C. He, X. Li, V.P.W. Shim, Effect of interphase and strain-rate on the tensile properties of polyamide 6 reinforced with functionalized silica nanoparticles, Compos. Sci. Technol. 75 (2013) 62–69.

[9] M.Z. Rong, M.Q. Zhang, W.H. Ruan, Surface modification of nanoscale fillers for improving properties of polymer nanocomposites: a review, Mater Sci Technol. 22 (2006) 787-796.

[10] M. Naffakh, A.M. Díez, C. Marco, G.J. Ellis, M.A. Gómez, Opportunities and challenges in the use of inorganic fullerene-like nanoparticles to produce advanced polymer nanocomposites, Prog. Polym. Sci. 38 (2013) 1163-1231.

[11] M. Masmoudi, M. Abdelmouleh, R. Abdelhedi, Infrared characterization and electrochemical study of γ-methacryloxypropyltrimethoxysilane grafted in to surface of copper, Spectrochim. Acta Part A: Mol. Biomol. Spectrosc. 118 (2014) 643-650.

[12] Y.Z. Wang, G.L. Chen, C. Yue, L. Ao, Z.Y. Sun, Y.S. Zhang, T.Y Lan, L.W Zu, Preparation and characterizations of nano-TiO_2 modified with polyacrylonitrile, Russ J Phys Chem A. 89 (2015) 1275-1279.

[13] E. Ukaji, T. Furusawa, M. Sato, N. Suzuki, The effect of surface modification with silane coupling agent on suppressing the photo-catalytic activity of fine TiO_2 particles as inorganic UV filter, Appl. Surf. Sci. 254 (2007) 563-569.

[14] Z.J. Li, B. Hou, Y. Xu, D. Wo, Y.H. Sun, W. He, F. Deng, Comparative study of sol-gel-hydrothermal and sol-gel synthesis of titania-silica composite nanoparticles, J. Solid State Chem. 178 (2005) 1395-1405.

[15] J. Zhao, M. Milaniva, M.C.G.W. Warmoeskerken, V. Dutschk, Surface modification of TiO_2 nanoparticles with silane coupling agents, Colloids Surf. A: Physicochem. Eng. Asp. 413 (2012) 273-279.

[16] C.D. Wagner, Sensitivity factors for XPS analysis of surface atoms, J. Electron Spectrosc. Relat. Phenom. 328 (1988) 99-102

[17] J.G. Yu, H.G. Yu, B. Chen, X.J. Zhao, J.C. Yu, W.K. Ho, The Effect of Calcination Temperature on the Surface Microstructure and Photocatalytic Activity of TiO_2 Thin Films Prepared by Liquid Phase Deposition, J. Phys. Chem. B. 107 (2003) 13871-13879.

[18] K. Terabe, K. Kato, H. Miyazaki, S. Yamaguchi, A. Imai, Y. Iguchi, Microstructure and crystallization behaviour of TiO_2 precursor prepared by the sol-gel method using metal alkoxide, J. Mater. Sci. 29 (1994) 1617-1622.

[19] J.C. Yu, J.G. Yu, K.W. Ho, Z.T. Jiang, L.Z. Zhang, Effects of F^- Doping on the Photocatalytic Activity and Microstructures of Nanocrystalline TiO_2 Powders. Chemistry of Materials. 14 (2002) 3808-3816.

[20] X.W. Li, W. Chen, C.Q. Bian, J.B. He, N. Xu, G. Xue, Surface modification of TiO_2 nanoparticles by polyaniline, Appl. Surf. Sci. 217 (2003) 16-22.

[21] X.L. Miao, M.F. Zhu, Y.G. Li, Q.H. Zhang, H.Z. Wang, Synthesis of dental resins using diatomite and nano-sized SiO_2 and TiO_2, Prog. Nat. Sci.: Mater. Int. 22 (2012) 94-99.

[22] Y. Rong, H.Z. Chen, H.Y. Li, M. Wang, Encapsulation of titanium dioxide particles by polystyrene via radical polymerization, Colloids Surf A: Physicochem Eng Asp. 253 (2005) 193-197.

[23] N. Leventis, S. Mulik, X. Wang, A. Dass, V.U. Patil, C. Sotiriou-Leventis, H. Lu, G.

Churu, A. Capecelatro, Polymer nano-encapsulation of templated mesoporous silica monoliths with improved mechanical properties, J. Non-Cryst. Solids. 354 (2008) 632-644.

[24] H.J. Song, Y.J. Jo, S.Y. Kim, J. Lee, C.K. Kim, Characteristics of ultrafiltration membranes fabricated from polysulfone and polymer-grafted silica nanoparticles: Effects of the particle size and grafted polymer on the membrane performance, J. Membrane Sci. 466 (2014) 173-182.

[25] M. Nowicki, A. Richter, B. Wolf, H. Kaczmarek, Nanoscale mechanical properties of polymers irradiated by UV, Polymer. 44 (2003) 6599-6606.

[26] R.G. Horn, Surface forces and their action in ceramic materials, J. Am. Ceram. Soc. 73 (1990) 1117-1135.

[27] L.W. Wang, W. Sigmund, K. Aldinger, Systematic approach for dispersion of silicon nitride powder in organic media II, dispersion of the powder, J. Am. Ceram. Soc. 83 (2000) 697-702.

[28] L.J. Xiang, K.J. Jiao, J. Wei, B.Z Jiang, Tensile modulus of polymer nanocomposites, Polym Eng Sci. 42 (2002) 983-993.

[29] H.F. Wang, W.J. Han, H.B. Tian, Y.M. Wang, The preparation and properties of glass powder reinforced epoxy resin, Mater Lett. 59 (2005) 94-99.

CHAPTER THREE

Evaporation-induced surface modification of poly(p-phenylene benzobisoxazole) fibers with polyetherimide encapsulated nano-TiO_2

Chapter 3: Evaporation-induced surface modification of poly(p-phenylene benzobisoxazole) fibers with polyetherimide encapsulated nano-TiO_2

3.1 Introduction

Poly(p-phenylene benzobisoxazole) (PBO) fibers have excellent properties, including their high tensile strength, high modulus, high thermal stability, and low weight, and they are widely used as reinforcement for advanced composites in the aerospace, marine, and automobile industries [1, 2]. However, the chemical inactivity and smooth surface of PBO fibers mean that they show poor interfacial adhesion with matrix resins, and this greatly restricts their application [3-5]. Great efforts have been made to improve the interfacial adhesion between PBO fibers and the matrix resin, using techniques such as chemical treatment [3, 4, 6], plasma treatment [7-13], enzymatic surface treatment [5], coupling agents [14, 15], and surface grafting treatment [1, 2, 16-19]. Another problem with PBO fibers, besides their chemical inactivity and smooth surfaces, is their sensitivity to solar irradiation, especially ultraviolet light. The structure and properties of PBO fibers and their composites thus deteriorate on light irradiation [20-22]. Data from Toyobo showed that the PBO fiber strength decreased by more than 60% after only 4 months of exposure at Ohtsu, Japan [23, 24]. Therefore, the development of measures to enable the production of safe and reliable PBO fiber-reinforced composites is necessary. Song et al. found that adhesion of UV absorbers to the PBO fiber surface improved the photostability of the fibers [24]. They also applied $(POSS/TiO_2)_n$ multi-coatings to a PBO fiber surface to improve its UV

resistance [21]. Zhang et al reported that nano-ZnO hybrid sizing effectively shielded the UV-aging of PBO fibers [20]. However, few researchers have used the long chain polymer as a carrier to make the fillers adsorbed on the fiber surface.

Evaporation-induced technology has been widely used in many fields, such as evaporation-induced self-assembly [25-27]. In this work, to endow PBO fibers with rougher interface and better UV resistance, PEI was chose as a carrier to make the nano-TiO_2 adsorbed on PBO fiber surface by evaporation-induced surface modification method. PBO fibers were immersed in dilute solutions containing polyetherimide (PEI)-encapsulated nano-TiO_2 and free PEI chains, and then allowed the solvent to evaporate from the impregnated PBO fiber. The effect of ultrasonic time in the modification on the morphology and UV resistance of treated PBO fibers was also investigated.

3.2 Materials and methods

3.2.1 Materials

TiO_2 nanoparticles (STR-100N, TiO_2 content: >95%, crystal structure: rutile 100%) with an average particle size of 16 nm and a specific surface area of 100 m^2/g were supplied by Sakai, Japan. *N*-methyl-2-pyrrolidone (NMP) was obtained from Kanto, Japan. 3-(Trimethoxysilyl)propyl methacrylate (γ-MPS, 98%) was purchased from Acros Organics, USA. Polyetherimide (PEI) was purchased from Sigma-Aldrich, USA. PBO fibers (HM, 664-H12RD) with a filament diameter of 11 μm were supplied by Toyobo, Japan. The pristine PBO fibers were washed with acetone at room temperature for 48 h to remove surface sizing agents and/or contaminants. The fiber obtained after this process was denoted the untreated PBO fiber.

3.2.2 Preparation of the nano-TiO_2 treatment solution

The nano-TiO_2 treatment solution was prepared from TiO_2 nanoparticles (0.1 wt%) in NMP. After sonication in an ice bath for 25 min, γ-MPS (100 wt% of the TiO_2 nanoparticles) was added and the mixture was stirred for 6 h at ambient temperature. PEI particles (100 wt% of the TiO_2 nanoparticles) were then added and the mixture was stirred at 70 °C for 2 h to give the nano-TiO_2 treatment solution.

3.2.3 Evaporation-induced surface modification of PBO fibers

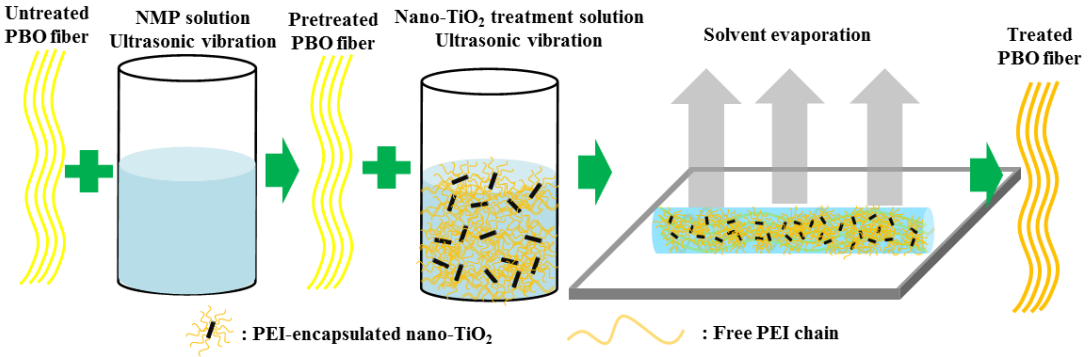

Fig. 3-1. Schematic illustration of evaporation-induced surface modification of poly(p-phenylene benzobisoxazole) (PBO) fibers.

The treated fibers were fabricated in several steps as illustrated in Fig. 3-1. A bundle of untreated PBO fibers (12 cm) was immersed in NMP and sonicated for 15 min, after which the fiber surface was well-infiltrated with the solvent. In addition, adsorption of NMP on the surface helped to transfer the solute from regions of high concentration to regions of low concentration in the subsequent treatment. Then, the infiltrated PBO fibers were placed into the nano-TiO_2 treatment solution, sonicated in an ice bath for different lengths of time (10, 20, and 30 min), and allowed to stand in the nano-TiO_2 treatment solution for 24 hours. Finally, the pretreated PBO fibers were placed on a Teflon plate in a fume hood at ambient temperature for 1 week to allow

evaporation of the solvent and yield the treated PBO fibers. The ultrasonic vibration time of samples in NMP solvent or Nano-TiO_2 treatment solution is shown in Table 3-1.

Table 3-1. Formulation of treated poly(p-phenylene benzobisoxazole) (PBO) fibers.

Sample	Ultrasonic vibration in NMP solvent/min	Ultrasonic vibration in Nano-TiO_2 treatment solution/min
PBO-10	15	10
PBO-20	15	20
PBO-30	15	30

3.2.4 Characterization

The surface morphologies of the fibers were examined using scanning electron microscopy (SEM, JSM-6010LA, JEOL, Japan) and field-emission scanning electron microscopy (FE-SEM) (S4800; Hitachi, Japan). Their surface chemical compositions were analyzed using energy-dispersive X-ray spectroscopy (EDS, JSM-6010LA, JEOL, Japan). The coating thickness was calculated through the observation of the fiber cross-section by transmission electron microscope (TEM, JEOL-2100F, Japan). Thermogravimetry (TG, Thermo plus TG-8120, Rigaku, Japan) was also measured. The surface roughness was analyzed using atomic force microscopy (AFM, SPA-400-AFM, Seiko, Japan). A single PBO fiber was fastened on a steel sample mount and a tapping mode was used to scan the fiber surface. Roughness analysis was performed on images obtained over 4×4 μm using the instrument software (SPIWin).

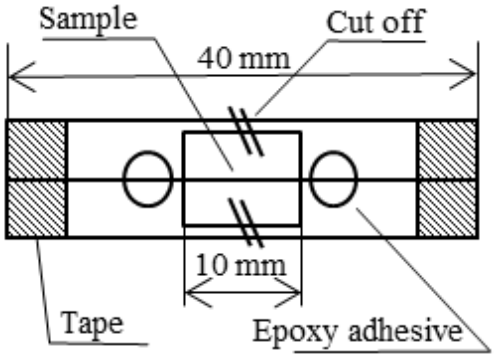

Fig. 3-2. Testing tab for single fiber tensile tests.

The samples were subjected to UV irradiation (365 nm) using a high-pressure mercury lamp (100 W, HLR100T-2, SEN Light Corp, Japan) under air-cooled conditions. The intensity of incident light (40 mW/cm^2) was measured using an ultraviolet radiometer UIT-201 (Ushio, Japan). A paper tab with an opening in the center (shown in Fig. 3-2) was used because the single fibers are very thin and smooth [22]. Single fiber tensile strength tests were carried out before and after UV irradiation using an EZ-SX 50N tensile tester (Shimadzu, Japan) with a strain rate of 1 mm/min at 20 °C and a relative humidity of 65%. For each sample, at least 35 specimens were tested.

3.3 Results and discussion

3.3.1 Surface morphology observation

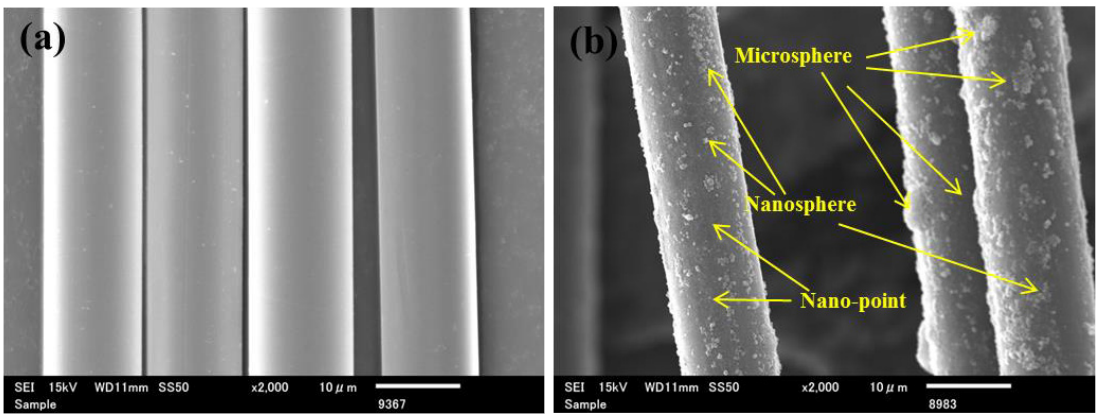

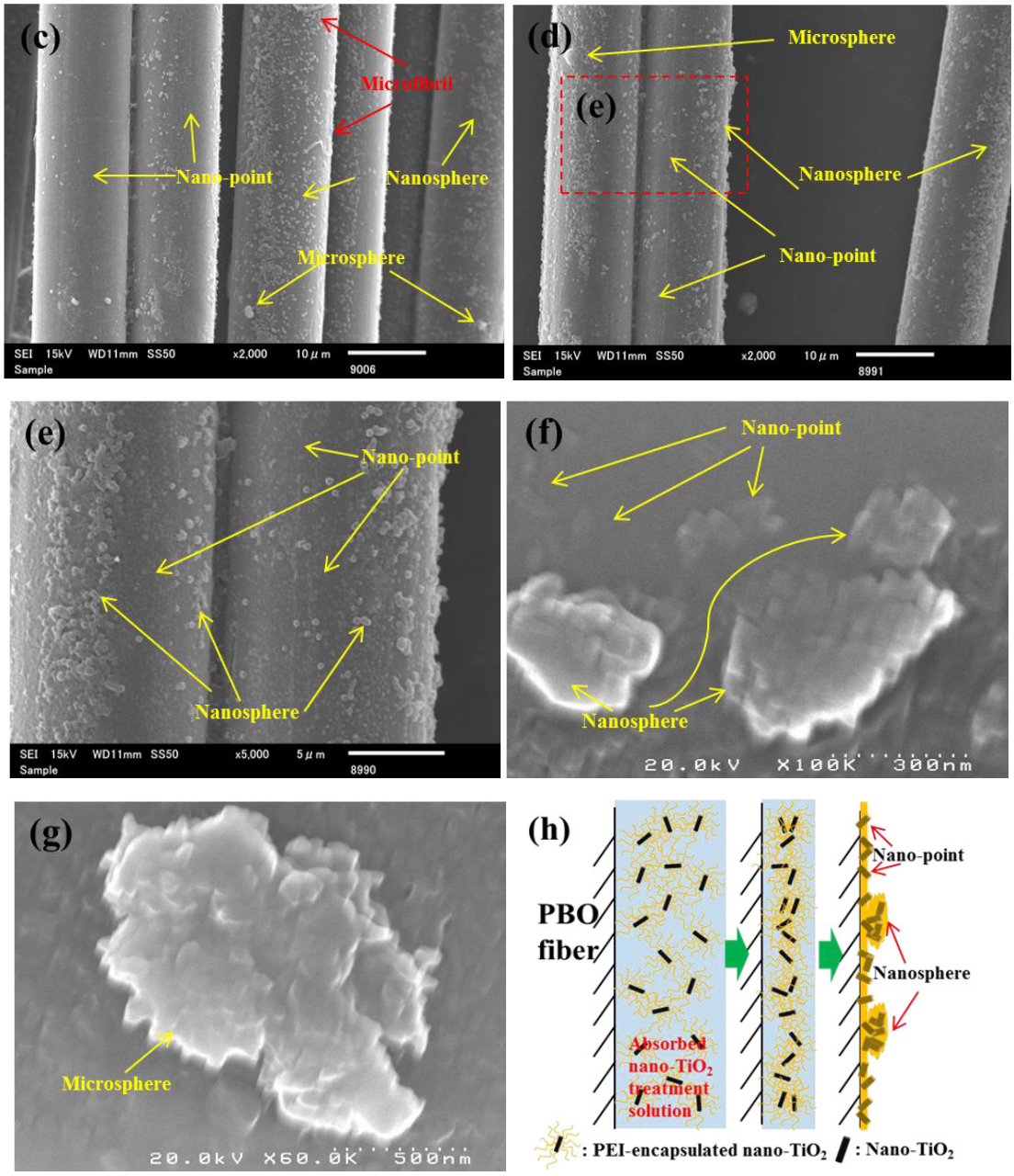

Fig. 3-3. Scanning electron micrographs of poly(p-phenylene benzobisoxazole) (PBO) fibers: (a) untreated; (b) PBO-10; (c) PBO-30; (d), (e) PBO-20 at different levels of magnification. Field-emission scanning electron micrographs of (f) nanospheres and nano-point; (g) a microsphere on PBO-20. (h) Schematic illustration of the nano-TiO_2 solvent evaporation process on the fiber surface.

The adhesion properties at the interface between the fiber and the resin were considerably affected by the fiber surface morphology [28]. The surface morphology was observed using SEM and FE-SEM, and the results are shown in Fig. 3-3. It is evident that the surfaces of the untreated PBO fibers are neat and smooth (Fig. 3-3a). Fig. 3-3b~e shows PBO fibers treated using the evaporation-induced surface modification method with different lengths of sonication in the nano-TiO_2 treatment solution. There are three kinds of dots with different sizes appeared on the surface of treated PBO fibers. These three kinds of dots are named “nano-point”, “nanosphere” and “microsphere” with size getting bigger which have been marked with words and arrows in the figures, respectively. As nano-TiO_2 is the most important component of UV absorption, the most important thing is to confirm whether “nano-point”, “nanosphere” and “microsphere” contain nano-TiO_2. So field-emission scanning electron microscopy (FE-SEM) was used to obtain higher magnification surface morphologies of the treated fibers. Fig. 3-3f~g shows some nano-points, and nanospheres and one microsphere on PBO-20 at different levels of magnification. As nano-TiO_2 used in this work were rodlike particles with Width 16 nm (provided by the company) and length 50-100 nm (confirmed by TEM, as shown in Fig. 3-6b). As shown in Fig. 3-3f, the flat edges of rodlike nano-particles can be seen obviously in both nano-points and nanospheres. We can confirm that the nanospheres are formed by the agglomeration of rodlike nano-particles which must be PEI-encapsulated nano-TiO_2 and the nano-points are some PEI-encapsulated nano-TiO_2 which were not agglomerate. Sharp edges still can be seen around the microsphere which must be nano-TiO_2 inside as shown in Fig. 3-3g. From Fig. 3-3f and Fig. 3-3g, it can be inferred that well dispersed PEI-encapsulated nano-TiO_2 formed nano-points, the initial agglomeration of

PEI-encapsulated nano-TiO_2 formed nanospheres, and seriously agglomerate formed microsphere.

As shown in Fig. 3-3b, as well as the uniformly distributed nano-points and nanospheres, there were many microspheres resulting from seriously agglomeration of PEI-encapsulated nano-TiO_2 after 10 min sonication in nano-TiO_2 treatment solution. After 30 min sonication, nano-points and nanospheres were both uniformly distributed on the fiber surface (Fig. 3-3c), but the PBO fiber cortex was damaged. Microfibrils could also be observed on the fiber surface (red arrows in Fig. 3-3c). Fig. 3-3d and 3-3e shows the PBO fiber after 20 min sonication in nano-TiO_2 treatment solution. As shown in Fig. 3-3e, besides uniformly distributed nano-points the fibers were covered with some nanospheres with an average diameter of 400 nm.

From these SEM images, we inferred the formation mechanism of the coating of nano-TiO_2, which is illustrated schematically in Fig. 3-3f. After two ultrasonic processes with appropriate length of time, the nanoparticles are more easily spread on the fiber surface and less agglomeration is observed. Then, in the subsequent impregnation process, more nanoparticles are adsorbed onto the fiber surface. Finally, evaporation of NMP in the solvent evaporation process induces well dispersed PEI-encapsulated nano-TiO_2 to form a uniform coating layer (also confirmed by TEM, as shown in Fig. 3-6) and agglomerated PEI-encapsulated nano-TiO_2 to form nanospheres or microspheres on the surface owing to the solution's surface tension.

3.3.2 Surface roughness

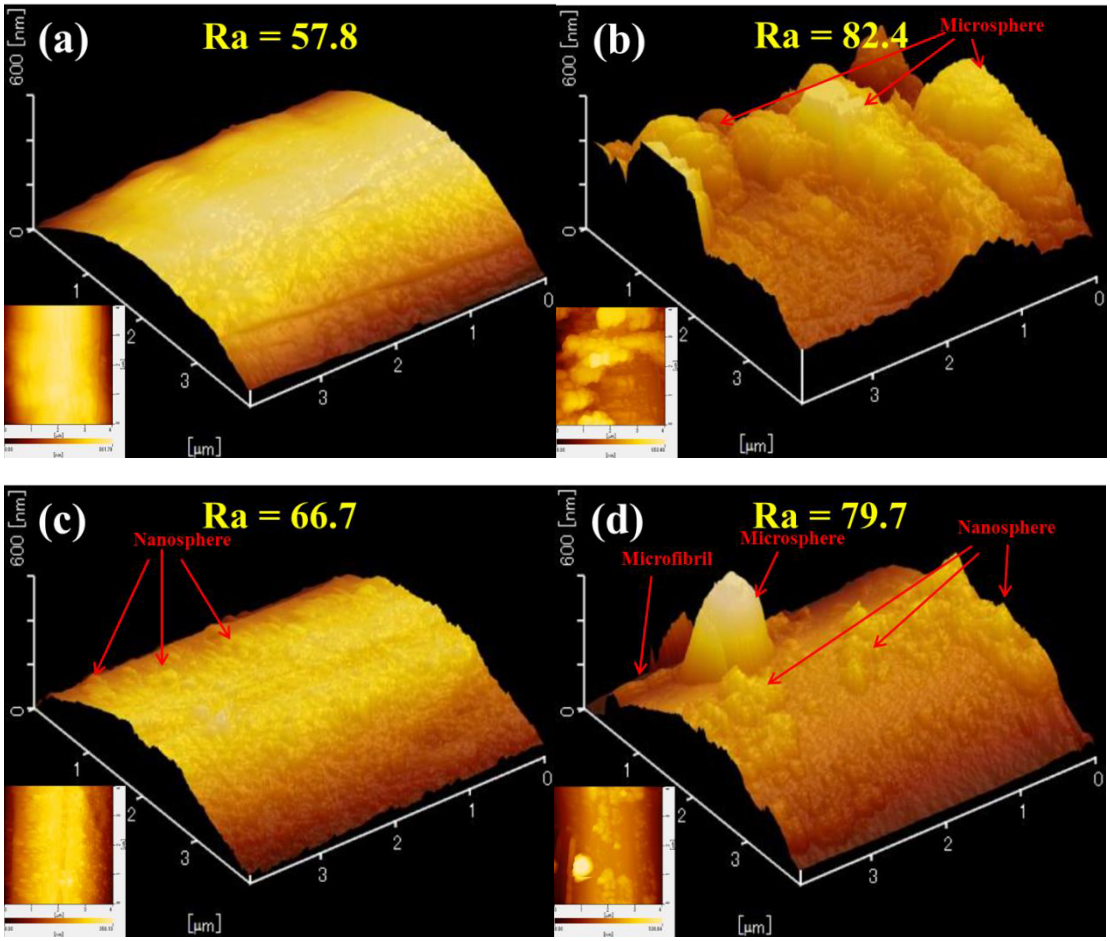

Fig. 3-4. Three-dimensional atomic force microscopy images of poly(p-phenylene benzobisoxazole) (PBO) fibers: (a) untreated; (b) PBO-10; (c) PBO-20; (d) PBO-30.

The surface roughness of reinforcement fibers considerably influences the interfacial adhesion properties between the fiber and matrix; a rougher surface provides more contact areas and mechanical interlocking [29]. When roughness is over a range of scales from microns to nanometers, which may strengthen the interface by redistributing the stress to dissipate bulk energy when the bond is stressed [30]. Furthermore, roughened fiber surfaces have a better wettability, which also contributes to their better

adhesion [31]. Fig. 3-4 presents three-dimensional AFM images of PBO fibers. The corresponding surface roughness data of different treated fibers is inserted in the figure, respectively.

The untreated PBO fibers had a relatively smooth surface (Ra = 57.8), as shown in Fig. 3-4a, but all treatments produced a rough surface. The sonication time in the nano-TiO_2 treatment solution had a clear effect on the surface morphology of the PBO fibers (Fig. 3-4b~d). When the fibers were sonicated for short time, the TiO_2 particles were not completely dispersed, and instead agglomerated to form many microspheres accumulated on the fiber surface as shown in Fig. 3-4b, which was also confirmed by SEM observation (Fig. 3-3b). So PBO-10 had the highest roughness (Ra = 82.4). It is clear from Fig. 3-4c that the coating of PBO-20 (20 min sonication) was uniformly adsorbed on the fiber surface (Ra = 66.7). Long sonication time (PBO-30) also led to some agglomeration, which is shown clearly in Fig. 3-4d. In addition, long sonication time damage to the fibers, which can be inferred from the appearance of microfibril on the fiber surface which is marked in Fig. 3-4d. So the roughness of PBO-30 was larger than that of PBO-20. The AFM test results are consistent with the SEM/FE-SEM observations.

3.3.3 EDS analysis

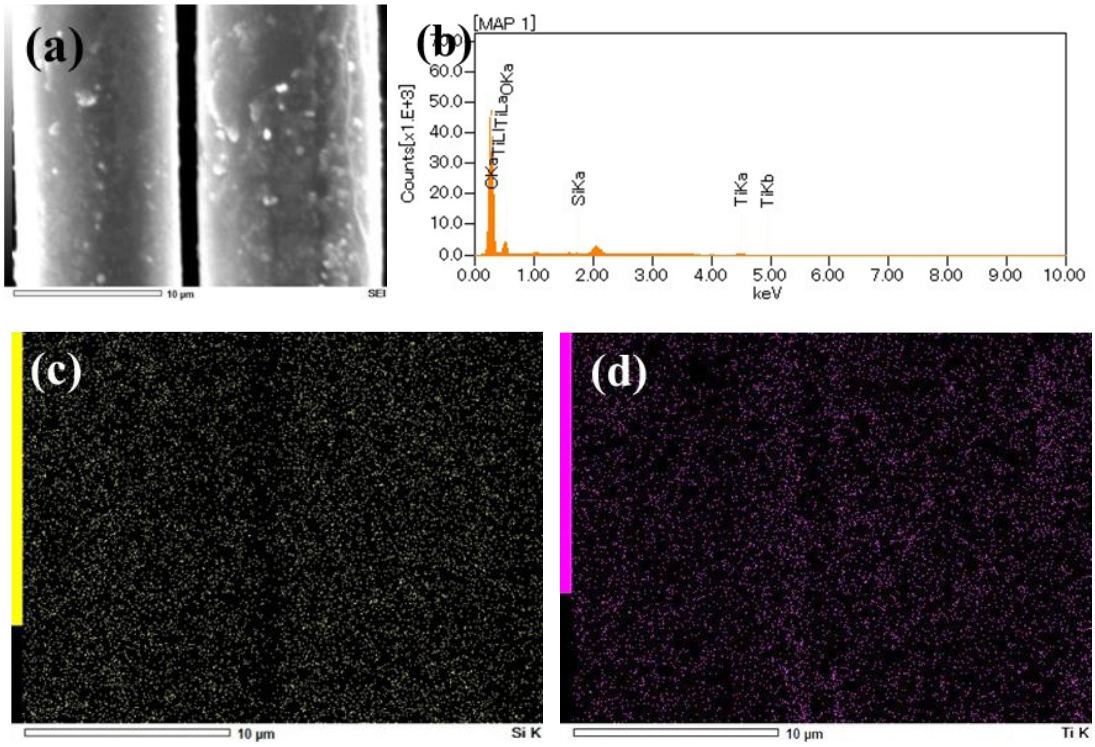

Fig. 3-5. Energy-dispersive X-ray spectroscopy of the PBO-20 surface: (a) analysis area; (b) element counts; (c) surface distribution of Si; (d) surface distribution of Ti.

Fig. 3-5a~d shows the EDS analysis of the PBO-20 surface; in addition to C and O as shown in Fig. 3-5b, we also observed the elements Si and Ti. Fig. 3-5c and 3-5d show element distribution analysis diagrams for Si and Ti, respectively. The Si derives from the γ-MPS that was used to react with the hydroxyl groups on the nano-TiO_2 particle surface (see section 3.2.2), and the Ti comes from the nano-TiO_2 particles. Thus, both Si and Ti derive from the modified nano-TiO_2 particles. These element distribution analysis diagrams indicate that the modified nano-TiO_2 particles are uniformly absorbed on the PBO surface. The elements observed in the EDS analysis and their corresponding amounts are listed in Table 3-2; Because of the high C and O content in PBO fibers and

PEI, and little amount of nano-TiO_2 adsorption which was calculated by TG analysis, compared with C and O, the content of Si and Ti on the treated PBO-20 surface is very low.

Table 3-2. Elements observed on the treated PBO-20 surface and their corresponding amounts.

Elements	Weight (%)	Atom (%)
C	80.42	84.91
O	18.72	14.84
Si	0.12	0.06
Ti	0.74	0.20
Total	100.00	100.00

3.3.4. TEM observation

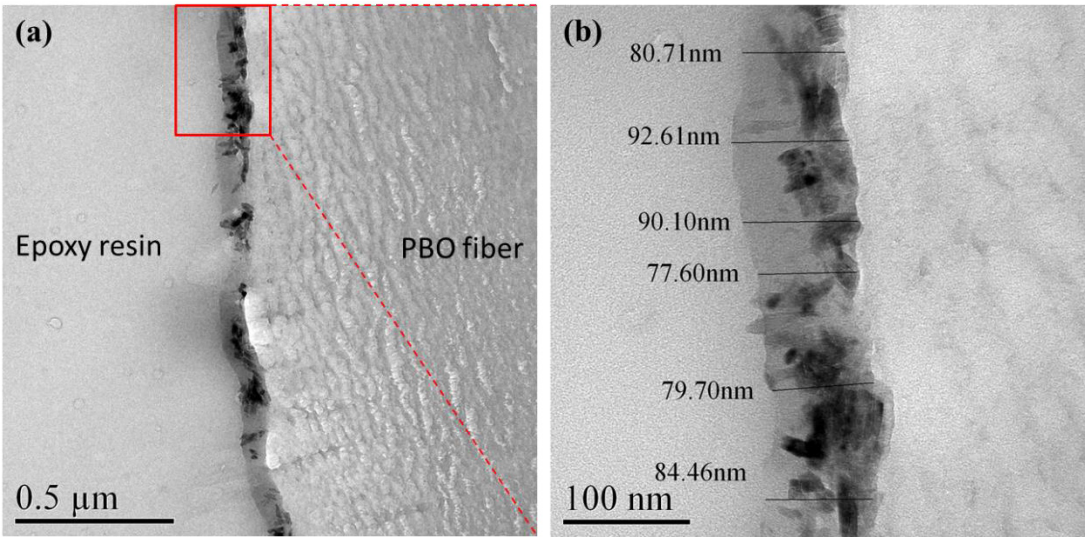

Fig. 3-6. Transmission electron microscope micrographs of the fiber cross-section (PBO-20) at different levels of magnification: (a) ×10K, (b) ×40K.

For clear observation of the fiber cross-section, a single fiber (PBO-20) was embedded into epoxy resin, and then a 120 nm film was cut perpendicular to the fiber

axis after the epoxy resin was cured, finally the resulting specimens were observed by TEM. A uniform layer (average thickness of 84.20 nm) with nanoparticles between epoxy resin and PBO fiber can be obviously seen in Fig. 3-6a. And the thickness of the layer was marked in Fig. 3-6b at a higher magnification. It can be clearly seen from TEM micrographs that the fiber surface was uniformly covered by a coating layer with nanoparticles. And the nanoparticles were uniformly distributed in the coating layer without serious agglomerations.

3.3.5 TG analysis

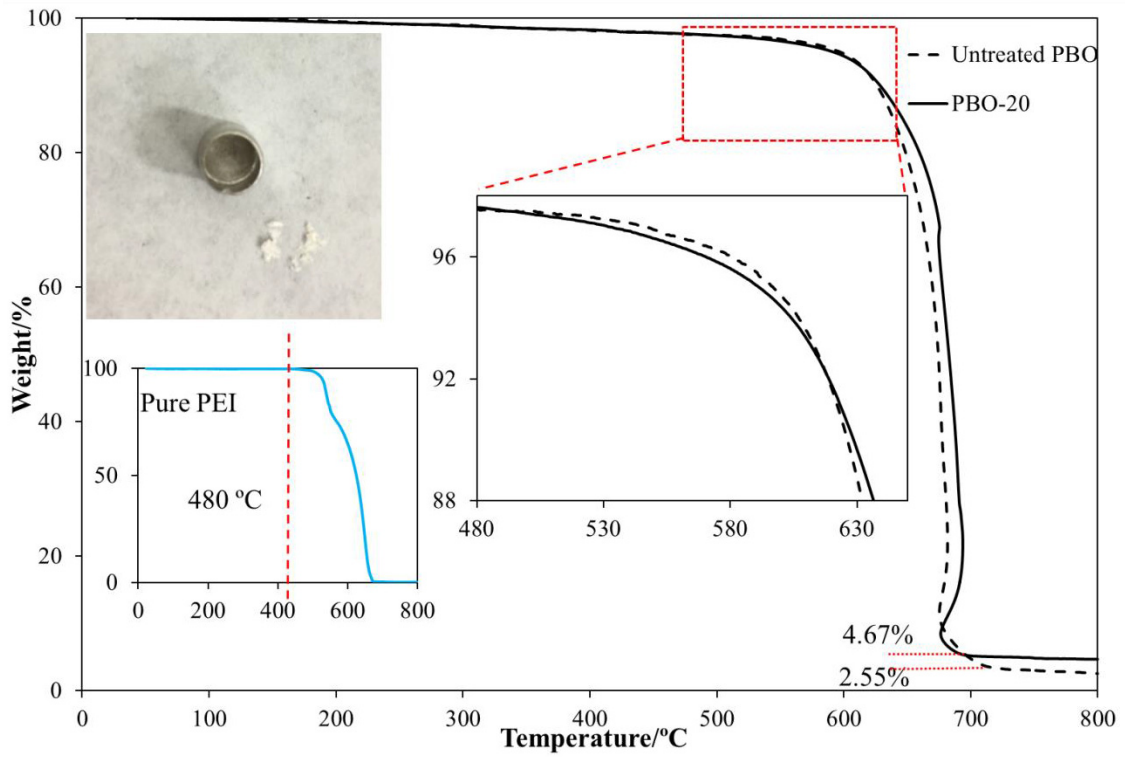

Fig. 3-7. Thermogravimetric curves of poly(p-phenylene benzobisoxazole) (PBO) fibers: (a) untreated; (b) PBO-20.

The thermal stability of the untreated and treated PBO fibers was studied by TG, as depicted in Fig. 3-7 all samples exhibited excellent thermal stability. For the untreated

PBO fibers, the weight loss before 300 °C corresponds to the elimination of water and residual solvent, and the dramatic weight loss between 600 and 800 °C was due to the decomposition of the PBO fibers [2]. Compared with the untreated PBO fibers, PBO-20 showed a little more weight loss from 500 to 600 °C, as shown in the enlarged drawing of the TG curve. This is due to the decomposition of PEI, which is a component of the surface coating on the PBO-20 fiber surface. For comparison, the TG curve of pure PEI is shown in the lower left-hand corner of Fig. 3-7. However, after 600 °C, the curve of the untreated PBO fibers dropped faster than that of PBO-20 until the curve become flat. This is a consequence of the coating of inorganic nanoparticles on the fiber surface, which improved the thermal stability. The residual mass fractions of the untreated PBO fibers and PBO-20 were 2.55% and 4.67%, respectively. Neglecting the thermal decomposition products of γ-MPS, we deduced that the maximum mass fraction of TiO_2 nanoparticles on the PBO-20 fiber surface was about 2.12%. As expected, a white residue of TiO_2 was observed after the decomposition of PBO-20 was complete (photograph in the upper left-hand corner of Fig. 3-7).

3.3.6 Mechanical properties

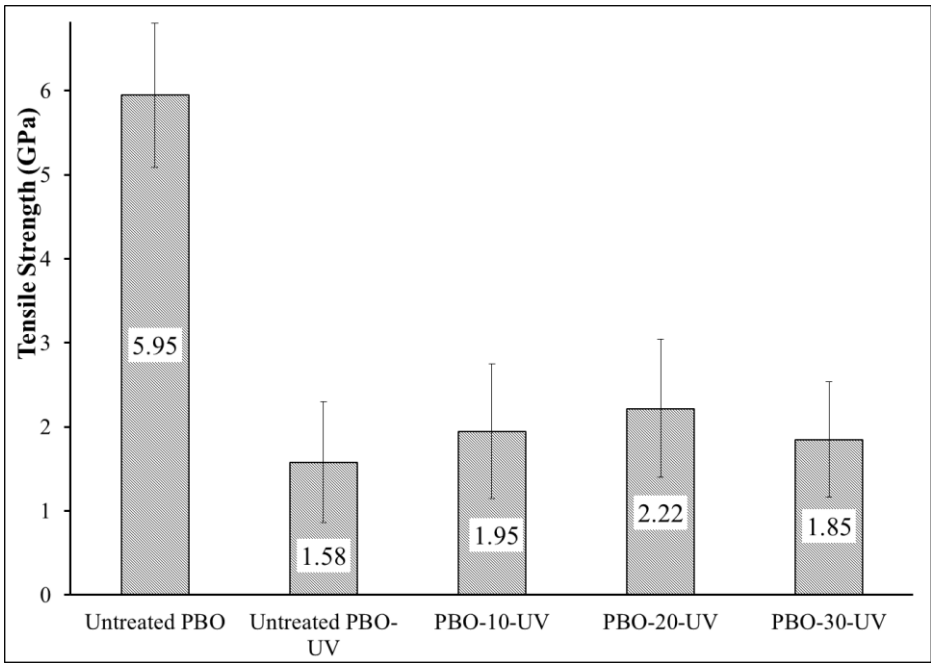

Fig. 3-8. Single fiber tensile strength of poly(p-phenylene benzobisoxazole) (PBO) fibers after UV irradiation.

The single fiber tensile strengths of PBO fibers after UV irradiation are presented in Fig. 3-8. The tensile strength of the untreated PBO fiber was 5.95 GPa. After UV irradiation (40 mW/cm^2) for about 30 h, the tensile strength of the PBO samples was clearly reduced, as shown in Fig. 3-8. The tensile strength of the untreated PBO fibers decreased to 1.58 GPa, only 26.6% of the original strength. The tensile strength of the treated PBO fibers also decreased, but owing to the uniform coating layer of nano-TiO_2 particles, which exhibit good absorption and scattering of UV light, the decrease was smaller than that observed for the untreated PBO fibers. The tensile strength of PBO-20 after 30 h UV irradiation was 2.22 GPa, which is 37.3% of the untreated PBO fiber. Due to agglomeration of nano-TiO_2 particles, the tensile strength of PBO-10 after 30 h UV irradiation was 1.95 GPa, which is 32.8% of the untreated PBO fiber. In addition, the

sample with the longer sonication process (PBO-30) had a tensile strength of 1.85 GPa after 30 h UV irradiation, which is just 31.1% of the untreated PBO fibers. That is because long sonication times resulted in the loss of parts of the coating and damage to the fibers, which was confirmed by SEM and AFM analysis.

3.4 Conclusions

In summary, besides some nanospheres resulted from the initial agglomeration of PEI-encapsulated nano-TiO_2, a uniform coating layer with nano-TiO_2 particles was adsorbed on PBO fiber surfaces using evaporation-induced surface modification method. TEM micrographs indicated that the fiber (PBO-20) surface was uniformly covered with a coating layer with nanoparticles. SEM, AFM, and EDS analysis showed that the nano-TiO_2 particles were uniformly distributed on the fiber (PBO-20) surface. And the roughness of the treated PBO fiber surface increased. In addition, the single fiber tensile strength of the treated PBO fibers increased after UV irradiation.

References

[1] L. Chen, Y.Z. Du, Y.D. Huang, P.F. Ng, B. Fei, Facile fabrication of hierarchically structured PBO-$Ni(OH)_2$/NiOOH fibers for enhancing interfacial strength in PBO fiber/epoxy resin composites, Compos. Sci. Technol. 129 (2016) 86-92.

[2] L. Chen, Y.Z. Du, Y.D. Huang, F. Wu, H.M. Cheng, B. Fei, J.H. Xin, Hierarchical poly(p-phenylene benzobisoxazole)/graphene oxide reinforcement with multifunctional and biomimic middle layer, Compos. A. 88 (2016) 123-130.

[3] T. Zhang, D.Y. Hu, J.H. Jin, S.L. Yang, G. Li, J.M. Jiang, XPS study of PBO fiber surface modified by incorporation of hydroxyl polar groups in main chains, Appl. Surf. Sci. 256 (2010) 2073-2075.

[4] M. J. Jian, J. Z. Hui, L. Guang, J. H. Jin, L. Y. Sheng, Poly(P-phenylene benzoxazole) fibre chemically modified by the incorporation of sulfonate groups, J. Appl. Polym. Sci. 109 (2008) 3133.

[5] J.L. Wang, G.Z. Liang, W. Zhao, Z.P. Zhang, Enzymatic surface modification of PBO fibres, Surf Coat Technol. 201 (8) (2007) 4800-4804.

[6] G. Wu, Y. Shyng, Effects of basic chemical surface treatment on PBO and PBO fiber reinforced epoxy composites, J. Polym. Res. 12 (2005) 93-102.

[7] K. Tamargo-Martíneza, A. Martínez-Alonsoa, M. Graciab, J.I. Paredesa, J.M.D. Tascóna, M.A. Montes-Morán, Tailoring of the interfacial properties of polymeric single fibre-reinforced epoxy composites by non-oxidative plasma treatments, Compos. A. 50 (2013) 102-109.

[8] C.S. Zhang, P. Chen, D. Liu, B.C. Wang, W. Li, X.T. Kang, Aging behavior of PBO fibers and PBO-fiber-reinforced PPESK composite after oxygen plasma treatment, Surf. Interface Anal. 41 (2008) 187-192.

[9] Q. Wang, P. Chen, C.X. Jia, M.X. Chen, B. Li, Improvement of PBO fiber surface and PBO/PPESK composite interface properties with air DBD plasma treatment, Surf. Interface Anal. 44 (2012) 548-553.

[10] F. Guo, Z.Z. Zhang, H.J. Zhang, W.M. Liu, Effect of air plasma treatment on mechanical and tribological properties of PBO fabric composites, Compos. A. 40 (2009) 1305-1310.

[11] C.S. Zhang, C.Y. Li, B.Y. Wang, B. Wang, H. Cui, Effects of atmospheric air plasma treatment on interfacial propertiesof PBO fiber reinforced composites, Appl. Surf. Sci. 276 (2013) 190-197.

[12] P. Chen, C. Zhang, X. Zhang, B. Wang, W. Li, Q. Lei, Effects of oxygen plasma

treatment power on surface properties of poly(p-phenylene benzobisoxazole) fibers, Appl. Surf. Sci. 255 (2008) 3153-3158.

[13] R.Y. Zhang, X.L. Pan, M.W. Jiang, S.J. Peng, Y.P. Qiu, Influence of atmospheric pressure plasma treatment on surface properties of PBO fiber, Appl. Surf. Sci. 261 (2012) 147-154.

[14] J.W. Gu, T. Bai, J. Dang, J.J. Feng, Q.Y. Zhang, Surface functionalization of HMPBO fibers with MSA/KH550/GlycidylEthyl POSS and improved interfacial adhesion, Polym Compos. 35 (2014) 611-616.

[15] J.W. Gu, J. Dang, W.C Geng, Q.Y Zhang, Surface Modification of HMPBO Fibers by Silane Coupling Agent of KH-560 treatment assisted by ultrasonic vibration, Fiber. Polym. 13 (2012) 979-984.

[16] C.H. Zhang, W.J. Yuan, S.G. Wang, X.F. Liang, Effect of MWCNTs irradiation grafting treatment on the surface properties of PBO fiber, J Appl Polym Sci. 121 (2011) 3455-3459.

[17] C. Zhang, H. Xu, Z. Jiang, F. Zhu, Y. Huang, Carbon nanotubes grafting PBO fiber: a study on the interfacial properties of epoxy composites, Polym. Composite. 33 (2012) 927-932.

[18] J. Qian, J. Wu, X. Liu, Q. Zhuang, Z. Han, Improvement of interfacial shear strengths of polybenzobisoxazole fiber/epoxy resin composite by n-TiO_2 coating, J Appl Polym Sci. 127 (2013) 2990-2995.

[19] L. Chen, F. Wei, L. Liu, W. Cheng, Z. Hu, G. Wu, et al, Grafting of silane and graphene oxide onto PBO fibers: multifunctional interphase for fiber/polymer matrix composites with simultaneously improved interfacial and atomic oxygen resistant properties, Compos Sci Technol. 106 (2015) 32-38.

[20] C.H. Zhang, Y.D. Huang, W.J. Yuan, J.N. Zhang, UV aging resistance properties of PBO fiber coated with nano-ZnO hybrid sizing, J. Appl. Polym. Sci. 120 (2011) 2468-2476.

[21] B. Song, L. Meng, Y. Huang, Preparation and characterization of $(POSS/TiO_2)_n$ multi-coatings based on PBO fiber surface for improvement of UV resistance, Fiber. Polym. 14 (2013) 375-381.

[22] Horikawa, N., et al, Tensile fracture behavior of UV light irradiated PBO fiber, J. Solid Mech. Mater. Eng. 3 (2009) 1-9.

[23] B. Song, Q. Fu, L.H. Ying, X.Y. Liu, Q.X. Zhuang, Z.W. Han, Study on photo aging of poly(p-phenylene benzobisoxazole) fibre, J Appl Polym Sci. 124 (2012) 1050-1058.

[24] B. Song, Q.X. Zhuang, L.H. Ying, X.Y. Liu, Z.W. Han, Photostabilisation of poly(p-phenylenebenzobisoxazole) fibre, Polym Degrad Stabil. 97 (2012) 1569-1576.

[25] J. Bahadur, D. Sen, S. Mazumder, B. Paul, A. Khan, G. Ghosh, Evaporation-induced self assembly of nanoparticles in non-buckling regime: volume fraction dependent packing, J Colloid Interface Sci. 351 (2010) 357-364.

[26] H.S. Ki, J.H. Yeum, S.J. Choe, J.H. Kim, I.W. Cheong, Fabrication of transparent conductive carbon nanotubes/polyurethane-urea composite films by solvent evaporation-induced self-assembly (EISA), Compos Sci Technol. 69 (2009) 645-650.

[27] J.R. Lee, J.H. Won, J.H. Kim, K.J. Kim, S.Y. Lee, Evaporation-induced self-assembled silica colloidal particle-assisted nanoporous structural evolution of poly(ethylene terephthalate) nonwoven composite separators for high-safety/high-rate lithium-ion batteries, J. Power Sources. 216 (2012) 42-47.

[28] X.Y. Zhang, P. Chen, D.B. Han, Q. Yu, Z.F. Ding, X.L. Zhu, Effect of

thermoplastic coating on interfacial adhesion of oxygen-plasma-pretreated PBO/PPESK composites, Appl. Surf. Sci. 266 (2013) 110-117.

[29] Z. Liu, P. Chen, X. Zhang, Q. Yu, K. Ma, Z. Ding, Effects of surface modification by atmospheric oxygen dielectric barrier discharge plasma on PBO fibers and its composites, Appl. Surf. Sci. 283 (2013) 38-45.

[30] D. Liu, P. Chen, J.J. Mu, Q. Yu, C. Lu, Improvement and mechanism of interfacial adhesion in PBO fiber/bismaleimide composite by oxygen plasma treatment, Appl. Surf. Sci. 257 (2011) 6935-6940.

[31] D. Liu, P. Chen, Q. Yu, K.M. Ma, Z.F. Ding, Improved mechanical performance of PBO fiber-reinforcedbismaleimide composite using mixed O_2/Ar plasma, Appl. Surf. Sci. 305 (2014) 630-637.

CHAPTER FOUR

Preparation of a sub-100-nm-thick polyetherimide coating layer with nano-TiO_2 particles on poly(p-phenylene benzobisoxazole) fibers surface

Chapter 4: Preparation of a sub-100-nm-thick polyetherimide coating layer with nano-TiO_2 particles on poly(p-phenylene benzobisoxazole) fibers surface

4.1 Introduction

Poly(p-phenylene benzobisoxazole) (PBO) fibers were developed by the US Air Force and commercialized by Toyobo as Zylon [1]. The company commercially produces two types of PBO fibers; standard type AS and high modulus type HM [2]. As a new structural material, PBO fibers have low density, high strength, high modulus (HM), good chemical resistance, and good thermal stability [3-9]. Because of these favorable features, PBO fibers have great potential applications such as fiber reinforced composites [10-12], tendons for scientific balloon, high strength tethers, tension structures, and body armor [4,13-16].

However, PBO fibers have a critical problem like photodegradation under UV exposure, which can deteriorate structures and properties of PBO fiber and corresponding products [17]. According to the report provided by Toyobo, both AS and HM PBO fibers lost 65 % of their strength after 6 months exposure at Ohtsu, Japan, or after 500 h exposure in a Xenon light weatherometer [14, 18]. Therefore, measures of protecting PBO fibers from UV effects are needed.

To overcome such an undesired characteristic, some researches have been undertaken to protect high performance fibers form UV light [19-21]. Jin et al. prepared a photoaging-resistant PBO fiber containing a light stabilizer (OB-1) by in situ polymerization and dry-jet wet-spinning [14]. Won et al. used low density polyethylene

loaded with different content of TiO_2 and white pigment as protective film for high performance fibers from UV light [13]. Song et al. prepared a (polyhedral oligomeric silsesquioxane/TiO_2)$_n$ multi-coating on PBO fibers via layer-by-layer assembly [22]. They also added UV absorbers to PBO fiber surfaces by coordination bond formation and physical adsorption [23]. Zhang et al. focused on the UV shielding efficiency of PBO fibers with a ZnO nanoparticle/epoxy hybrid coating [16].

In this work, Rutile titanium dioxide (TiO_2) was chose as the UV absorber to protect PBO from UV light. Rutile titanium dioxide (TiO_2) with outstanding optical properties, such as absorption of UV light, transparency at the visible wavelength ranges and high refraction index (2.6-2.9) is one of the most important inorganic UV absorbers [22]. Development of nanotechnology endows rutile TiO_2 nanoparticles with larger specific surface area, higher surface energy and activity, and more efficient UV adsorption.

Polyetherimide (PEI) is a high performance polymer material, has many excellent properties, such as good mechanical behaviors (high specific strength), heat and radiation resistance, and hydrolytic stability [24-26]. So in our previous study [27], nano-TiO_2 particles were modified with 3-methacryloxypropyltrimethoxysilane (γ-MPS) and polyetherimide (PEI) in *N*-methyl-2-pyrrolidone (NMP) using an anchoring grafting method. γ-MPS was hydrolyzed by water that had absorbed to the surface of the TiO_2 nanoparticles, which would lead to hydrogen bonding between the silanols and the TiO_2 nanoparticles. And the PEI chains were not chemically bonded to theγ-MPS modified TiO_2 nanoparticles but absorbed by the Van der Waals force, which acted to anchor the PEI chains to the γ-MPS modified TiO_2 nanoparticles. The suspension of treated nano-TiO_2 obtained using this method has excellent dispersion stability.

Therefore, the suspension with nano-TiO_2 particles modified with γ-MPS and PEI using an anchoring grafting method was selected as the treatment suspension in this work. After evaporation of the suspension of PEI encapsulated nano-TiO_2 particles absorbed around the fiber surface, a coating layer with nano-TiO_2 particles was physical adsorbed on PBO fibers. The effects of this evaporation-induced surface modification on the structure and properties of PBO fibers were studied. X-ray photoelectron spectroscopy, transmission electron microscope and thermogravimetric analysis were used to confirm the presence, distribution, and content of nano-TiO_2 particles. And the single-filament tensile strength of the PBO fibers before and after UV irradiation was also measured.

4.2 Experimental

4.2.1 Materials

TiO_2 nanoparticles (STR-100N, TiO_2 content: >95%, crystal structure: rutile 100%) with an average particle size of 16 nm and specific surface area of 100 m^2/g were supplied by Sakai Chemical Industry, Japan. PEI was purchased from Sigma-Aldrich, USA; γ-MPS (98%) from Acros Organics, USA; and NMP from Kanto, Japan. PBO fibers (HM 664-H12RD, diameter: 11 μm) with a filament tensile strength of 5.95 GPa were purchased from Toyobo, Japan. The pristine PBO fibers were washed with acetone for 48 h at ambient temperature to remove surface sizing agents and/or contaminants. The obtained fibers are denoted as untreated PBO fibers.

4.2.2 Preparation of the nano-TiO_2 treatment suspension

The nano-TiO_2 treatment suspension was prepared from TiO_2 nanoparticles in NMP. After sonication in an ice bath for 25 min, γ-MPS was added and the mixture was stirred using a magnetic stirring heater (300 r/min) for 6 h at ambient temperature. PEI

particles were then added and the mixture was stirred using a magnetic stirring heater (300 r/min) at 70 °C for 2 h to give the nano-TiO_2 treatment suspension. The experimental condition of 2 h was derived from a large number of experiments. Under this condition, the dispersion stability of nano-TiO_2 suspension was the best as shown in our previous study [27]. Although PEI was not completely dissolved, the upper liquid was used as the treatment suspension. The contents of the different compositions in each treatment suspension are shown in Table 4-1.

Table 4-1. Compositions of fiber treatment suspensions.

Sample	TiO_2 (wt.%)	PEI (wt.%)	γ-MPS (wt.%)	NMP(mL)
I-a	-	-	-	-
I-b	0.1	-	-	100
I-c	0.02	0.1	0.1	100
I-d	0.1	0.1	0.1	100
I-e	0.5	0.1	0.1	100
I-f	0.1	0.02	0.1	100
I-g	0.1	0.05	0.1	100
I-h	0.1	0.2	0.1	100
I-i	0.1	0.5	0.1	100
II-a	0.05	0.05	0.05	100
II-b	0.25	0.25	0.25	100
II-c	0.5	0.5	0.5	100
III-a	0	0.1	0	100

4.2.3 Evaporation-induced surface modification of PBO fibers

Treated PBO fibers were fabricated in several steps as follows: A bundle of untreated PBO fibers was immersed in NMP for 15 min. Then, the NMP-infiltrated PBO fibers were placed in the nano-TiO_2 treatment suspension, which was sonicated in an ice bath for 20 min and then allowed to stand for 24 h. Finally, the pretreated PBO

fibers were placed on a Teflon plate in a fume hood at ambient temperature for one week to allow the solvent to evaporate and provide the treated fibers. This process is shown schematically in Fig. 4-1.

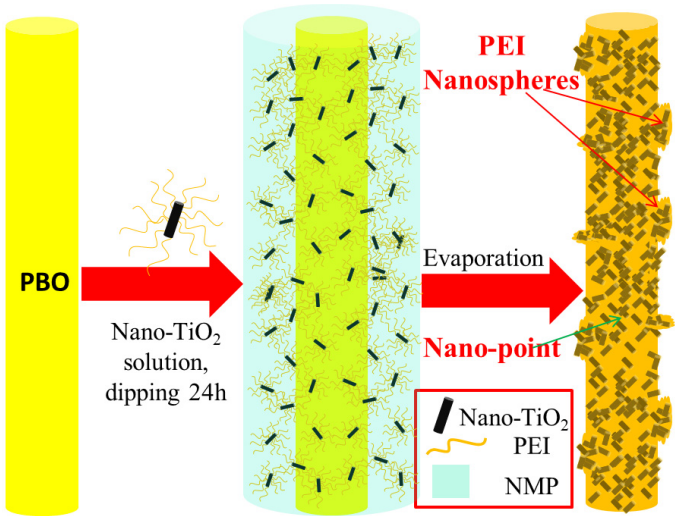

Fig. 4-1. Schematic illustration of preparation of a sub-100-nm-thick coating layer on PBO fibers.

4.2.4 Characterization

The surface morphologies of the fibers were examined using scanning electron microscopy (SEM; JSM-6010LA, JEOL, Japan), and their surface chemical compositions were probed by X-ray photoelectron spectroscopy (XPS; AXIS-ULTRA, Kratos, Japan). Binding energies were referenced to the C 1s peak of adventitious carbon at 284.3 eV. The coating layer was investigated through the observation of the treated fiber cross section by a transmission electron microscope (TEM, JEOL-2100F, Japan). Thermogravimetric analysis (TGA) was conducted on a simultaneous thermal analyzer (Thermo plus TG-8120, Rigaku, Japan). The sample was placed in a platinum crucible and the weight of each sample was controlled at 3-6 mg. The temperature was

increased from ambient temperature to 800 °C under an air atmosphere (0.2L/min) at a heating rate of 10 °C/min.

The samples were subjected to UV irradiation (365 nm) from a high-pressure mercury lamp (100 W, HLR100T-2, SEN Light Corp, Japan) for 30 h under air-cooled conditions. The intensity of incident light (40 mW/cm^2) was measured using a UV radiometer (UIT-201, Ushio, Japan). A paper tab with an opening in the center (10×10 mm) and epoxy adhesive were used because a single fiber is very thin and smooth [3]. Single-fiber tensile strength tests were carried out after UV irradiation using a tensile tester (EZ-SX, Shimadzu, Japan) with a strain rate of 1 mm/min at 20 °C and a relative humidity of 65% referring to JIS R 7606:2000. A 5 N load sensor was used to measure the loads. The gauge length was fixed to 25 mm. The tensile strength was calculated using eq. (1).

$$\sigma_f = \frac{4F_f}{\pi {d_f}^2} \times 10^{-9} \qquad (1)$$

where σ_f was the single fiber tensile strength (MPa), F_f was the maximum tensile load (N), d_f was the diameter of single fiber (μm). The value of test was more than 35 successful measurements.

The adhesive durability of the modified components was evaluated using an ultrasonic exposure test, which was carried out in water for 30 min with an ultrasonicator (300 W, 38 kHz, US-106, SND Co., Ltd, Japan)

4.3 Results and discussion

4.3.1 XPS analysis of the fiber surface

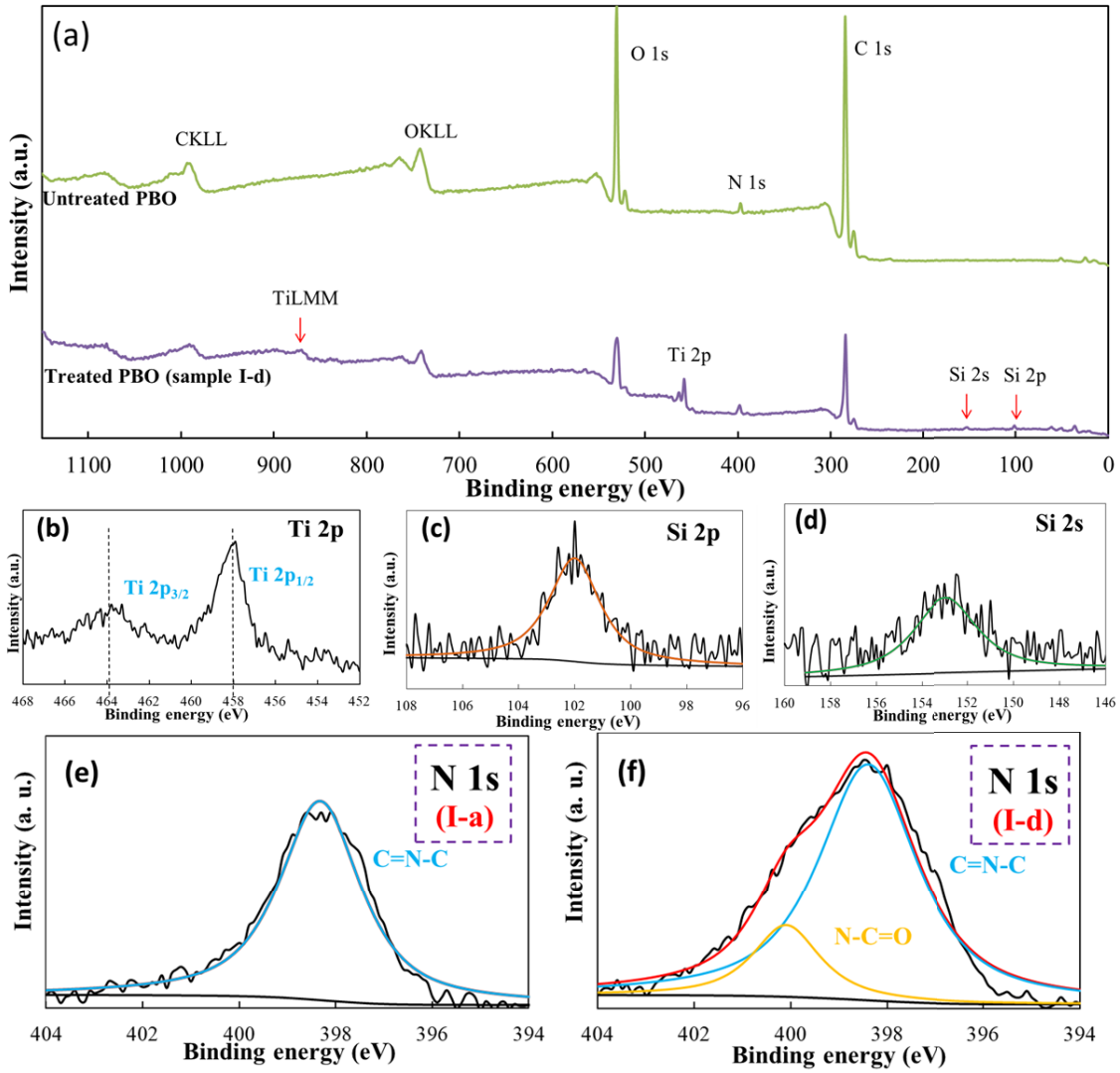

Fig. 4-2. (a) Survey XPS curves for untreated and treated PBO fibers; (b) Ti 2p spectra for treated PBO fibers (sample I-d); (c) Si 2p spectra for sample I-d; (d) Si 2s spectra for sample I-d; N 1s spectra for (e) untreated PBO fibers (sample I-a) and (f) sample I-d.

The surfaces of treated PBO fibers and untreated PBO fibers were investigated by XPS. Wide-scan spectra of sample I-d, which possessed a favorable surface coating, and

untreated PBO fibers in the binding energy range of 0-1150 eV were obtained to identify the surface elements and conduct a quantitative analysis, as shown in Fig. 4-2a. Both spectra contained were C 1s, O 1s, and weak N 1s peaks. There were many remarkable differences between the spectra of the untreated and treated PBO fibers. The surface chemical elements of the untreated PBO fibers were only oxygen, nitrogen, and carbon. In contrast, the spectrum of the treated PBO fiber contained some new distinctive peaks. Peaks appeared at 458.0 and 464.0 eV as shown in Fig. 4-2b corresponding to Ti $2p_{1/2}$ and Ti $2p_{3/2}$, respectively, suggesting that nano-TiO_2 particles were successfully dispersed on the fiber surface [28, 29]. In addition, peaks at 102.0 eV (Fig. 4-2c)and 152.5 eV (Fig. 4-2d) corresponding to Si 2p and Si 2s, respectively, appeared, consistent with the presence of γ-MPS [30-32].

The N 1s peak positions were derived from peak deconvolution. The untreated PBO fiber displayed only one C=N-C peak at 398.6 eV, as shown in Fig. 4-2e [33-35]. After surface modification, a new peak at 400.1 eV ascribed to N-C=O of PEI appeared as illustrated in Fig. 4-2f [36]. This confirmed the presence of PEI on the surface of sample I-d.

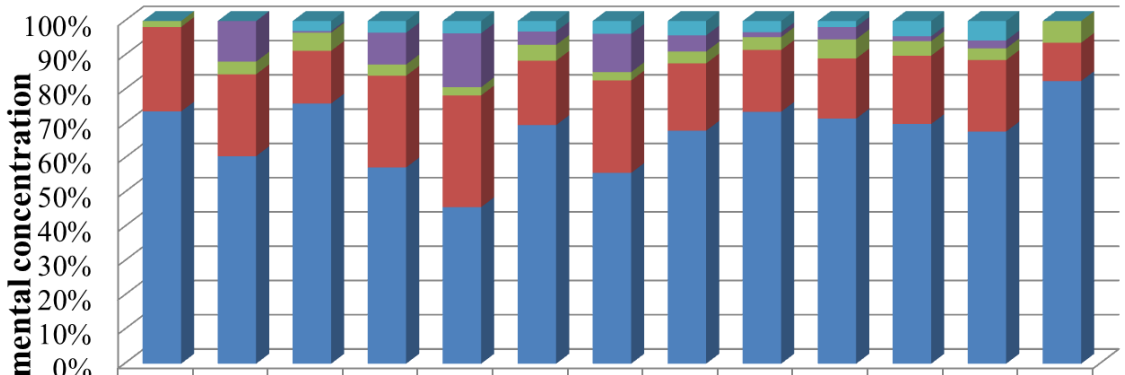

	I-a	I-b	I-c	I-d	I-e	I-f	I-g	I-h	I-i	II-a	II-b	II-c	III-a
Si	0	0	2.95	3.4	3.56	3.05	3.75	4.21	3.28	1.75	4.46	5.68	0
Ti	0	11.86	0.44	9.28	15.75	3.9	11.15	4.7	1.39	3.58	1.41	2.32	0
N	1.73	3.69	5.31	3.3	2.39	4.65	2.47	3.46	3.78	5.61	4.24	3.39	6.34
O	24.66	23.88	15.36	26.75	32.61	18.77	26.95	19.65	18.02	17.53	19.95	20.89	11.17
C	73.62	60.57	75.94	57.27	45.69	69.64	55.69	67.99	73.53	71.54	69.95	67.81	82.49

Fig. 4-3. Surface elemental compositions of untreated and treated PBO fibers.

Fig. 4-3 presents the surface elemental compositions of untreated and treated PBO fibers. Comparing the data of sample I-a and I-b, it can be seen that the appearance of nano-TiO_2 on fiber surface leaded to an increase in the Ti content from 0 to11.86%. The increase of N and C content and the decrease of O content were found from the data contrast between I-a and III-a, which was caused by the PEI coating on the PBO surface.

When PBO fibers treated with suspensions in which the contents of PEI and γ-MPS were fixed at 0.1 wt.%, and the contents of nano-TiO_2 were 0.02, 0.1, and 0.5 wt.% (I-c, I-d and I-e), respectively, the Ti content was increased from 0.44% to 15.75% as confirmed in the XPS analysis on these three samples.

When PBO fibers treated with suspensions in which the contents of nano-TiO_2 and γ-MPS were fixed at 0.1 wt.%, and the contents of PEI were 0.02, 0.05, 0.1, 0.2, and 0.5 wt.% (I-f, I-g, I-d, I-h and I-i), respectively, It can be seen that the Ti content in the

surface layer increased firstly and then decreased, although the nano-TiO_2 content in the treatment suspensions was the same. It was because when the PEI content was very low, it could enable linking between the particles and led to aggregation and settling under the force of gravity [27], which decreased the Ti content on the fiber surface. However, with the increase of PEI content, the fiber surface was mostly covered by PEI, resulting in a decrease in the percentage of Ti component.

When the content ratio of nano-TiO_2 to PEI was fixed and the content of nano-TiO_2 and PEI was changed from 0.05 to 0.5 wt.% (II-a, II-b and II-c), it can been seen from the XPS data that, there was no regular change in the content of Ti, but the content of Si content increased as the content of γ-MPS increased.

4.3.2 Effect of the content ratio of nano-TiO_2 to PEI on fiber coating formation

SEM images of untreated PBO fibers and treated PBO fibers modified with different treatment suspensions are shown in Fig. 4-4. The surface of the untreated PBO fiber is smooth and neat (Fig. 4-4a). Fig. 4-4b displays the surface morphology of PBO fibers modified with treatment suspension in which the solute was only nano-TiO_2. The nanoparticles were not evenly distributed, but concentrated in the gaps between fibers. Agglomerated microspheres were also present.

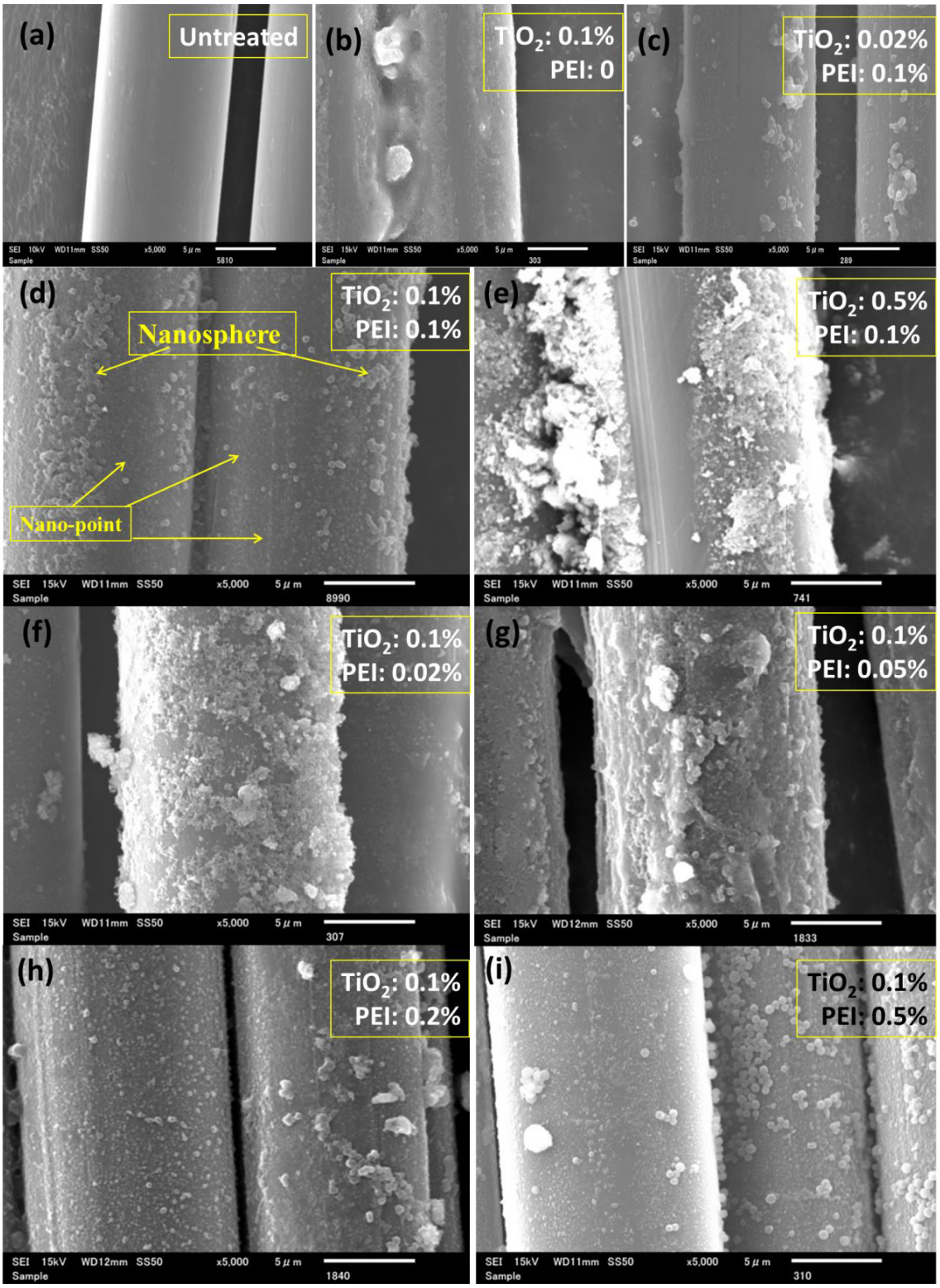

Fig. 4-4. SEM images of (a) untreated PBO fibers (sample I-a) and (b)-(i) PBO fibers treated in the suspension with different content ratios of nano-TiO_2 to PEI.

Fig. 4-4c, d, and e illustrate the surface morphology of PBO fibers treated with suspensions in which the contents of PEI and γ-MPS were fixed at 0.1 wt.%, and the contents of nano-TiO_2 were 0.02, 0.1, and 0.5 wt.%, respectively. Besides some nanospheres with uniform size, there were many nano-points uniformly distributed on the fiber surface as shown in Fig. 4-4d, which were proved to be nano-TiO_2 particles inside. This was because in the treatment suspension, the PEI concentration on the particle surface was high enough to cause steric stabilization; an additional stabilization mechanism may also have existed [27]. As a result, nano-TiO_2 particles were uniformly distributed on the fiber surface. However, the fiber surface was coated with agglomerates for the sample depicted in Fig. 4-4e. In this case, because of the high nano-TiO_2 content, the nanoparticles were not completely covered with γ-MPS or PEI, which enabled joining of the particles and led to aggregation. As shown in Fig. 4-4c, because of less concentration of nano-TiO_2 and more interaction between PEI and γ-MPS, there were even no obvious white particles but some agglomerated nanospheres.

Fig. 4-4f, g, h, i, and d show the surface morphology of PBO fibers treated with treatment suspensions in which the contents of nano-TiO_2 and γ-MPS were fixed at 0.1 wt.% and those PEI were 0.02, 0.05, 0.1, 0.2, and 0.5 wt.%, respectively. As depicted in Fig. 4-4f~g, the fiber surfaces were covered with agglomerates. Also, the low content of PEI, which could not completely cover the nanoparticles, resulted in aggregation of the particles. In Fig. 4-4d, h, and i, nano-TiO_2 nanoparticles were uniformly distributed on the fiber surface because of the higher PEI content.

Comparison of these SEM images and previous dispersion stability tests of modified nano-TiO_2 indicate that the higher the stability of the treatment suspension, the better the dispersion of nanoparticles on the fiber surface after solvent evaporation.

Therefore, the content ratio of nano-TiO_2 to PEI strongly influences not only the stability of the treatment suspension but also this evaporation-induced surface modification.

4.3.3 Effect of the contents of nano-TiO_2 and PEI on PBO fiber coating formation

To study the effect of the content of nano-TiO_2 and PEI on the treatment results, the content ratio of nano-TiO_2 to PEI was fixed and the content of nano-TiO_2 and PEI was changed from 0.05 to 0.5 wt.%. The compositions of these treatment suspensions are listed in Table 4-1 (II-a~c).

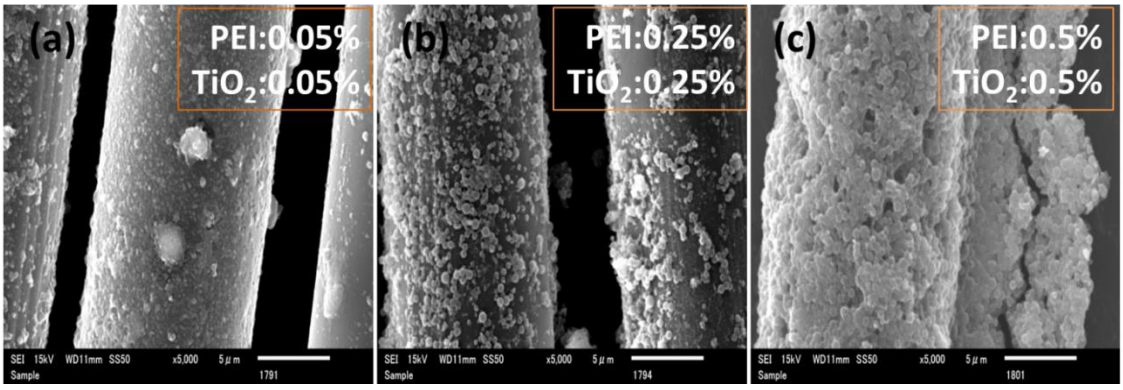

Fig. 4-5. SEM images of treated PBO fibers with different contents of nano-TiO_2 and PEI: (a) 0.05%, (b) 0.25%, and (c) 0.5%.

Together with the sample I-d, these four samples should in theory have the same content ratio of nano-TiO_2 to PEI, but because PEI is difficult to dissolve, the actual content ratio between PEI and nano-TiO_2 in sample II-a was the lowest, TiO_2 nanoparticles were not completely covered with PEI, which resulted in agglomeration, as shown in Fig. 4-5a. With increasing solutes' content, the number of nanospheres increased and the dispersion of nano-TiO_2 particles became worse, as illustrated in Fig. 4-5b. This was because the viscosity of the suspension increased, which hindered the

evaporation process. When the content of nano-TiO_2 and PEI was 0.5 wt.%, the fiber surface was completely coated with nanospheres, which made the fibers much thicker (Fig. 4-5c). The experimental results indicate that to form a sub-100-nm-thick coating layer on the PBO fiber surface, the treatment suspension must be really dilute and the content ratio of nano-TiO_2 to PEI must be appropriate.

4.3.4 Effect of evaporation method on fiber coating formation

Using sample I-d, four different evaporation environments were evaluated: evaporation at ambient temperature in a fume hood for a week (named fume hood evaporation), in a drying oven at 60 °C for 2 days (named drying oven evaporation), on a hotplate at 60 °C for 2 days (named hotplate evaporation), and in a vacuum drying oven at 60 °C for 2 days (named vacuum drying oven evaporation). Heating could shorten the evaporation time, but the dispersion of nanoparticles on the fiber surface became difficult to control as the temperature increased. Therefore, in this experiment, the heating temperature was set at 60 °C.

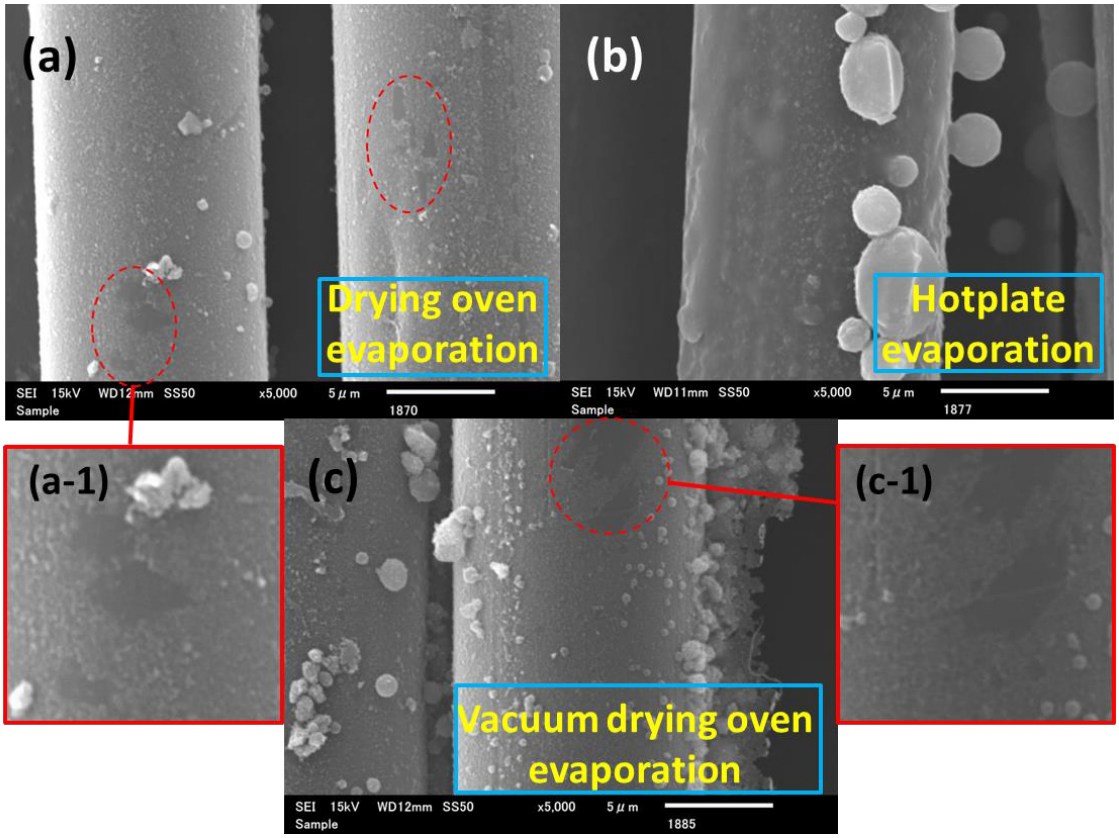

Fig. 4-6. SEM images of PBO fibers treated using different evaporation methods: (a) drying oven evaporation, (b) hotplate evaporation, and (c) vacuum drying oven evaporation.

After drying in an oven at 60 °C for 2 days, nano-points were uniformly dispersed on the fiber surface and nanospheres were almost absent, as shown in Fig. 4-6a. PEI solvent flowed away from the surface more easily at higher temperature. After the loss of PEI, the surface layer became even thinner. The coating was lost in some regions, which are indicated by red circles and enlarged in the magnified image (Fig. 4-6a-1). This phenomenon also occurred in the sample dried in a vacuum oven at 60 °C for 2 days (Fig. 4-6c and Fig. 4-6c-1), and because of the lower pressure, agglomerates formed in the gaps between fibers. During heating on the hotplate, the heating of the top

and bottom of fibers was uneven, resulting in an uneven coating layer on the fiber surface and the formation of PEI microspheres of varying size, as shown in Fig. 4-6b. Comparing the four samples reveals that low pressure leads to agglomeration, uneven heating leads to surface irregularities, and heating leads to a thinner coating. Among the investigated evaporation methods, oven drying at 60 °C gave the closest result to that of ambient-temperature drying in a fume hood.

4.3.5 TEM observation of a treated PBO fiber cross section

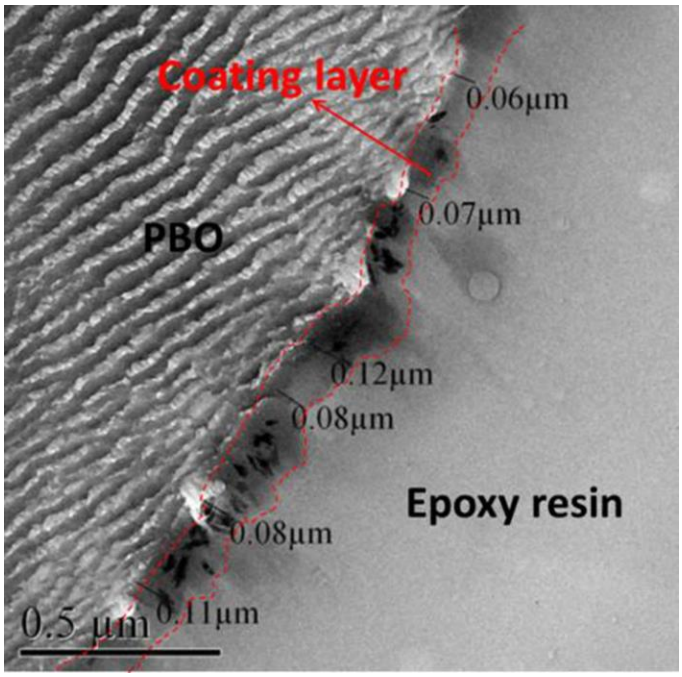

Fig. 4-7. TEM micrographs of a fiber cross section (sample I-d) at magnifications of ×40,000.

To observe the cross section of a treated PBO fiber, a single treated PBO fiber (sample I-d) was embedded in epoxy resin. The resulting 120-nm-thick film was cut perpendicular to the fiber axis after the epoxy resin was cured before being observed by TEM. A uniform coating layer (average thickness of 86.7 nm) with nano-TiO_2 between

PBO fibers and epoxy resin can be seen in Fig. 4-7. The TEM images clearly reveal that the fiber surface was uniformly covered by a coating layer of nano-TiO_2.

4.3.6 TGA

TGA curves for untreated and treated PBO fibers are presented in Fig. 4-8. For the untreated PBO fiber, the weight loss below 600 °C corresponds to the elimination of water and residual solvent [37], and the sharp weight loss between 600 and 700 °C is attributed to the decomposition of PBO fibers [38]. The two treated samples sample I-d and sample I-i both lost more weight between 500 and 600 °C than the untreated PBO fiber, which is ascribed to the decomposition of PEI on the fiber surface. Sample I-i displayed an even greater weight loss than sample I-d between 500 and 600 °C. This indicates that the PEI content on the surface of sample I-i was higher than that of sample I-d, which was consistent with the PEI contents of the treatment suspensions used to produce sample I-d and I-i. This result also means that the higher the content of PEI in the treatment suspension, the greater the amount of PEI adsorbed on the PBO fiber surface. The TGA curves for these two samples both intersected with that of the untreated PBO fiber (see the enlarged image). This clearly shows that the treated samples contained components that decompose more easily than PBO, that is, PEI, as well as components that enhance the thermal stability of the sample; i.e., nano-TiO_2 particles. The difference of PEI content between sample I-d and I-i can also be seen from the corresponding temperatures of the intersections of their TGA curves with that of the untreated fibers.

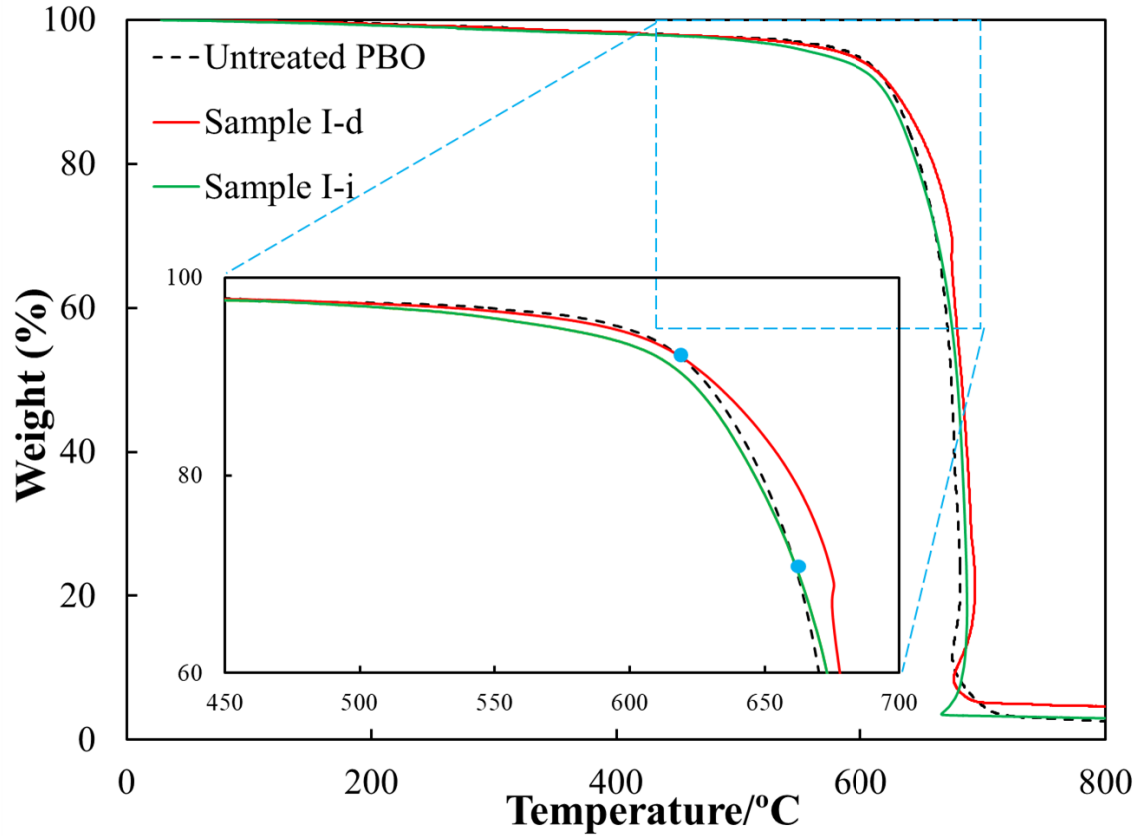

Fig. 4-8. TGA curves of untreated PBO fibers and treated PBO fibers (sample I-d and I-i).

The residual masses of the untreated PBO fibers, sample I-d, and sample I-i were 2.55%, 4.67%, and 3.01%, respectively. Neglecting the weight loss caused by the thermal decomposition products of γ-MPS, the maximum mass fractions of TiO_2 nanoparticles on the treated PBO fiber surface for sample I-d and I-i were 2.12% and 0.46%, respectively. This result shows that less nano-TiO_2 particles were adsorbed on the PBO fiber surface of sample I-i, which had higher PEI content, than that of sample I-d, even though the nano-TiO_2 content in the treatment suspension was the same. Because there was some non-adsorbed PEI, an additional stabilization mechanism may have existed, such as depletion stabilization, because the free polymer molecules may

have promoted the flocculation or stabilization of the colloidal dispersions. Depletion stabilization occurs via a depletion interaction that depends on the concentration of the free polymer [27]. The concentration of free PEI in sample I-d must have been lower than the critical concentration (C^+) for the onset of depletion flocculation, and thus exhibited depletion stabilization. The concentration of free PEI in sample I-i must have been greater than C^+ for the onset of depletion flocculation, so this sample displayed depletion flocculation. The nano-TiO_2 content in the dispersion was decreased by depletion flocculation, as was the nano-TiO_2 content absorbed on the fiber surface. Because of its higher content of nano-TiO_2 particles, sample I-d displayed better thermal stability than that of sample I-i; as illustrated in the TGA curves, the sharp weight loss temperature of sample I-d was lower than that of sample I-i.

4.3.7 Mechanical property

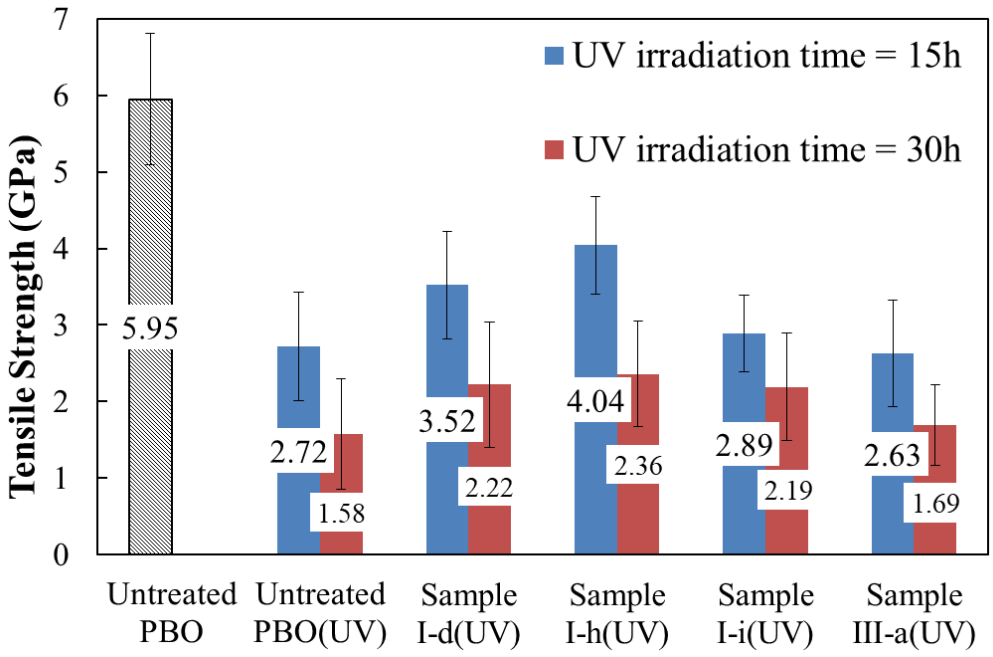

Fig. 4-9. Single-fiber tensile strength of treated and untreated PBO fibers after UV irradiation.

Fig. 4-9 shows the tensile strength of different samples after 15 and 30 hours of UV irradiation. The sample only coated with PEI (Sample III-a) was tested to compare with that of untreated PBO fibers after UV irradiation. The results reveal that the single-fiber tensile strength of the untreated PBO fiber decreased sharply after UV irradiation. The single fiber tensile strength of untreated PBO was 5.95 GPa before UV irradiation; after 15 hours of UV irradiation, the single fiber tensile strength decreased to 2.72 GPa, and the single fiber tensile strength was only 1.58 GPa after 30 hours of UV irradiation, which means PBO fiber is especially poor in UV resistance [18]. After UV irradiation for 15 and 30 hours, the single fiber tensile strengths of sample III-a were 2.63 and 1.69 GPa, respectively. Comparing the results between untreated PBO and sample III-a, it can be seen that a single PEI coating could not protect PBO fiber from UV irradiation.

In addition, the tensile strengths of sample I-d, I-h, and I-i, which had uniform PEI coating with nano-TiO_2, were also measured to compare with that of untreated PBO fibers after UV irradiation. The single-fiber tensile strengths of these three samples also decreased after UV irradiation. However, the nano-TiO_2 particles dispersed on the fiber surface, which exhibit good absorption and scattering of UV light, meant that the decrease of tensile strength was smaller than that observed for the untreated PBO fiber. The residual strengths of sample I-d, I-h, and I-i were 3.52, 4.04 and 2.89 after 15 hours of UV irradiation, respectively; and after 30 hours of UV irradiation the residual strengths were 2.2, 2.36, and 2.19 GPa, respectively. The residual strength of sample I-h was higher than that of sample I-d. It was shown that the treatment process of sample I-h was better than that of sample I-d. The low residual strength of sample I-i was ascribed to its lower content of nano-TiO_2 particles on the PBO fiber surface, which was

confirmed by TGA. The detailed results of single-fiber tensile strength are listed in Table 4-2.

Table 4-2. Single-fiber tensile strength of PBO fibers after UV irradiation.

Samples	UV irradiation time	
	15 hours	30 hours
	Single-fiber tensile strength/GPa	Single-fiber tensile strength/GPa
Untreated PBO(UV)	2.72 ± 0.71	1.58 ± 0.72
Sample I-d(UV)	3.52 ± 0.70	2.22 ± 0.82
Sample I-h(UV)	4.04 ± 0.64	2.36 ± 0.69
Sample I-i(UV)	2.89 ± 0.50	2.19 ± 0.70
Sample III-a(UV)	2.63 ± 0.70	1.69 ± 0.53

4.3.8 Adhesive durability

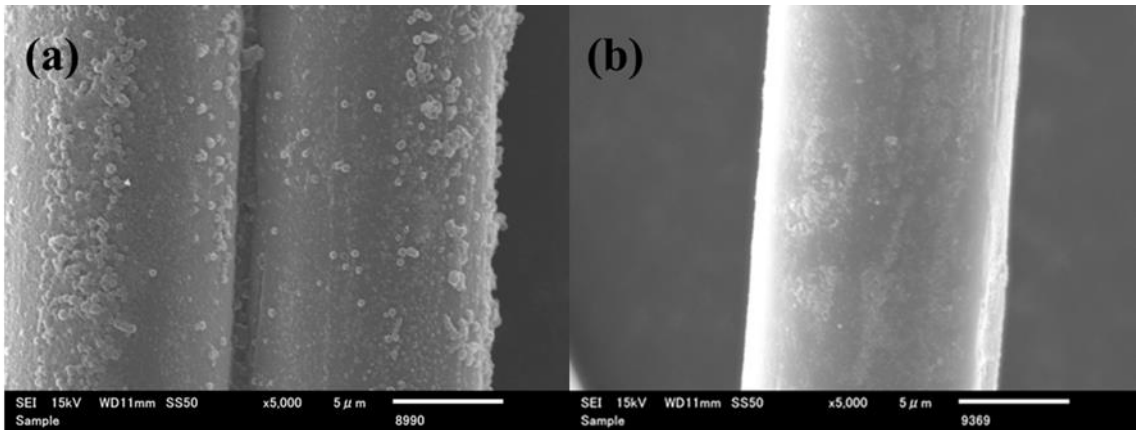

Fig. 4-10. Scanning electron microscopy images of the sample I-d surface before and after ultrasonic exposure for 30 min.

Optimizing the adhesive durability of the nanoparticles on the modified fiber surface is a very difficult problem. Here, the adhesive durability of the coating on the PBO fiber surface was evaluated with an ultrasonic exposure test, and the SEM image of the fiber after the test is shown in Fig. 4-10. If we contrast Fig. 4-10a and Fig.4-10b,

it is clear that the nanospheres were almost all removed by ultrasonication. This is because the contact area between the nanospheres and the coating or the fiber surface was relatively small, and the nanospheres were thus easily removed under an external force (ultrasonic exposure for 30 min). However, the uniform coating of the nano-point still remains in most areas of the fiber surface, which indicates that the PEI coating layer with nano-TiO_2 particles absorbed on the PBO fiber surface has adhesive durability.

4.4 Conclusions

In this work, a sub-100-nm-thick coating layer was prepared on PBO fibers by evaporating the suspension of polyetherimide encapsulated nano-TiO_2 particles. The results suggested that the content ratio of nano-TiO_2 to PEI, the contents of nano-TiO_2 and PEI, and the evaporation method strongly influenced the surface modification of the PBO fibers. After suitable treatment, TiO_2, γ-MPS, and PEI existed on the PBO fiber surface, as confirmed by XPS analysis. Meanwhile, a PEI coating layer (average thickness of 86.7 nm) with nano-TiO_2 particles was clearly observed by TEM observation of a treated PBO fiber cross section. Single-fiber tensile strength of treated and untreated PBO fibers after 15 and 30 hours of UV irradiation was tested. The results indicate that the UV resistance of the PBO fibers was improved after the surface modification, which is very important for the applications of PBO fibers in outdoor environment. In addition, this surface coating method could be widely applied to many other cases of chemical inert surface coating.

References

[1] P. Chen, C. Zhang, X. Zhang, B. Wang, W. Li, Q. Lei, Effects of oxygen plasma treatment power on surface properties of poly(p-phenylene benzobisoxazole) fibers,

Appl. Surf. Sci. 255 (2008) 3153-3158.

[2] T. Kitagawa, K. Funaki, Morphological studies of poly-p-phenylenebenzobisoxazole (PBO) fibers on the process that determines the direction of the crystal a-axis along the radius direction during the formation of fiber structures, Polymer. 82 (2016) 246-254.

[3] N. Horikawa, Y. Nomura, T, Kitagawa, Tensile fracture behavior of UV light irradiated PBO fiber, J. Solid Mech. Mater. Eng. 3 (2009), 1-9.

[4] B. Song, Q. Fu, L.H. Ying, X.Y. Liu, Q.X. Zhuang, Z.W. Han, Study on photoaging of poly(p-phenylene benzobisoxazole) fiber, J. Appl. Polym. Sci. 124 (2012) 1050-1058.

[5] T. Kitagawa, H. Murase, K. Yabuki, Morphological study on poly-p-phenylenebenzobisoxazole (PBO) fiber, J. Polym. Sci., Part B: Polym. Phys. 36 (1998) 39-48.

[6] C.H. Zhang, W.J. Yuan, S.G. Wang, X.F. Liang, Effect of MWCNTs irradiation grafting treatment on the surface properties of PBO fiber, J. Appl. Polym. Sci. 121 (2011) 3455-3459.

[7] T. Zhang, J.H. Jin, S.L. Yang, G. Li, J.M. Jiang, UV accelerated aging and aging resistance of dihydroxy poly(p-phenylene benzobisoxazole) fibers, Polym. Adv. Technol. 22 (2011) 743-747.

[8] L. Chen, Z. Hu, F. Zhao, L.X. Xing, B. Jiang, Y.D. Huang, Enhanced interfacial properties of PBO fiber via electroless nickel plating, Surf. Coat. Technol. 235 (2013) 669-675.

[9] J.L. Wang, G.Z. Liang, W. Zhao, Z.P. Zhang, Enzymatic surface modification of PBO fibres, Surf. Coat. Technol. 201 (2007) 4800-4804.

[10] C.S. Zhang, P. Chen, D. Liu, B.C. Wang, W. Li, X.T. Kang, Aging behavior of PBO fibers and PBO-fiber-reinforced PPESK composite after oxygen plasma treatment, Surf. Interface Anal. 41 (2008) 187-192.

[11] F. Guo, Z.Z. Zhang, X.H. Xu, W. Jiang, K. Wang, Tribological properties of PBO fabric composites modified by poly (vinyl alcohol), J. Appl. Polym. Sci. 130 (2013) 1313-1320.

[12] J. Qian, J. Wu, X. Liu, Q. Zhuang, Z. Han, Improvement of interfacial shear strengths of polybenzobisoxazole fiber/epoxy resin composite by n-TiO2 coating, J. Appl. Polym. Sci. 127 (2013) 2990-2995.

[13] J. Won, M.A. Said, A.F.M. Development of UV protective sheath for high performance fibers for high altitude applications, Seyam, Fibers Polym. 14 (2013) 647-652.

[14] J.H. Jin, G. Li, S.L. Yang, J.M. Jiang, Effects of light stabilizer on the ultraviolet stability of poly-p-phenylenebenzobisoxazole (PBO) fibers, Iran. Polym. J. 21 (2012) 739-745.

[15] P.J. Walsh, X.B. Hu, Environmental effects on poly-p-phenylenebenzobisoxazole fibers. II. Attempts at stabilization, J. Appl. Polym. Sci. 102 (2006) 3819-3829.

[16] C.H. Zhang, Y.D. Huang, W.J. Yuan, J.N. Zhang, UV aging resistance properties of PBO fiber coated with nano-ZnO hybrid sizing, J. Appl. Polym. Sci. 120 (2011) 2468-2476.

[17] Y.W. Jang, B.G. Min, K.H. Yoon, Enhancement in compressive strength and UV ageing-resistance of poly(p-phenylene benzobisoxazole) nanocomposite fiber containing modified polyhedral oligomeric silsesquioxane, Fibers Polym. 18 (2017) 575-581.

[18] ZYLON® (PBO fiber) Technical Information (2005). http://www.toyobo-global.com/seihin/kc/pbo/zylon-p/bussei-p/technical.pdf (accessed April 29, 2018).

[19] Y. Chen, Q. Zhang, Q. Han, Y. Mi, S. Sun, C. Feng, H. Xiao, P. Yu, C. Yang, Synthesis of polysiloxane with 5,5-dimethylhydantoin-based N-halamine pendants for biocidal functionalization of polyethylene by supercritical impregnation, J. Appl. Polym. Sci. 134 (2017) 44721.

[20] A. Naylor, S.M. Howdle, The preparation of novel blends of Ultra High Molecular Weight Polyethylene with polymethacrylate based copolymers using supercritical carbon dioxide, J. Mater. Chem. 15 (2005) 5037-5042.

[21] Y. Chen, X.S. Zhong, Q. Zhang, Synthesis of CO_2-Philic Polysiloxane with N-Halamine Side Groups for Biocidal Coating on CottonInd. Eng. Chem. Res. 51 (2012) 9260-9265.

[22] B. Song, L. Meng, Y. Huang, Preparation and characterization of $(POSS/TiO_2)_n$ multi-coatings based on PBO fiber surface for improvement of UV resistance, Fibers Polym. 14 (2013) 375-381.

[23] B. Song, Q.X. Zhuang, L.H. Ying, X.Y. Liu, Z.W. Han, Photostabilisation of poly(p-phenylenebenzobisoxazole) fibre, Polym. Degrad. Stabil. 97 (2012) 569-1576.

[24] J. Zhong, A.I. Isayev, Properties of polyetherimide/graphite composites prepared using ultrasonic twin-screw extrusion, J. Appl. Polym. Sci. 132 (2015) 41397.

[25] T. Liu, Y.J. Lei, Z.L. Chen, X.Z. Wang, S.K. Luo, Effects of processing conditions on foaming behaviors of polyetherimide (PEI) and PEI/polypropylene blends in microcellular injection molding process, J. Appl. Polym. Sci. 132 (2015)

41443.

[26] Y. Zhang, M. Zhong, B. Luo, J. Li, Q. Yuan, X.J. Yang, The performance of integrally skinned polyetherimide asymmetric nanofiltration membranes with organic solvents, J. Membr. Sci. 544 (2017) 119-125.

[27] P. Zhu, B. Liu, L.M. Bao, Preparation of double-coated TiO_2 nanoparticles using an anchoring grafting method and investigation of the UV resistance of its reinforced PEI film, Prog. Org. Coat. 104 (2017) 81-90.

[28] G. Li, F. Wang, P. Liu, Z.M. Chen, P. Lei, Z.S. Xu, Z.X. Li, Y.F. Ding, S.M. Zhang, M.S. Yang, Polymer dots grafted TiO_2 nanohybrids as high performance visible light photocatalysts, Chemosphere. 197 (2018) 526-534.

[29] J. Lee, Z. Li, L.Z. Zhu, S.H. Xie, X. L. Cui, Ti^{3+} self-doped TiO_2 via facile catalytic reduction over $Al(acac)_3$ with enhanced photoelectrochemical and photocatalytic activities, Appl. Catal. B: Environ. 224 (2018) 715-724.

[30] M.R. Turner, E. Duguet, C. Labrugere, Characterization of silane-modified ZrO_2 powder surfaces, Surf. Interface Anal. 25 (1997) 917-923.

[31] Z. Han, B. Zhu, R. Chen, Z. Huang, C. Zhu, X. Zhang, Effect of silver-supported materials on the mechanical and antibacterial properties of reinforced acrylic resin composites, Mater. Des. 65 (2015) 1245-1252.

[32] T. Murakami, S. Takemoto, N. Nishiyama, M. Aidab, Zirconia surface modification by a novel zirconia bonding system and its adhesion mechanism, Dent. Mater. 33 (2017) 1371-1380.

[33] D. Liu, P. Chen, J.J. Mu, Q. Yu, C. Lu, Improvement and mechanism of interfacial adhesion in PBO fiber/bismaleimide composite by oxygen plasma treatment, Appl. Surf. Sci. 257 (2011) 6935-6940.

[34] D. Liu, P. Chen, Q. Yu, K.M. Ma, Z.F. Ding, Improved mechanical performance of PBO fiber-reinforced bismaleimide composite using mixed O_2/Ar plasma, Appl. Surf. Sci. 305 (2014) 630-637.

[35] L. Chen, F. Wei, L. Liu, W. Cheng, Z. Hu, G. Wu, Grafting of silane and graphene oxide onto PBO fibers: Multifunctional interphase for fiber/polymer matrix composites with simultaneously improved interfacial and atomic oxygen resistant properties, Compos. Sci. Technol. 106 (2015) 32-38.

[36] S. Basu,; M. Heuchel,; T. Weigel,; K. Kratz,; A. Lendlein, Integrated process for preparing porous, surface functionalized polyetherimide microparticles, Polym. Adv. Technol. 26 (2015) 1447-1455.

[37] J.W. Gu, J. Dang, W.C. Geng, Q.Y. Zhang, Surface modification of HMPBO fibers by silane coupling agent of KH-560 treatment assisted by ultrasonic vibration, Fibers Polym. 13 (2012) 979-984.

[38] L. Chen, Y.Z. Du, Y.D. Huang, F. Wu, H.M. Cheng, B. Fei, J.H. Xin, Hierarchical poly(p-phenylene benzobisoxazole)/graphene oxide reinforcement with multifunctional and biomimic middle layer, Compos. A. 88 (2016) 123-130.

CHAPTER FIVE

Preparation of Polyetherimide nanoparticles on carbon fiber surface via evaporation induced surface modification method and its effect on tensile strength and interfacial shear strength

Chapter 5: Preparation of Polyetherimide nanoparticles on carbon fiber surface via evaporation induced surface modification method and its effect on tensile strength and interfacial shear strength

5.1 Introduction

Carbon fibers (CFs) have been widely used as reinforcements for advanced composites because of their excellent mechanical properties, high thermal and electrical conductivities, excellent corrosion resistance, low linear thermal expansion coefficient, and low density [1, 2]. CF-reinforced epoxy composites remain the most widely used fiber-reinforced composite materials because of the simplicity and low cost of their production process. However, the potential of CF-reinforced epoxy composites has not yet been fully exploited because of the chemically inert CF surface, which makes it difficult to achieve the desired interfacial adhesion with the matrix [1].

In investigations of this interfacial adhesion, fiber-reinforced composites are considered to consist of three main components: the fibers, which are the load-bearing components; the matrix, which holds the fibers together and transfers the applied load between fibers; and the fiber–matrix interphase, which determines the adhesion property between the fibers and matrix [3]. During the last decade, extensive research has been devoted to improving the fiber–matrix interphase using surface treatment of the CFs using techniques such as chemical grafting, electromechanical methods, plasma treatment, radiation, or surface coating [4-6]. However, in addition to providing a coating, these methods generate oxygen functional groups via strong oxidizing reactions,

which lead to drawbacks on the CF surface that cause a decrease of the fiber strength [7, 8]. However, with recent developments in materials science and technology, an increasing number of new materials that have begun to be used as coating components have been invented, such as carbon nanotubes [9-11], graphene oxide [12, 13], and graphene nanoplatelets [2, 14].

In addition to inorganic coatings, research has also been conducted on organic coatings, including studies on the tensile properties of polyimide-coated CFs [15, 16]; the interfacial shear strength (IFSS) of CFs coated with high-performance polymers such as poly(arylene ether phosphine oxide) (PEPO), Udel®P-1700, and Ultem®1000, water-soluble poly(hydroxy ether ethanol amine), water-dispersed carboxy-modified poly(hydroxyether), and water-insoluble poly(hydroxy ether) [17]; the effect of polyamide coatings on CFs on the mechanical properties of carbon/epoxy composites [18]; the effect of hygrothermal aging on the interlaminar shear strength of carbon–epoxy composites based on fibers coated with Nylon 6,6 [19]; and the role of a polyamide interphase on CFs reinforcing an epoxy matrix [20]. However, in recent years, there has been little research in this area because most new polymer materials (such as polyether ether ketone, polyphenylene sulfide, and polyetherimide (PEI)) are difficult to dissolve in common organic solvents. In addition, it is difficult to accurately control the coating thickness using this dip-coating method, and the fibers adhere to each other, preventing the resin from entering during the preparation of fiber-reinforced composite materials.

In this study, PEI was used to prepare a coating material. The PEI was dissolved in *N*-methyl-2-pyrrolidone (NMP) to prepare a dilute solution of PEI, taking advantage of the low volatility of NMP and the PEI concentration to accurately control the coating

morphology. The effect of the coating on the single fiber strength and the effect of the coating morphology on the IFSS were also studied.

5.2 Experimental section

5.2.1 Materials

CFs (T300, diameter: 7 μm) were supplied by TORAY, Japan. The pristine CFs were washed with acetone for 48 h at ambient temperature to remove surface sizing agents and/or contaminants. The obtained fibers are referred to as desized CFs. PEI (melt index 9 g/10 min (337 °C/6.6 kg)) was purchased from Sigma–Aldrich, USA, and NMP was purchased from Kanto, Japan. All the chemicals were used as received.

5.2.2 Evaporation-induced surface modification

Different amounts of PEI particles were dissolved in NMP at 70 °C for 2 h to obtain dilute PEI solutions with different concentrations.

The treated CFs were fabricated in several steps. First, a bundle of desized CFs was immersed in NMP for 15 min. Then, the NMP-infiltrated CFs were placed in the PEI solution, which was sonicated in an ice bath for 20 min and then allowed to stand for 24 h. Finally, the pretreated CF bundle was placed on a Teflon plate in a fume hood at ambient temperature for 1 week to allow the solvent to evaporate and obtain the treated fibers. The detail compositions and processes used for fiber treatment are listed in Table 5-1.

Table 5-1. Compositions and processes used for fiber treatment.

Sample	PEI (wt.%)	260°C heat for 40 min
Desized CF	-	-
CF-0.02	0.02	-
CF-0.05	0.05	-
CF-0.1	0.1	-
CF-0.2	0.2	-
CF-0.3	0.3	-
0.02-heat	0.02	√
0.05-heat	0.05	√
0.1-heat	0.1	√
0.2-heat	0.2	√
0.3-heat	0.3	√

5.2.3 Characterization of CFs

The surface chemical compositions of the CFs were probed using X-ray photoelectron spectroscopy (XPS; AXIS-ULTRA, Kratos, Japan). The binding energies were referenced to the C1s peak of aliphatic carbon at 284.3 eV. The surface morphologies of the fibers were examined using scanning electron microscopy (SEM; VE-9800, KEYENCE, Japan). The surface morphology and roughness were also examined using atomic force microscopy (AFM; SPA-400-AFM, Seiko, Japan). A single CF was fastened on a steel sample mount, and tapping mode was used to scan the fiber surface. Roughness analysis was performed on images obtained over an area of 4×4 μm using the instrument software (SPIWin). And its function of sample tilt correction for background tilt removal was used (1st order plane fitting was selected for all samples in our test). The possible formation mechanism of the PEI nanoparticles on the CF surfaces was also investigated by cross-section observation of CF using field-emission scanning electron microscopy (FE-SEM; S4800, Hitachi, Japan). Single-fiber tensile strength tests were performed using a tensile tester (EZ-SX,

Shimadzu, Japan) with a strain rate of 1 mm/min at 20 °C and a relative humidity of 65%. For each sample, at least 35 specimens were tested in the single-fiber tensile strength tests.

To assess the interfacial properties of PEI coated CF in epoxy resin, the single fiber fragmentation test (SFFT) was employed [2, 3]. The dog-bone specimens for SFFT were prepared by suspending an individual carbon fiber in the PTFE mold, fixing the ends of the carbon fiber on the mold and surrounding it with epoxy resin. The samples were then cured at room temperature for 24 h and 50 °C for 12 h. Finally, the dog-bone samples were fixed to a micro-tension device. The measurement under a tensile load was taken at a crosshed speed of 0.1mm/min. During the test, entire single fiber fragmentation was monitored by optical microscope and the number of fiber fragmentation was counted within the gauge length of 26 mm.

When the length of fiber fragmentation becomes too short to effectively transfer load from the matrix, the number of fractures will no longer increase with increasing stress (saturation point). The number of fractures was used to calculate the critical fracture length and interfacial shear strength by the follow equations:

$$\tau_{\mathrm{IFSS}} = \frac{\delta_f d_f}{2 l_c}$$

$$l_c = \frac{4}{3} l_{average}$$

Where

τ_{IFSS}: interfacial shear strength

δ_f: single fiber tensile strength

d_f: fiber diameter

l_c: critical fiber length

$l_{average}$: average fiber length

5.3 Results and discussion

5.3.1 Chemical characterization of CFs

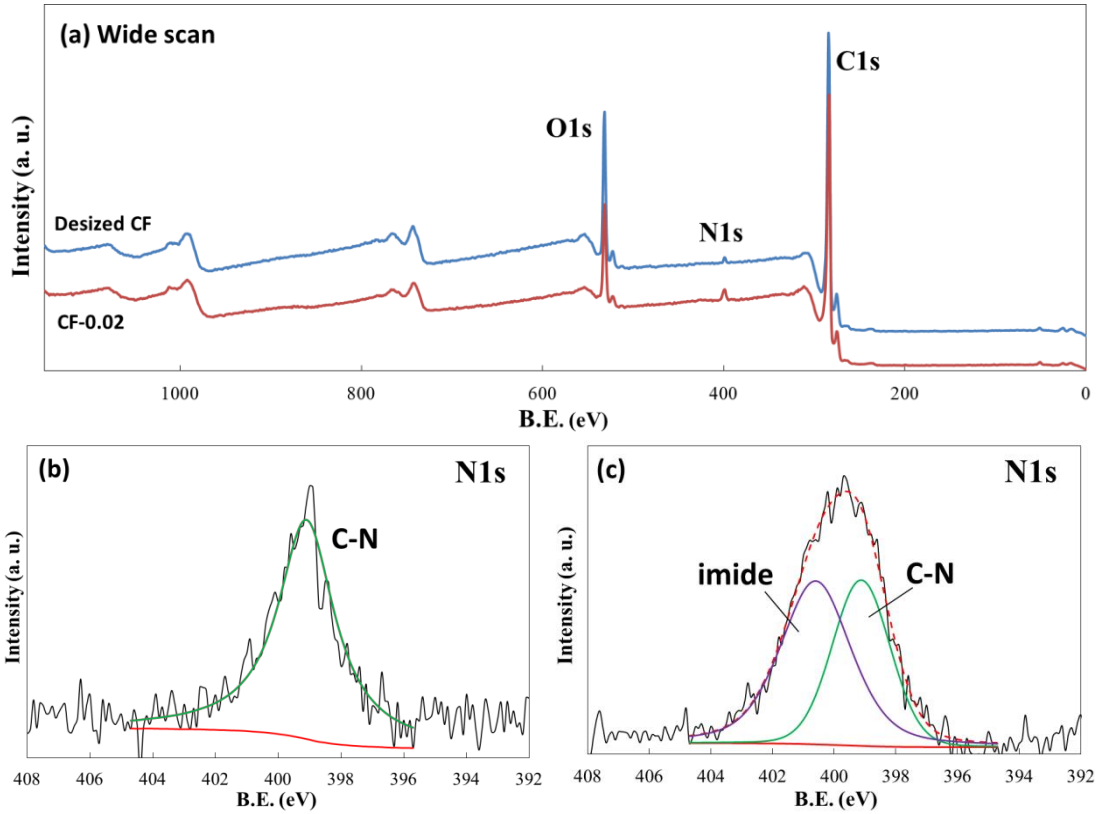

Fig. 5-1. (a) Wide-scan survey XPS spectra of CFs. XPS scan spectra of N1s: (b) desized CF and (c) CF-0.02.

The chemical compositions of the CF surfaces were assessed using quantitative XPS analysis. CF-0.02 with the lowest PEI content was used as a representative for the modified samples. The detailed elemental compositions of the desized CF and CF-0.02 determined using XPS are presented in Fig. 5-1a. The presence of carbon, oxygen, and a small amount of nitrogen was confirmed on the surface of the desized CF and CF-0.02. A comparison of the elemental composition of treated CF and that of the desized CF revealed an obvious increase of N1s content for treated CF as shown in Table 5-2. And

the N1s/C1s ratio of the desized CF was only 0.007, the N1s/C1s ratio of treaded CF was obviously increased from 0.026 to 0.034. The increased N content was attributed to the successful absorption of PEI on the CF surface, which affected the fiber surface elemental composition.

XPS N1s spectra were also obtained to determine the difference in the chemical compositions of the desized and modified CFs, and the results of the chemical analysis are presented in Fig. 5-1b~c. As observed from the N1s spectrum in Fig. 5-1b, the energy position of the nitrogen (399.1 eV) is indicative of C-N bonding. This peak was attributed to N-containing residue, perhaps due to the incomplete oxidation of the PAN source [21, 22]. After modification, a new peak appeared at 400.6 eV in addition to the C-N bonding from the CFs, which was assigned to an imide as shown in Fig. 5-1c. Because the characteristic structure of PEI is an imide [23, 24], this result supports the successful coating of the fiber surface with PEI.

Table 5-2. Relative elemental contents (at%) of fiber surfaces.

Sample	Relative content of elements/%			N1s/ C1s
	C1s	O1s	N1s	
Desized CF	85.34	14.03	0.63	0.007
CF-0.02	86.50	10.96	2.55	0.030
CF-0.05	82.89	14.77	2.34	0.028
CF-0.1	82.53	15.25	2.22	0.027
CF-0.2	83.85	13.41	2.74	0.033
CF-0.3	84.04	13.35	2.61	0.031
0.02-heat	84.99	12.24	2.77	0.033
0.05-heat	84.76	12.86	2.39	0.028
0.1-heat	83.93	13.63	2.44	0.029
0.2-heat	84.57	13.27	2.16	0.026
0.3-heat	85.26	11.88	2.86	0.034

5.3.2 Surface topography of CFs

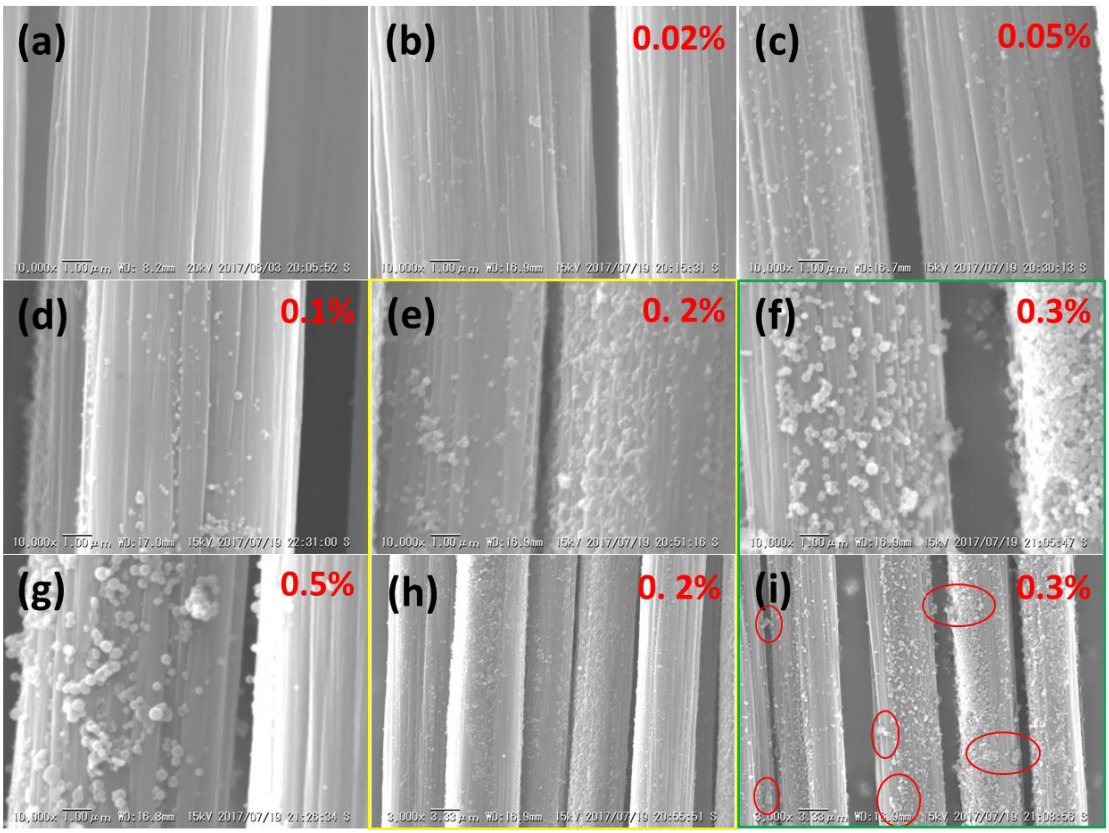

Fig. 5-2. SEM images of (a) desized CF and (b-g) CF treated with different PEI concentrations; (h-i) sample 0.2% and 0.3% at magnifications of ×3000.

SEM images of the surface topographies of the CFs before and after the surface modification are presented in Fig. 5-2. The fiber surface of the desized CF appears to be relatively clean and smooth, with the clear appearance of narrow grooves distributed parallel to the longitudinal direction. The surface topographies of the CFs after treatment with different PEI concentrations are shown in Fig. 5-2b~g. With increasing PEI concentration, the shallow grooves disappeared, leaving only a few deep grooves. This phenomenon indicates that a thin layer of PEI coating has begun to appear on the fiber surface, which has filled the shallow grooves. In addition, some PEI nanoparticles

appeared after modification, with the PEI nanoparticle size clearly increasing with increasing PEI concentration. When the PEI concentration is higher than 0.2%, most of the nanoparticles on the CF surface are approximately spherical as show in Fig. 5-2f~g.

The surface topographies of samples 0.2% and 0.3% at lower magnification are shown in Fig. 5-2h~i. The nanoparticles were uniformly distributed on the fiber surface for the PEI concentration of 0.2%, as observed in Fig. 5-2h. However, upon further increasing the PEI concentration, nanoparticle aggregation occurred, as indicated by the red circles in Fig. 5-2i, which may have affected the degree of interfacial enhancement.

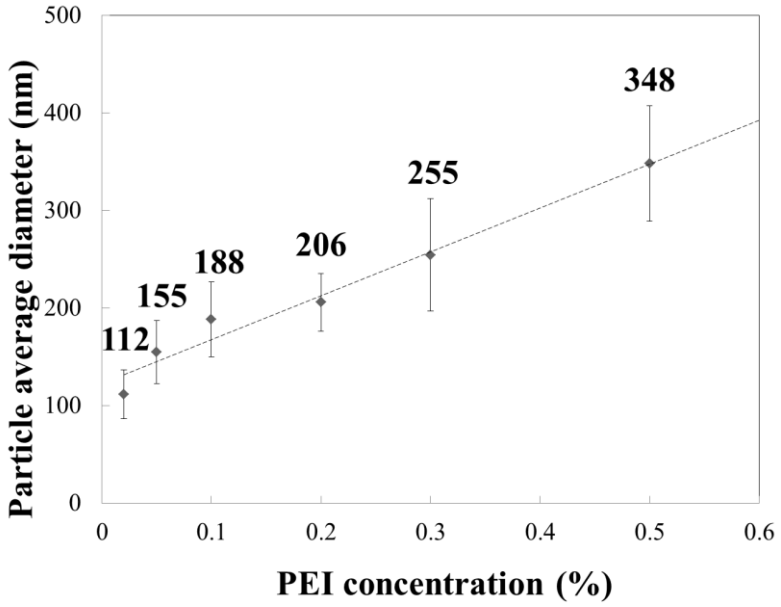

Fig. 5-3. Average particle diameter of particles on CF surface as a function of PEI concentration

The average diameters of the particles on the CF surface were calculated using SEM measurement function, at least 50 particles were measured in each SEM image, and the results are presented in Fig. 5-3. The average diameter of the PEI nanoparticles linearly increased with increasing PEI concentration, indicating that the size of the

nanoparticles on the fiber surface could be controlled by changing the PEI concentration.

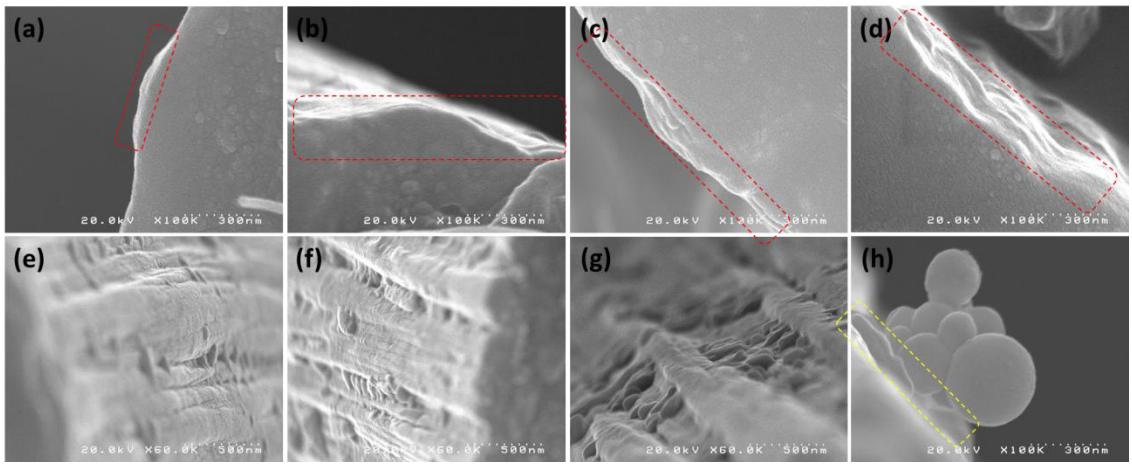

Fig. 5-4. Cross-section images of (a, e) CF-0.02; (b, f) CF-0.05; (c, g) CF-0.2; (d, h) CF-0.3.

Cross-section observation of different samples was also used to study the possible formation mechanism of the PEI nanoparticles on the CF surfaces. As marked in the red frames (Fig. 5-4a~d), the PEI layer can be seen on the treated CF surface, and the thickness of the PEI layer becomes thicker as the concentration increases. Combining with the SEM images and the FE-SEM images, the three-dimensional morphology of the nanoparticles can be obtained. From Fig. 5-4e~g it can be seen that the nanoparticles closest to the CF surface are hemispherical, and the nanoparticle size and the nanoparticle coverage rate increase with increasing concentration. Fig. 5-4h shows the agglomeration of nanoparticles from CF-0.3, from which the formation mechanism of PEI nanoparticles could be inferred. Two different morphologies of PEI nanoparticles can be seen, one is hemispherical closest to the CF surface as marked in the yellow frame (Fig. 5-4h), and the other is nearly spherical above the hemispherical

nanoparticles.

To understand the formation mechanism of the PEI nanoparticles on the CFs in this modification method, the CF surface can be divided into numerous identical areas, which can be called unit areas as show in Fig. 5-5. In dilute PEI solution, there must be a critical concentration (C′), blew which the PEI chains are dispersed in the solvent as individual chains that do not interact with each other and above which the PEI chains begin to entangle like a thread ball. Therefore, the dilute PEI solution can be divided into two types according to the concentration; type I of which the PEI concentration is less than C′ and type II of which the PEI concentration is higher than C′.

When the PEI concentration is higher than C′ (type II), the PEI chains can be divided into two parts, part I: individual chains that do not interact with each other; part II: the “thread balls” formed by the entanglement of the chains. The individual chains would be absorbed on CF surface to form the relatively flat layer, and the “thread balls” would be absorbed on CF surface to form the PEI nanoparticles. During PEI nanoparticle formation, the solvent in the “thread balls” is relatively difficult to evaporate; forming some separate solvent-containing “thread balls” before the evaporation ends, and then shrinks with evaporation, eventually forming spherical nanoparticles with no external influence. In addition, the “thread balls” near the surface forms hemispherical nanoparticles because of entanglement with the PEI chains adsorbed on the fiber surface; the “thread balls” far away from the surface forms spheres without any interference, which eventually accumulate on the surface of the fiber. The reason of the formation of accumulation is that the “thread balls” have both attraction and exclusion effects, eventually leading to mutual contact, but the “thread balls” are still independent, not fully integrated. And with the “thread ball” growing

larger with increasing PEI concentration, the size of the nanoparticles increased with increasing PEI concentration which has been shown in the SEM images (Fig. 5-2).

As the evaporation process is a dynamic process of increasing the concentration of solute as the solvent decreases, there must be a time the PEI concentration of type I is higher than C′ before the solvent is completely evaporated. The PEI chains still can be divided into two parts like in type II. This means that even when the concentration is extremely low, there is still particle formation, although the particle size may be extremely small.

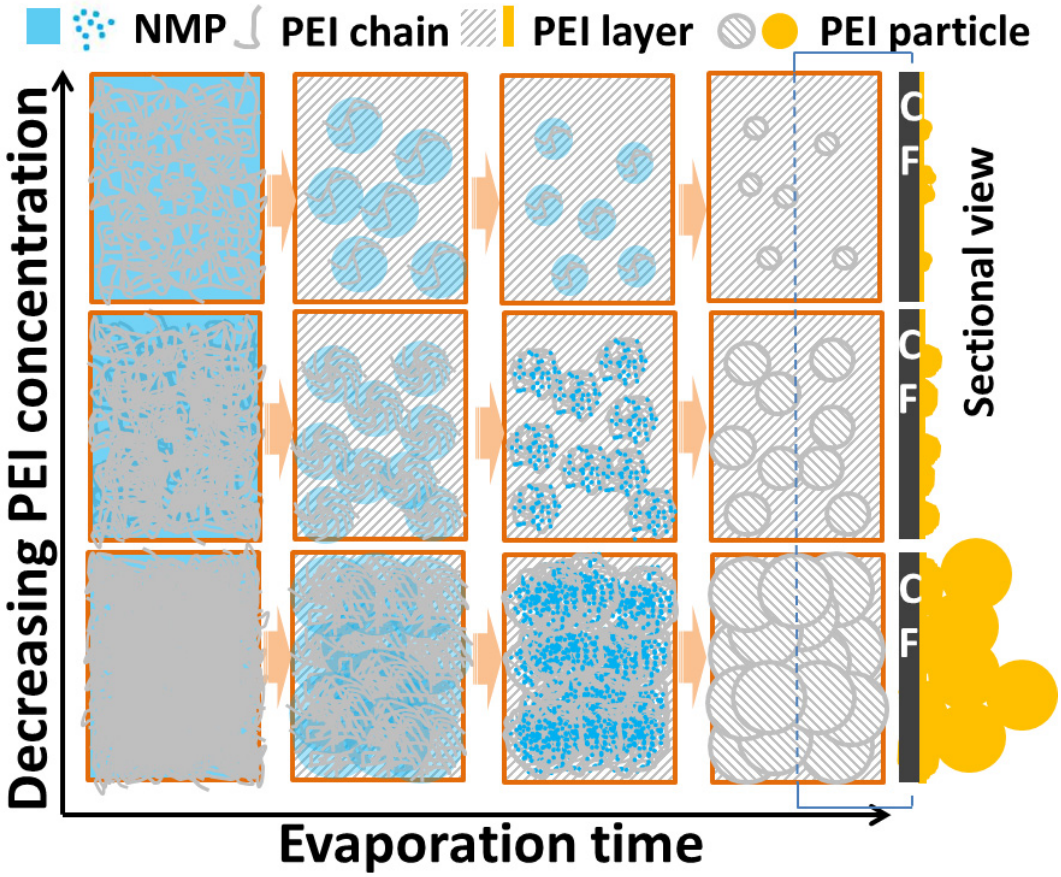

Fig. 5-5. Schematic illustration of the preparation process for PEI nanoparticles on CF surface.

The boiling point of NMP, which was used as the solvent in the modification, is 202 °C, and thus volatilizes very slowly at room temperature. Therefore, the PEI chains could shrink to form a hemispherical nanoparticle or a nanosphere under surface tension. This possible formation mechanism of the PEI nanoparticles on the CF surface is schematically illustrated in Fig. 5-5.

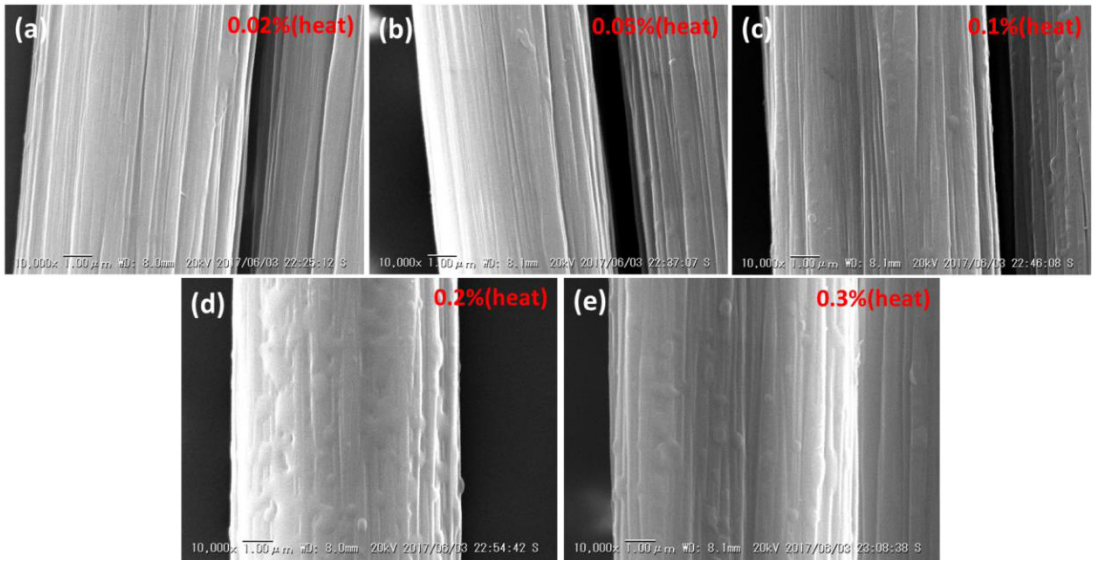

Fig. 5-6. SEM images of CFs treated with different PEI concentrations after heating for 40 min at 260 °C.

To study the effect of the PEI nanoparticles on the surface properties, samples treated with different PEI concentrations were heated at 260 °C for 40 min to melt the PEI nanoparticles. SEM images of the surface topographies of the treated samples after heating are presented in Fig. 5-6. For a PEI concentration of less than 0.05%, the PEI nanoparticles were completely melted, and some grooves were filled. For PEI concentrations greater than 0.1%, the PEI nanoparticles fused together, forming many flat PEI blocks.

AFM was used to characterize the surface roughness of the desized CF and treated

CF. The surface of the desized CF was relatively clean and smooth, as observed in Fig. 5-2a, leading to a relatively low surface roughness (Ra = 55.04 nm, Rq = 70.72 nm). As show in Fig. 5-2b~f and Table 5-3, the Ra value increased from 55.04 nm to 106.1 nm and the Rq value increased from 70.72 nm to 122.4 nm with increasing PEI concentration from 0% to 0.3%, most likely because increasingly more PEI nanoparticles were appeared because of the increased PEI concentration. It can be seen from Fig. 5-6d that all the PEI particles melted and fiber surface became even smoother than desized CF after heating, leading to a lowest surface roughness (Ra = 46.14 nm, Rq = 58.26 nm).

Compared the roughness data of Sample 0.2 with Sample 0.2-heat, it can be seen that the Ra value dramatically decreased from 96.95 nm to 46.14 nm and the Rq value decreased from 122.0 nm to 58.26 nm after the melting of PEI nanoparticles. So it can be seen that the appearance of PEI nanoparticles has a greater effect on the increase of roughness. Compared the roughness data of Sample CF with Sample 0.2-heat, it can be seen that when some grooves were filled, the Ra value slightly decreased a little from 55.04 nm to 46.14nm and the Rq value decreased from 70.72 nm to 58.26 nm. Detailed surface roughness data for the different samples is provided in Table 5-3.

Table 5-3. Root mean square roughness (Rq) and arithmetic average roughness (Ra) of CF samples.

Sample	Rq	Ra
CF	70.72 nm	55.04 nm
0.02	75.19 nm	66.07 nm
0.05	105.9 nm	83.52 nm
0.1	124.8 nm	93.22 nm
0.2	122.0 nm	96.95 nm
0.3	122.4nm	106.1 nm
0.2-heat	58.26 nm	46.14 nm

5.3.3 Mechanical properties of CFs

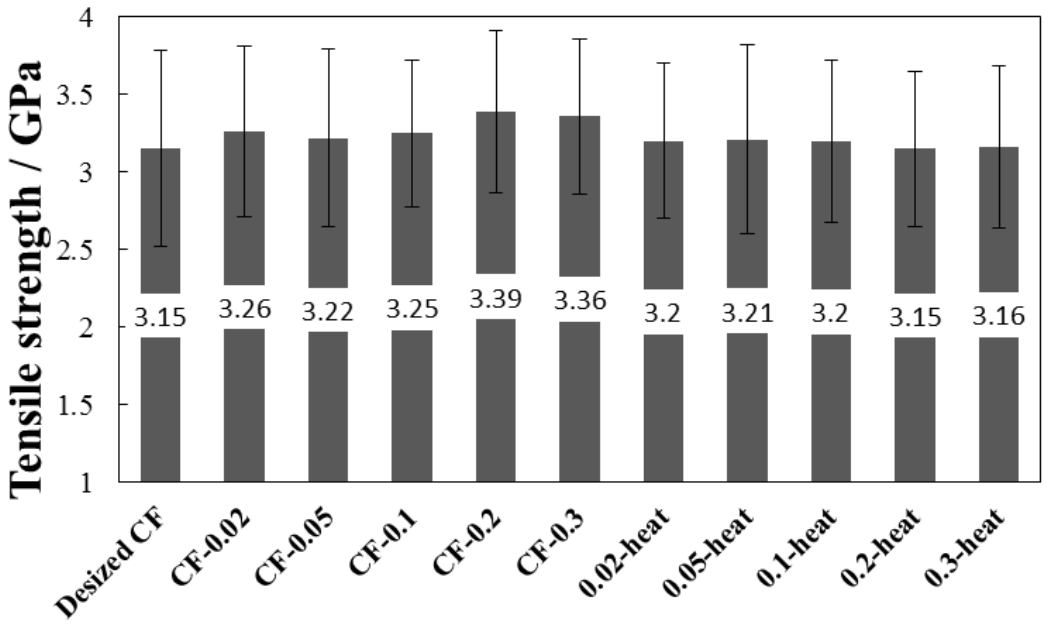

Fig. 5-7. Tensile strength of CFs.

The single-fiber strength is usually used to assess the effect of grafting modification on the tensile strength of the fiber; the detailed data is show in Fig. 5-7. Similar to previous studies, the addition of the PEI coating increased the single fiber strength [15, 25]. The introduction of the PEI coating on the CF surface could help heal

flaws or notches created during manufacturing process and reduce stress concentrations, resulting in an improved single fiber tensile strength [26]. For a PEI concentration of 0.2%, the single-fiber strength reached its maximum value (3.39 GPa).

After heating process during which some new defects could be formed, the strengths of all the coated samples decreased. However, the decrease in strength for the sample prepared with low PEI concentration was very slight; the decrease in strength for high PEI concentration was higher. It can be observed from the SEM images that for PEI concentrations of less than 0.05%, the PEI nanoparticles were completely melted; for PEI concentrations greater than 0.1%, the PEI nanoparticles fused together, forming many flat PEI blocks. These blocks could cause stress concentrations during fiber stretching, resulting in a higher decrease of the single-fiber tensile strength.

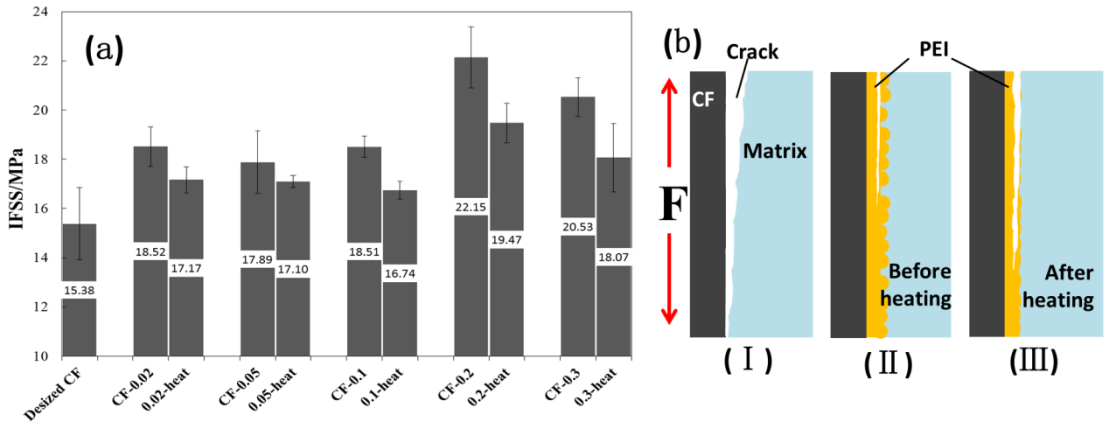

Fig. 5-8 (a) IFSS of CFs and (b) Schematic illustration of SFFT process: (I) desized CF; (II) treated CF before heating; (III) treated CF after heating.

The effect of CF surface modification on the IFSS as determined by single-fiber fragmentation (SFFT) is shown in Fig. 5-8a. The IFSS of the desized CF was only 15.38 MPa because of its clean and smooth surface. After modification, the surface roughness increased (as observed in the AFM results), which is thought to enhance the mechanical

interlocking between the fiber and resin. Therefore, the IFSS value increased after PEI modification. The IFSS increases were similar for PEI concentrations of less than 0.2%. At a PEI concentration of 0.2%, the IFSS value reached its maximum value, indicating that the highest interfacial strength was achieved for a uniform nanoparticle coating. When the concentration decreases, CF surface could not be covered by PEI nanoparticles completely and deterioration of this mechanical interlocking effect occurs. However, for a PEI concentration of 0.3%, the IFSS value also decreased. Because most of nanoparticles of 0.3% are nearly spherical, the combination of these nanoparticles with the PEI layer on the CF surface is relatively poor, in fact, weakening the interfacial strength. In addition, because of the presence of agglomeration, the epoxy resin did not uniformly contact the modified coating layer, resulting in the decrease of the IFSS.

To determine whether the appearance of nanoparticles increased the mechanical interlocking effect, the IFSS of the treated CF after heating was also tested. The IFSS values of all the heated samples clearly decreased, because of that the appearance of nanoparticles increases the contact area with the epoxy resin and improves the mechanical interlocking effect, making the fiber and resin more difficult to separate. This possible enhancement mechanism provided by the PEI nanoparticles in the CF-epoxy resin composite is schematically illustrated in Fig. 5-8b.

5.4 Conclusion

PEI nanoparticles were prepared on CF surfaces via an evaporation-induced surface modification method for which the particle diameter could be controlled by changing the PEI concentration. A possible formation mechanism for the PEI particles was proposed: the volatilization process during this modification was very long because of the nonvolatile nature of NMP, the PEI chains could form some separate

solvent-containing balls before the evaporation ends, then shrinks with evaporation, eventually forming PEI nanoparticles. When the PEI concentration was not higher than 0.2%, the nanoparticle morphology was almost hemispherical; when the PEI concentration was over 0.2%, many spherical particles appeared above the hemispherical nanoparticles.

In addition, the single-fiber strength and IFSS between the CF and epoxy resin increased after the surface modification. The interfacial shear strength (IFSS) contrast test results with treated CF before and after heating show that the presence of PEI nanoparticles (hemispherical) had a great influence on IFSS. And at a PEI concentration of 0.2%, the IFSS value reached its maximum value, 44.02% more than that of desized CF.

References

[1] B. Jiang, T. Zhang, L.W. Zhao, Y.D. Huang, Interfacially reinforced carbon fiber composites by grafting modified methylsilicone resin, Compos. Sci. Technol. 140 (2017) 39-45.

[2] W.Z. Qin, F. Vautard, L.T. Drzal, J.R. Yu, Modifying the carbon fiber-epoxy matrix interphase with graphite nanoplatelets, Polym Compos. 37 (2016) 1549-1556.

[3] M.A. Downey and L.T. Drzal, Compos. Toughening of carbon fiber-reinforced epoxy polymer composites utilizing fiber surface treatment and sizing, Appl. Sci. Manuf. 90 (2016) 687-698.

[4] D.I. Chukov, A.A. Stepashkin, M.V. Gorshenkov, V.V. Tcherdyntsev, S.D. Kaloshkin, Surface modification of carbon fibers and its effect on the fiber–matrix interaction of UHMWPE based composites, J Alloys Compd. 586 (2014) 459-463.

[5] X. Yuan, B. Zhu, X. Cai, J. Liu, K. Qiao, J. Yu, Improved interfacial adhesion in carbon fiber/epoxy composites through a waterborne epoxy resin sizing agent, J Appl Polym Sci. 134 (2017) 44757.

[6] J. Jiang, X. Yao, C. Xu, Y. Su, L. Zhou, C. Deng, Influence of electrochemical oxidation of carbon fiber on the mechanical properties of carbon fiber/graphene oxide/epoxy composites, Compos. Part A: Appl. Sci. Manuf. 95 (2017) 248-256.

[7] S.A. Song, C.K. Lee, Y.H. Bang, S.S. Kim, A novel coating method using zinc oxide nanorods to improve the interfacial shear strength between carbon fiber and a thermoplastic matrix, Compos. Sci. Technol. 134 (2016) 106-114.

[8] J.D. Dong, C.Y. Jia, M.Q. Wang, Improved mechanical properties of carbon fiber-reinforced epoxy composites by growing carbon black on carbon fiber surface, Compos. Sci. Technol. 149 (2017) 75-80.

[9] W. Liu, S. Zhang, L. Hao, F. Yang, W. Jiao, X. Li, et al. Fabrication of carbon nanotubes/carbon fiber hybrid fiber in industrial scale by sizing process, Appl Surf Sci. 284 (2013) 914-920.

[10] P. Agnihotri, S. Basu, K.K. Kar, Effect of carbon nanotube length and density on the properties of carbon nanotube-coated carbon fiber/polyester composites, Carbon. 49 (2011) 3098-3106.

[11] Z. Zhao, K. Teng, N. Li, X. Li, Z. Xu, Mechanical, thermal and interfacial performances of carbon fiber reinforced composites flavored by carbon nanotube in matrix/interface, Compos Struct. 159 (2017) 761-772.

[12] D. Jiang, L. Liu, G. Wu, Q. Zhang, J. Long, Z. Wu, et al. Mechanical properties of carbon fiber composites modified with graphene oxide in the interphase, Polym Compos. 38 (2016) 2425-2432.

[13] F. Li, Y. Liu, C.B. Qu, H.M. Xiao, Y. Hua, G.X. Sui, Enhanced mechanical properties of short carbon fiber reinforced polyethersulfone composites by graphene oxide coating, Polymer. 59 (2015) 155-165.

[14] W.Z. Qin, F. Vautard, L.T. Drzal, J.R. Yu, Mechanical and electrical properties of carbon fiber composites with incorporation of graphene nanoplatelets at the fiber–matrix interphase, Compos Part B. 69 (2015) 335-341.

[15] T. Naganuma, K. Naito, J.M. Yang, J. Kyono, D. Sasakura, Y. Kagawa, The effect of a compliant polyimide nanocoating on the tensile properties of a high strength PAN-based carbon fiber, Compos Sci Technol. 69 (2009) 1319-1322.

[16] K. Naito, Tensile properties of polyimide composites incorporating carbon nanotubes-grafted and polyimide-coated carbon fibers, J. Mater. Eng. Perform. 23 (2014) 3245-3256.

[17] H.M. Kang, T.H. Yoon, M. Bump, J.S. Riffle, Effect of solubility and miscibility on the adhesion behavior of polymer-coated carbon fibers with vinil ester resins, J. Appl. Polym. Sci. 79 (2001) 1042-1053.

[18] P.C. Varelidis, R.L. McCullough, C.D. Papaspyrides, The effect on the mechanical properties of carbon/epoxy composites of polyamide coatings on the fibers, Compos Sci Technol. 59 (1999) 1813-1823.

[19] T Duvis, C.D Papaspyrides, Carbon-Epoxy Composites Based on Fibers Coated with Nylon 6,6: Hygrothermal Ageing versus Interlaminar Shear Strength, Polym Adv Technol. 5 (1994) 444-450.

[20] T. Skourlis, T. Duvis, C.D. Papaspyrides, The role of a polyamide interphase on carbon fibres reinforcing an epoxy matrix, Compos Sci Technol. 48 (1993) 119-125.

[21] X.Z. Zhang, Y.D. Huang, T.Y. Wang, Surface analysis of plasma grafted carbon fiber, Appl Surf Sci. 253 (2006) 2885-2892.

[22] A.L. Woodhead, M.L. Souza, J.S. Church, An investgation into the surface heterogeneity of nitric acid oxidized carbon fiber, Appl. Surf. Sci. 401 (2017) 79-88.

[23] S. Basu, M. Heuchel, T. Weigel, K. Kratz, A. Lendlein, Integrated process for preparing porous, surface functionalized polyetherimide microparticles, Polymer. Adv. Tech. 26 (2015) 1447-1455.

[24] J.F. Watts, G. Beamson, D. Briggs (Eds.), High resolution XPS of organic polymers: The Scienta ESCA 300 database, John Wiley & Sons, Chichester (1992), ISBN 0471 935921.

[25] H. He, K. Li, F. Gao, Improvement of the bonding between carbon fibers and an epoxy matrix using a simple sizing process with a novolac resin, Constr. Buid. Mater. 116 (2016) 87-92.

[26] M. Sharma, S. Gao, E. Mäder, H. Sharma, L.Y. Wei, J. Bijwe, Carbon fiber surfaces and composite interphases, Compos Sci Technol. 102 (2014) 35-50.

CHAPTER SIX

Conclusions

Chapter 6: Conclusions

This thesis mainly focused on three parts: 1. Preparation of double-coated TiO_2 nanoparticles using an anchoring grafting method and investigation of the UV resistance of its reinforced PEI film; 2. Evaporation-induced surface coating of poly(p-phenylene benzobisoxazole) fibers with polyetherimide encapsulated nano-TiO_2; 3. Preparation of Polyetherimide nanoparticles on carbon fiber surface via evaporation induced surface modification method and its effect on tensile strength and interfacial shear strength. The conclusions are collected in this chapter.

In Chapter 1, an introduction on surface modification of high performance fibers, polymer grafted nanoparticles, fiber surface modification with inorganic nanoparticles, and polymer coating on fiber surface was made.

In Chapter 2, double-coated TiO_2 nanoparticles (TMP) were prepared using a single-pot fabrication method in NMP. These particles contained a chemically bonded layer of γ-MPS and a layer of PEI that was absorbed via Van der Waals forces. All fabrication and experimental processes were conducted in NMP, which prevented the agglomeration of particles during the centrifugal drying process. The double-coated TiO_2 nanoparticles (TMP) exhibited improved dispersion in NMP because of steric stabilization of the polymer chains that were absorbed to the particle surface and depletion stabilization of the free polymer in the solvent. In the long-term dispersion stability test, we found that there was a common cycle during the process of the sedimentation in which the suspension shown turbid firstly, then upper clarification and lower turbidity appeared, and then a clear interface layer appeared, and then the part over the interface layer turbid again. The double-coated TiO_2 nanoparticles (TMP) also exhibited improved dispersion within the PEI nanocomposite films and increased interface adhesion between the TiO_2 nanoparticles and the PEI matrix. Therefore, the nanocomposite TMP/PEI film exhibited increased mechanical properties and UV resistance.

In Chapter 3, poly(p-phenylene benzobisoxazole) (PBO) fibers were modified

using the evaporation-induced surface coating method. Through this new method, nano-TiO_2 particles encapsulated with polyetherimide (PEI) chains were firmly adsorbed on the fiber surface. The results indicate that besides some nanospheres resulted from the initial agglomeration of PEI-encapsulated nano-TiO_2, a uniform coating layer with thickness of 84 nm was formed by absorption of polyetherimide (PEI)-encapsulated nano-TiO_2. This coating method changed the surface morphology of the PBO fibers, enhanced the surface roughness, and increased the poor UV resistance of untreated PBO fibers.

In Chapter 4, to improve the UV resistance of poly(p-phenylene benzobisoxazole) (PBO) fibers, a sub-100-nm-thick coating layer was prepared on PBO fibers by evaporating the suspension of polyetherimide encapsulated nano titanium dioxide (TiO_2) particles absorbed around the fiber surface. The effects of this evaporation-induced surface modification on the structure and properties of PBO fibers were investigated. The content ratio of nano-TiO_2 particles to PEI, the contents of nano-TiO_2 particles and PEI, and the evaporation method greatly influenced the surface modification of the PBO fibers, as confirmed by scanning electron microscopy observation. The ultraviolet (UV) resistance of the PBO fibers was improved after surface modification, which confirmed by single-fiber tensile strength test.

In Chapter 5, PEI nanoparticles were prepared on CF surfaces via an evaporation-induced surface modification method for which the particle diameter could be controlled by changing the PEI concentration. A possible formation mechanism for the PEI particles was proposed: the volatilization process during this modification was very long because of the nonvolatile nature of NMP, the PEI chains could form some separate solvent-containing balls before the evaporation ends, then shrinks with evaporation, eventually forming PEI nanoparticles. When the PEI concentration was not higher than 0.2%, the nanoparticle morphology was almost hemispherical; when the PEI concentration was over 0.2%, many spherical particles appeared above the hemispherical nanoparticles.

List of publications

1. Peng Zhu, Bing Liu, Limin Bao, Preparation of double-coated TiO_2 nanoparticles using an anchoring grafting method and investigation of the UV resistance of its reinforced PEI film, *Progress in Organic Coatings*, 104 (2017) 81-90, DOI: 10.1016/j.porgcoat.2016.12.009. (**Accepted**)
2. Peng Zhu, Bing Liu, Limin Bao, Evaporation-induced surface coating of poly(p-phenylene benzobisoxazole) fibers with polyetherimide encapsulated nano-TiO_2, *Progress in Organic Coatings*, 146 (2018) 43-50, DOI: 10.1016/j.porgcoat.2017.11.017. (**Accepted**)
3. Peng Zhu, Bing Liu, Limin Bao, Preparation of a sub-100-nm-thick polyetherimide coating layer with nano-TiO_2 particles on poly(p-phenylene benzobisoxazole) fibers surface, *Journal of Applied Polymer Science*, DOI:10.1002/app.46852. **(Accepted)**
4. Peng Zhu, Fangtao Ruan, Limin Bao, Preparation of Polyetherimide nanoparticles on carbon fiber surface via evaporation induced surface modification method and its effect on tensile strength and interfacial shear strength, *Applied Surface Science*, 454 (2018) 54-60, DOI: 10.1016/j.apsusc.2018.04.232. (**Accepted**)
5. Bing Liu, Peng Zhu, Limin Bao, et al. Investigation of the recycling of continuous-fiber-reinforced thermoplastics. *Journal of Thermoplastic Composite Materials*, DOI: 10.1177/0892705718759388. (**Accepted**)

Scientific presentation

International conference

1. Peng Zhu, Limin Bao, Fabrication of surface-modified TiO_2 nano particle composite, The 9th International Silk Conference (ISC2016), Liuzhou, China, 8-10/09/2016, ISC16-1-47. (Oral)
2. Peng Zhu, Limin Bao, Preparation of double-coated TiO_2 nanoparticles and investigation of the UV resistance of its reinforced PEI film, The 12th China-Japan Joint Conference on Composite Materials (CJJCC-12), Kochi, Japan, 14-18/09/2016, 2D-04. (Oral)
3. Peng Zhu, Limin Bao, EVAPORATION-INDUCED SURFACE MODIFICATION OF PBO FIBER AND INVESTIGATION ITS UV RESISTANCE, 21st International Conference on Composite Materials(ICCM-21), Xi'an, China, 20-25/08/2017.(Oral)

Domestic conference

1. 朱　鵬, 鮑　力民. 表面改質した TiO_2 ナノ粒子コンボジットの創製, 日本機械学会　北陸信越支部　第５３期総会・講演会, 信州大学工学部, 05/03/2016.（口頭）

Acknowledgement

It is my pleasure to express my gratitude to all those who have contributed to my study.

First of all, I would like to thank my supervisor Prof. Limin Bao in Shinshu University, for giving me the opportunity to study and giving me a lot of useful advices.

Naturally, these studies have joint efforts with many other researchers. Thanks also would be given to my group-mates for their joining part of experiment work, as well for pleasant and enjoyable work environment that they made.

This work was supported by Grants for Excellent Graduate Schools, MEXT, Japan; and this work was also supported by Institute for Fiber Engineering (IFES), Interdisciplinary Cluster for Cutting Edge Research (ICCER), Shinshu University, Japan.

Finally, I dedicate my greatest thanks to my parents for their silent support. And thanks to my wife and my son, I must apologize for spending too much time in the lab without accompanying them often. Thank you all!